Dissertation

Submitted to the

Combined Faculty of Natural Sciences and Mathematics of

the Ruperto Carola University Heidelberg, Germany

for the degree of

Doctor of Natural Sciences

Presented by

José Ramón Robador Arteta (M. Sc.)

Born in: Bilbao, Spain

Oral examination: 14th of November, 2019

Crosstalk between melanoma cells and the blood-brain barrier:

Impact on coagulation and brain metastasis to identify new anti-metastatic targets

Referees:

Prof. Dr. rer.nat. Viktor Umansky

Prof. Dr. med. Stefan Werner Schneider

This thesis is dedicated to my family and the whole group of Experimental dermatology in the UKE, in particular to Dr. Alexander T. Bauer who guided and supported me during this time.

Table of content

I. Abstract

Brain metastasis is associated with a high risk for venous thromboembolism (VTE), which determines the prognosis of the patient. We postulated that von Willebrand factor (VWF), a procoagulant glycoprotein stored in endothelial cells (ECs) and platelets, contributes to VTE and promotes metastasis in the brain. Previously, it was shown that EC activation and the subsequent formation of luminal VWF fibers mediate the recruitment of platelets promoting tumor-associated vessel occlusion and pulmonary metastasis. However, little is known about the function of VWF within the specialized vascular bed of the blood-brain barrier. The aim of this project is to determine the contribution of VWF in the pathophysiology of brain metastasis.

Using *in vitro* approaches significant lower levels of VWF were detected in primary human microvascular brain ECs compared to macrovascular human umbilical vein ECs. This was reflected by a restricted release of VWF and low numbers of luminal VWF fibers upon tumor cell-induced brain EC activation. In line, brain microvessels of wild type mice showed low amounts of stored VWF and few VWF-platelet aggregates. However, immunofluorescence analyses of brain tissue from patients with brain metastasis revealed a strong formation of luminal VWF-platelet aggregates mediating vessel occlusions. These findings were confirmed in the *ret* transgenic mouse model, which develops spontaneous melanoma with metastasis in the brain: metastatic *ret* mouse brains showed a strong formation of intravascular VWF-platelet aggregates. Importantly, this phenomenon was already observed in brains of ret transgenic mice without visible cerebral metastasis, suggesting that luminal VWF fibers are involved in initial steps of the brain metastatic cascade. High resolution microscopy techniques revealed the contribution of activated platelets in the formation of luminal VWF networks in the brain. Consistent with this, aggregometry assays and *in vitro* microfluidic model of brain microcirculation showed that the lack of VWF in platelets (VWF-/-) resulted in a reduced platelet aggregation. Additionally, impedance measurements and transmigration assays demonstrated that blocking platelet activation with the low molecular weight heparin Tinzaparin reduces the impact of platelet-mediated endothelium disruption and the transmigration of tumor cells. Furthermore, systemic anticoagulation using Tinzaparin reduced platelet accumulation and VWF networks in ret mouse brains. The impact of anticoagulation on brain metastasis formation was examined after intracardiac injection of melanoma

cells in mice treated with Tinzaparin. Quantification of brain metastasis showed that Tinzaparin attenuates the metastatic load compared to non-treated control mice.
In summary, our findings provide new insights into the mechanisms by which platelet-derived VWF promotes cerebral thrombosis and identifies platelet activation as a promising therapeutic target for the prevention of brain metastases.

II. Zusammenfassung

Tumorpatienten mit Hirnmetastasen haben ein hohes Risiko venöse Thromboembolien (VTE) zu erleiden, was mit einer beschleunigten Tumorprogression und einer schlechten Prognose betroffener Patienten assoziiert ist. Aus dieser Erkenntnis resultiert die Hypothese, das Gerinnungsprotein von Willebrand Faktor (VWF), welches in Endothelzellen und zirkulierenden Blutplättchen gespeichert wird, nicht nur die Entstehung einer Thrombose vermittelt, sondern auch eine Metastasierung in das Gehirn fördert. In früheren Arbeiten konnte gezeigt werden, dass eine Tumorzelle das vaskuläre Endothel aktiviert. Die Konsequenz dieser Interaktion ist die Freisetzung von VWF, welcher unter Scherfluss fadenartige Netzerke ausbildet, Blutplättchen bindet und so thrombotische Gefäßverschlüsse und eine erfolgreiche Metastasierung in die Lunge unterstützt. Obwohl VWF folglich die Tumorprogression beeinflusst, bleibt dessen Funktion im spezialisierten Endothel der Blut-Hirn-Schranke unklar. Ziel der hier formulierten Arbeit war es daher, den Einfluss von VWF auf die Pathophysiologie von Hirnmetastasen zu untersuchen.

Es konnte gezeigt werden, dass primäre humane mikrovaskuläre Endothelzellen des Gehirns *in vitro* deutlich weniger VWF exprimieren, als makrovaskuläre Endothelzellen der Nabelschnurvene. Folglich belegten Stimulationsexperimente und Immunfluoreszenzen eine limitierte VWF Freisetzung und luminale Fadenbildung des zerebralen Endothels nach Aktivierung durch Melanomzellüberstand. Dieser Befund konnte auch *in vivo* an Gewebeschnitten von Maushirnen verifiziert werden, wobei nur wenig VWF und einzelne Thrombozyten in zerebralen Blutgefäßen detektiert wurden. Im Gegensatz dazu wurde in Gewebeproben humaner Hirnmetastasen und im *ret* transgenen Mausmodell, welches spontan maligne Melanome und Metastasen im Gehirn entwickelt, eine starke Zunahme luminaler VWF-Plättchen Aggregate beobachtet. Interessanterweise zeigte die gleiche Analyse VWF Fäden und Mikrothrombosierungen im zerebralen Gefäßsystem bevor Metastasen detektiert werden konnten. Das ist ein relevanter Befund, der eine plausible Erklärung für frühe Schritte in der Metastasierung liefert. Weiterhin konnten durch Implementierung hochauflösender Fluoreszenzmikroskopie, aktivierte Thrombozyten identifiziert werden, welche VWF Netzwerke freisetzen. Durch Aggregometrie und mikrofluidische Systeme zur Simulation der zerebralen Mikrozirkulation konnte gezeigt werden, dass VWF-defiziente Blutplättchen transgener Mäuse ein reduziertes

Aggregationsverhalten aufweisen. In diesem Zusammenhang wurde der Einfluss von Antikoagulatien auf die Thrombozyten mit Impedanzmessungen und Transmigrationsversuchen untersucht. Hierbei zeigte sich, dass das niedermolekulare Heparin Tinzaparin durch Blutplättchen induzierte lokale Änderungen der der endothelialen Barriere und eine Tumorzelltransmigration hemmt. In Übereinstimmung führte die Behandlung von tumortragenden *ret* transgenen Mäusen mit Tinzaparin zu einer signifikanten Verminderung von Plättchenaktivierung, VWF-Fadenbildung und Mikrothrombosierung im Gehirn. Letztlich konnte eine Therapie mit Tinzaparin nach intrakardialer Injektion von Melanomzellen, welche durch eine Bildung zerebralen Metastasen charakterisiert sind, deutlich die Metastasierung ins Gehirn reduzieren.

Zusammenfassend liefern die Befunde neue mechanistische Einblicke, inwieweit thrombozytärer VWF tumorassoziierte Thrombophilie und die Metastasierung in das Gehirn fördert. Eine gezielte Hemmung der Plättchenaktivierung liefert somit vielversprechende Therapieoptionen zur Behandlung von Krebspatienten.

III. Publications and scientific stay

Clinical Cancer Research (Under revision)

Platelets promote cerebral hypercoagulation and metastases via secretion of von Willebrand factor

Jose Ramon Robador (first coauthorship)*, Frank Thomas Mayer*, Manuel Feinauer, Frank Winkler, Anna Berghoff, Maria A. Brehm, Daniela Hirsch, Marisse C. Asong, Kai Nowak, Marcel Seiz-Rosenhagen, Viktor Umansky, Christian Gorzelanny, Stefan Werner Schneider and Alexander Thomas Bauer.

Clinical Cancer Research (Under revision)

Clot formation and brain metastasis

Manuel J. Feinauer, Anna S. Berghoff, **Jose Ramon Robador**, Gergely Solecki, Julia K. Grosch, Matthia A. Karreman, Katharina Gunkel, Bogdana Kovalchuk, Alexander Thomas Bauer, Matthias Osswald, Y. Schwab, Stefan Werner Schneider, Wolfgang Wick, Frank Winkler.

Neuro-Oncology (Under revision)

ALCAM promotes brain metastasis in non-small-cell lung cancer through interaction with the vascular endothelium

Justine Münsterberg & Desirée Loreth, Laura Brylka, Stefan Werner, Jana Karbanova Monja Gandrass, Svenja Schneegans, Katharina Besler, **Jose Ramon Robador**, Alexander Bauer, Michaela Wrage, Katrin Lamszus, Jakob Matschke, Yogesh Vashist, Güntac Uzunoglu, Stefan Steurer, Andrea Kristina Horst, Letizia Olivera-Ferrer, Markus Glatzel, Thorsten Schinke, Denis Corbeil, Klaus Pantel, Cecile Maire, Harriet Wikman.

Conference presentations:

03/2019	**Oral presentation at the GTH-Congress 2019, Berlin, Germany:** "Platelet-derived von Willebrand factor fosters intracranial hypercoagulation in metastatic brains of mice and humans" Jose R. Robador, Frank T. Mayer, Viktor Umansky, Christian Gorzelanny, Frank Winkler, Stefan W. Schneider and Alexander T. Bauer Selected abstract for the session: "Basic Science Highlights" on Saturday, March 2, 2019.
11/2017	**Poster presentation at the HALLMARKS OF SKIN CANCER (HoSC) CONFERENCE. Heidelberg, Germany:** "von Willebrand factor fibers mediate platelet aggregation promoting local disruption of the blood brain barrier in brain metastasis" Jose R. Robador, Thomas F. Mayer, Marisse Assong, Viktor Umansky, Frank Winkler, Alexander T. Bauer and Stefan W. Schneider
03/2016	**Poster presentation at the 45th Annual Meeting of the ADF, Vienna, Austria:** "Von Willebrand factor fibers in tumor vasculature mediate tumor

progression and inflammation in malignant melanoma”

Jose R. Robador, Alexander T. Bauer, L.Görtz, Jan Suckau, Anna Desch, Viktor Umansky and Stefan W. Schneider

Scientific research visit:

10/2017-02/2018 **Research stay at the group of Prof. Dr. Anthony Dorling**: MRC Centre for Transplantation, King's College London.

IV. Abbreviations

ADAMTS-13	A disintegrin and metalloproteinase with a thrombospondin type 1 motif, member 13
Ang-2	Angiopoietin 2
ATIII	Antithrombin III
BMECs	Brain microvascular ECs
BSA	Bovine serum albumin
cDNA	Complementary DNA
CNS	Central nervous system
CTC	Circulating tumor cells
DNA	Deoxyribonucleic acid
DVT	Deep vein thrombosis
ECIS	Electric cell-substrate impedance sensing
ECM	Extracellular matrix
ECs	Endothelial cells
ELISA	Enzyme-linked immunoabsorbent assay
EMT	Epithelial-mesenchymal transition
ERK	Extracellular-related kinase
F	Coagulation factor
FCS	Fetal calf serum
H&E	Hematoxylin & Eosin
HBMEC	Human brain microvascular endothelial cells
HBRS	HEPES-buffered Ringer solution
HEPES	4-(2-hydroxyethyl)-1-piperazineethanesulfonic acid)
HUVEC	Human vein umbilical endothelial cells
IHC	Intracranial hemorrhage
IL-8	Interleukin-8
LMWH	Low molecular weight heparin
LTA	Light transmission aggregometry
MC1R	Melanocortin receptor 1
MMP	Matrix metalloproteinase
mRNA	Messenger RNA
NK	Natural killer cells
Oligo DT nucleotides	Oligo deoxythymidine nucleotides
PAR	Proteinase-activated receptor
PAR-1	Proteinase-activated receptor-1
PBS	Phosphate-buffered saline

PBS-T	Phosphate-buffered saline -Tween
PCR	Polymerase chain reaction
PFA	Paraformaldehyde
PS	Phosphatidylserine
PTX	Pertussis toxin
qPCR	Quantitative polymerase chain reaction
qRT-PCR	Quantitative real-time polymerase chain reactions
rcf	Relative centrifugal force
ret	*Ret* transgenic mouse
Ret Sn	Ret supernatant
rh	Recombinant human
RNA	Ribonucleic acid
RT	Room temperature
TEER	Transendothelial electrical resistance
TF	Tissue factor
TFPI	Tissue factor pathway inhibitor
UFH	Unfractionateded heparin
ULVWF	Ultra-large VWF fibers
UVR	Ultraviolet radiation
UVA	Ultraviolet A
UVB	Ultraviolet B
UVC	Ultraviolet C
VEGF-A	Vascular endothelial growth factor
VEGF-A_{165}	Recombinant human Vascular endothelial growth factor A_{165}
VEGF-C	Vascular endothelial growth factor C
VEGFR-1	VEGF receptor-1
VEGFR-2	VEGF receptor-2
VTE	Venous thromboembolism
VWF	Von Willebrand factor
$VWF^{-/-}$	Von Willebrand factor deficient
WPB	Weibel-Palade body
Wt	Wild type

1. Introduction

1.1 Malignant melanoma

Malignant melanoma is a malignant neoplasm originating from the uncontrolled proliferation of degenerated melanocytes. Melanoma principally manifests on the skin (cutaneous melanoma) although it can also arise in mucosal surfaces, the uveal tract, and the leptomeninges (Matthews et al. 2017). The incidence of melanoma has substantially increased in the last decades (**Figure 1**) and the tendency suggests an increasing incidence in the next years (Guy et al. 2015). The American Cancer Society's estimated that about 96,480 new patients will be diagnosed with melanoma in 2019, being the fifth most common cancer in the United States (ACS). Similarly, in Europe, around 100,000 new cases are reported every year (Antoni et al. 2016).

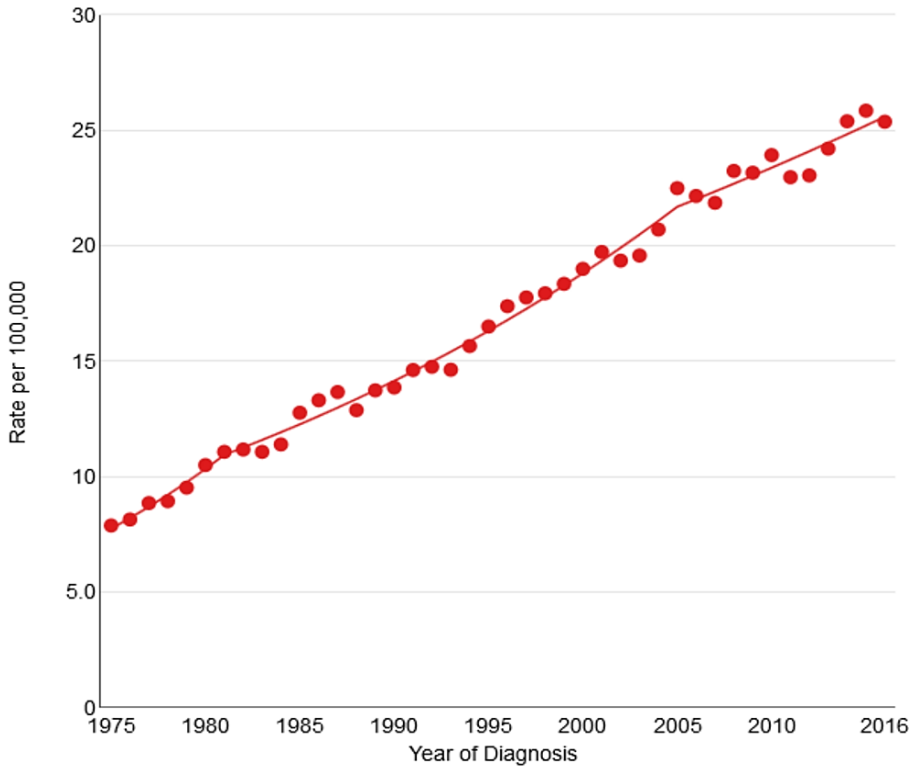

Figure 1. The incidence of malignant melanoma. The incidence for the occurrence of malignant melanoma per 100,000 inhabitants in the United States of America. Data were obtained from the American Cancer Society (ACS).

Although malignant melanoma accounts only for less than 5% of all skin malignancies, it is responsible for 80% of all the deaths from cutaneous cancer (Arlo

J. Miller and Martin C. Mihm 2008). When melanoma is diagnosed at an early stage, the lesion can be surgically resected and the prognosis is favorable with a 5-year survival rate of 98% (ACS). In contrast, in advanced stages, malignant melanoma shows an aggressive behavior with rapid systemic dissemination and very bad prognosis (Tas 2012). Therefore, a good understanding of the melanoma biology is required for the development of successful therapies improving the outcome of the patients.

1.1.1 Onset of malignant melanoma

Many environmental factors and a genetic predisposition influence the development of malignant melanoma. For instance, excessive exposure to ultraviolet radiation (UVR) can induce genetic lesions, which lead to the malignant transformation of melanocytes (Narayanan, Saladi, and Fox 2010). The UVR is divided into three classes: ultraviolet A (UVA [315–400 nm]), ultraviolet B (UVB [280– 315 nm]) and ultraviolet C (UVC [100–280 nm]) radiation (Tran, Schulman, and Fisher 2008). The UVB radiation is mainly responsible for the development of skin cancer (Glanz, Buller, and Saraiya 2007). The damaging effects of UVB radiation on the skin entail a direct damage of the DNA (formation of cyclobutane pyrimidine dimers), gene mutations, inhibition of the tumor immune surveillance, oxidative stress and inflammatory responses (Meeran, Punathil, and Katiyar 2008). Altogether favor the formation of a nevus, which has the potential to acquire a malignant phenotype and metastasize (Bald et al. 2014).

Regarding the genetic influence on the formation of cutaneous melanoma, Caucasian populations with light skin are predisposed to malignant melanoma due to a reduced production of melanin (Bradford 2009). Melanin is a photoprotective pigment produced by the skin melanocytes and distributed within the keratinocytes (Brenner and Hearing 2008). Melanin reduces the transmission of UVR through the epidermis, indeed, epidermis from Black people transmits significantly less UVR (7.4% of UVB and 17.5% of UVA) compared to Caucasian epidermis (24% of UVB and 55% UVA) (Gloster and Neal 2006). The reduced expression of melanin in Caucasian people is caused by a polymorphism in the melanocortin receptor 1 (MC1R) resulting in a lower pigmentation (Switonski, Mankowska, and Salamon

2013). Additionally, during the last years a better understanding of the molecular biology of malignant melanoma has contributed to identify a series of oncogenes associated with the emergence and progression of melanoma malignancy (**Table 1**). The occurrence of specific lesions in these oncogenes defines the etiology of the tumor (Kunz 2014). Nowadays, the identification and molecular-targeting of these oncogenes is implemented in the individual therapy of melanoma patients (Leonardi et al. 2018).

Table 1. Oncogenes and intracellular signaling molecules involved in the development of malignant melanoma.

Pathway	Gene or Protein	Function
RAS and MAPK	N-RAS	Oncogene
	BRAF	Oncogene
	Mitogen-activated protein kinase-extracellular related kinase (MEK)	Signal transduction
	Extracellular-related kinase 1 or 2 (ERK2 or ERK2) or mitogen activated protein kinase (MAPK)	Signal transduction
INK4A, CDK, and Rb	Cyclin-dependent kinase inhibitor 2A or inhibitor kinase 4 A (CDKN2A or INK4A)	Tumor suppressor gene
	Cyclin-dependent kinase (CDK4)	Cell growth promoter
	Cyclin D1 (CCND1)	Cell growth promoter
	Retinoblastoma (Rb)	Tumor suppressor gene
ARF and p53	Alternate reading frame (ARF)	Tumor suppressor gene
	Tumor protein 53 (p53)	Tumor suppressor gene
	Mouse double minute 2 (MDM2)	p53 ubiquitination
	BCL-2 associated X protein (BAX)	Induces cell death
PTEN and AKT	Phosphatase and tensin homologue (PTEN)	Tumor suppressor gene
	Phosphatidylinositol 3 kinase (PI3K)	Cell signaling molecule
	Protein kinase B (AKT or PKB)	Cell survival promoter
	BCL-2 antagonist of cell death (BAD)	Induces cell death
	Forkhead receptor (FKHR)	Cell growth suppressor

Note: Adapted from Miller and Mihm 2006.

According to the Clark model, the development of malignant melanoma can be divided into 5 steps (Clark et al. 1984) (**Figure 2**): **a**) The first step in melanoma development is the formation of a nevus. This is characterized by the proliferation of regular melanocytes due to defective activation of the proliferative pathways (mainly the mitogen-activated protein kinase [MAPK]/extracellular-related kinase [ERK] signaling pathways) (McCain 2013). **b**) The growth of the nevus is controlled by tumor suppressor genes, like the cyclin gene family (Flørenes et al. 2000). However, the accumulation of genetic lesions in these genes leads to a dysplastic phase characterized by uncontrolled proliferation of aberrant melanocytes. **c**) Next, the dysplastic nevus can enter into a new phase known as the radial growth, which is defined by the suppression of apoptotic mechanisms (i.e., by homozygous deletions in phosphatase and tensin homologue [PTEN]) (Agosto-Arroyo et al. 2017). **d**) Then, the nevus evolves towards an invasive or vertical growth phase associated with the penetration through the basement membrane and the formation of an intradermal nodule (Betti et al. 2016). **e**) At this point, metastatic melanoma cells can dissociate from the primary nevus (i.e., Slug (Snai2) expression causes cell-cell desmosome dissociation) and migrate through the stroma until they eventually arrive at the circulatory system (Shirley et al. 2012).

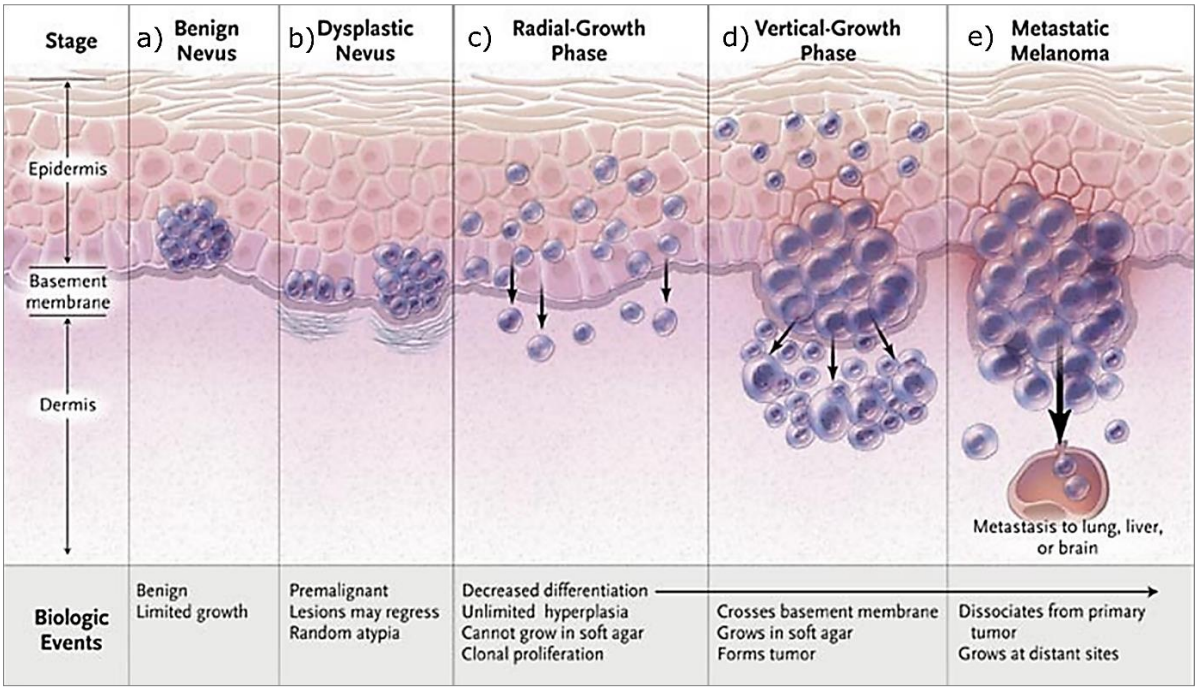

Figure 2. Tumor progression of malignant melanoma. Schematic overview showing different steps in the progression of malignant melanoma according to the Clark model. *Adapted from Miller and Mihm 2006*.

1.1.2 Mesenchymal transition of malignant melanoma

Invasion of distant organs by tumor cells implies a complex process which includes the access of tumor cells to the circulatory system, the dissemination through the lymphatic system or the bloodstream, arresting on a vessel wall and extravasation into a new tissue, and finally the metastatic colonization of the new tissue (Lambert, Pattabiraman, and Weinberg 2017).

To succeed, a tumor cell must develop a series of “abilities” which involve the remodeling of cell-cell interactions, the modification of cell polarity and the acquisition of motility skills, all generated by the activation of a new transcriptional program (Dongre and Weinberg 2019). This process is known as the epithelial-mesenchymal transition (EMT) (**Figure 3**).

In malignant melanoma, EMT is characterized by the downregulation of E-cadherin, an adhesion integrin important for the maintenance of cell-cell adhesion (Yan et al. 2016). In turn, the expression of N-cadherin is enhanced promoting the motility of melanoma cells (Mrozik et al. 2018). Additionally, the overexpression of matrix metalloproteinases (MMPs), such as MMP2 or MMP3, promotes the degradation of the basement membrane and facilitating tumor cell access to ECs (Liu et al. 2017). The expression of αVβ3 integrin in melanoma cells facilitates the interaction with ECs and favors the transmigration towards the circulatory system (Pearlman et al. 2017).

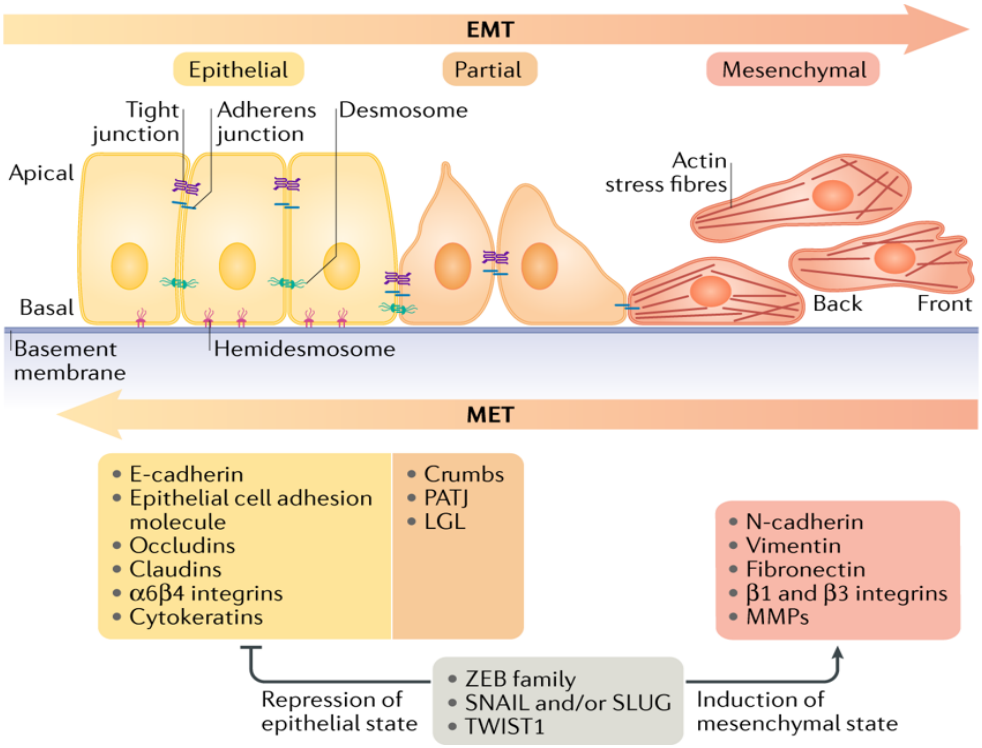

Figure 3. The Epithelial-mesenchymal transition. The initiation of the epithelial-mesenchymal transition (EMT) is promoted by the expression of EMT-inducing transcription factors which enhance the disassembly of the epithelial cells and induce changes in their morphology, their motility and their invasive capacities. *Adapted from Dongre and Weinberg 2019.*

1.1.3 Malignant melanoma dissemination

The dissemination of metastatic cells is the major cause of cancer mortality (Guan 2015). Commonly, malignant melanoma starts its spreading through the lymphatic system (Tejera-Vaquerizo et al. 2012). The secretion of vascular endothelial grow factor C (VEGF-C) by malignant melanoma cells induces the growth of lymphatic vessels towards the primary tumor (Fankhauser et al. 2017). In turn, the infiltration of lymph vessels around the tumor tissue generates a proinflammatory microenvironment that promotes tumor progression (Karlsson et al. 2017). Indeed, tumor-induced expression of the chemokine ligand 1 (CCL-1) in the lymph nodes fosters the migration of malignant melanoma cells towards the lymphatic system (Das et al. 2013). Additionally, it has been described that lymphatic endothelial cells promote the expression of EMT-inducing transcription factors in tumor cells by activation of Notch 3 and β1-integrin signals in tumor cells (L. Liu et al. 2014; Pekkonen et al. 2018). Moreover, given the role of the lymphatic system in the

drainage of the extracellular fluids into the blood (Ji 2006), it has been suggested that lymphatic vessels may favor the communication between the tumor tissue and the blood stream facilitating the hematogenous dissemination to distant organs (Joyce and Pollard 2009).

Tumor cell dissemination through the circulatory system is a complex process that can be divided in different steps. To intravasate into the blood stream, a tumor cell interact with the endothelium and transmigrate through the EC barrier (Reymond, D'Água, and Ridley 2013). In the blood, the shear stress and the immune surveillance greatly reduce the chances of a tumor cell to survive (Rejniak 2016). Therefore, circulating tumor cells (CTCs) rapidly bind to platelets (Labelle et al.2012.), which protect cancer cells from immune recognition, shear stress and facilitate CTC attachment to the endothelium (Leblanc and Peyruchaud 2016a). Attached CTCs interact with the ECs to extravasate into the new tissue (Bendas and Borsig 2012). In the new location, the metastatic cell must evade the immune response, adapt to the new microenvironment and then, proliferate (Chaffer and Weinberg 2011) (**Figure 4**).

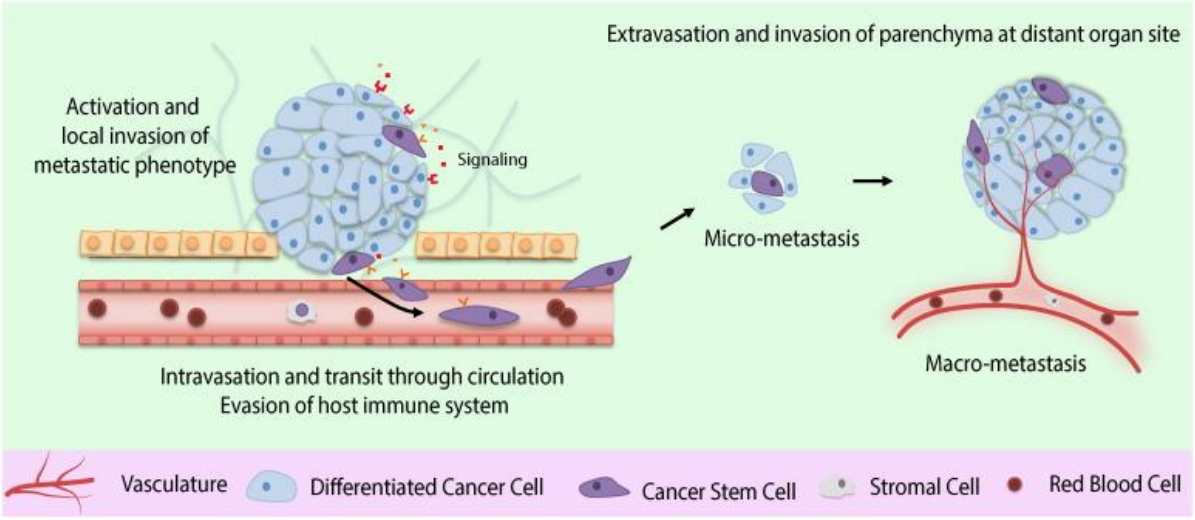

Figure 4. The hematogenous dissemination of a metastatic cell. The hematogenous dissemination of a metastatic cell can be divided in four major phases: (I) the activation of a metastatic phenotype (EMT) in a tumor cell. (II) The intravasation and circulation of metastatic cell through blood stream. (III) The extravasation in a foreign tissue. (IV) The proliferation and invasion of the distant organ (Ganapathy, Moghe, and Roth 2015).

Interestingly, malignant melanoma exhibits a high incidence of metastasis to the lung (10-40%), the liver (14-20%) and the central nervous system (2-20%)

(Belhocine et al. 2006) and when this occurs the survival of patients is considerably reduced, with a 5-year survival rate of only 5-19% (Sandru et al. 2014).

1.1.4 Therapeutic options

Considering the characteristics of the tumor, such as its stage, metastasis locations and the genetic features different treatments are implemented: at early stages, the primary treatment consists on the surgical resection of the primary tumor including safety margins according to the Breslow thickness (Melanoma Research Alliance), usually this procedure is combined with adjuvant therapies which improve the clinical responses (Kwak et al. 2019). For disseminated melanoma, chemotherapy was the most common treatment option for many years. However, the capacity of tumor cells to develop drug resistance reduced the efficacy of this kind of treatments (Soengas and Lowe 2003). Nowadays, chemotherapy has been substituted by other therapies, and may be used in a palliative treatment (Wilson and Schuchter 2016).

In the early nineties, immunotherapy appeared as a promising treatment option for cancer patients in advanced stage. Immunotherapy aims to activate the immune system to seek and destroy tumor cells: immunotherapy fosters the anti-tumor activity of T-cells, B lymphocytes, natural killer cells and dendritic cells, and in addition, inhibits pro-tumorigenic cells like regulatory T-cells and myeloid derived suppressor cells (Oiseth and Aziz 2017). The introduction of immune-checkpoint inhibitors, such as the anti-Programmed cell death protein 1 (PD-1) antibodies nivolumab or pembrolizumab or the anti-Cytotoxic T-lymphocyte-associated protein 4 (CTLA-4) ipilimumab have revolutionized the treatment of melanoma patients during the last years. Indeed, it has been recently shown that the implementation of PD-1 inhibitors improves the response rates up to 44% with an 3-year overall survival of up to 52% (Hamid et al. 2013; Larkin et al. 2018).

However, is known that the immunogenic tumor microenvironment can influence the immune system response and affects the efficacy of immunotherapies (Gasser, Lim, and Cheung 2017). In the last decade, the discovering of a series of mutations in genes involved in the proliferation and aggressiveness of melanoma cells (**section 1.1.1**) has promoted the development of promising molecular therapies, which target proteins derived from this mutated genes (Leonardi et al. 2018). For

example, in melanoma patients with BRAF mutation specific targeted therapies, with BRAF and MEK inhibitors combined with anti-PD-1 immunotherapies revealed a dramatic improvement of the prognosis of patients in advanced stage (Flaherty et al. 2012).

Taken together, the last advances in cancer therapy have demonstrated promising results in the survival of cancer patients (Domingues et al. 2018). However, the prolonged survival of patients suffering malignancies has brought a new challenge for the oncologists, an increased incidence of brain metastasis (Franchino, Rudà, and Soffietti 2018).

1.1.5 Melanoma brain metastasis

Brain metastases are the most frequent intracranial tumors: compared to primary tumors in the brain the incidence of brain metastasis is 3 to 10-fold higher (Davis et al. 2012). The most common primary cancers in patients with brain metastasis are pulmonary malignancies (36–64%), breast cancer (15–25%) and skin (melanoma) (5–20%) (Stelzer 2017).

It is important to note that the metastatic invasion of the brain differs from metastatic processes in other organs, mainly due to the special properties of the blood-brain barrier (BBB) constituted by the neurovascular unit. The principal element of the BBB is the cerebral blood vessel. Compared to other tissues, ECs from the BBB exhibit special characteristics. Intercellular boundaries are tightly sealed by the formation of tight junctions (TJs) and adherens junctions (AJs). Besides, cerebral ECs lack of fenestrae and exhibit a low transcytosis, which notably reduces both the paracellular and transcellular diffusion through the BBB (Obermeier, Daneman, and Ransohoff 2013). Additionally, astrocytes, pericytes and neurons form the neurovascular unit providing structural and functional support to the BBB (Wilhelm et al. 2013) (**Figure 5**). Therefore, the BBB presents a physical and functional barrier which maintains a strict regulation of the molecular and cellular trafficking between the peripheral blood and the CNS (W.-Y. Liu et al. 2012) This profound regulation of CNS homeostasis defends the neural tissue against, toxins, inflammatory processes and pathogen invasion (Daneman and Prat 2015). However, in malignant disease, this barrier function acts as a double-edged sword in the formation of cerebral metastasis (Fidler 2015). On the one hand, the BBB

limits the penetration of immune cells from the circulatory system into the brain parenchyma (Daneman and Prat 2015). On the other hand, a transient weakening of the BBB integrity allows the transmigration of tumor cells into the brain parenchyma (Blecharz et al. 2015), then, the BBB protects tumor cells from the immune response and drug delivery, limiting the therapeutic options for the patient (Wilhelm et al. 2013).

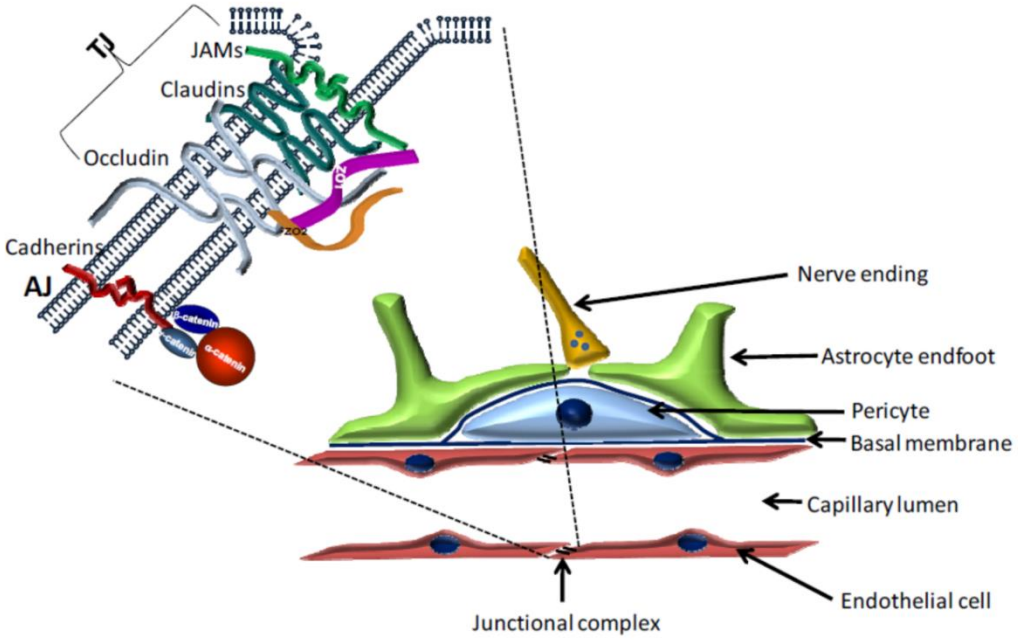

Figure 5. The blood-brain barrier. Brain ECs are interconnected by a continuous line of tight junctions (TJs) and adherens junctions (AJ). Brain pericytes, astrocytes and nerve-ending feet establish a close contact with brain ECs providing a structural and functional support to the blood-brain barrier. *Adapted from Wilhelm et al. 2013*.

As it was mentioned before, malignant melanoma is the third most common tumor of brain metastasis (Davis et al. 2012). Indeed, 75% of melanoma patients in stage IV develop cerebral metastasis (Davies et al. 2011) and this is associated with a very poor prognosis with a median survival of only 4 to 5 months (Vosoughi et al. 2018). The emergence of new treatments combining immune-checkpoint inhibitors with targeted therapies have significantly prolonged the survival of melanoma patients with brain metastasis (Harary, Reardon, and Iorgulescu 2019). However, despite the increased survival of these patients the development of a cerebral metastasis is still, with rare exceptions, a fatal complication (Fidler 2015). Therefore, to prevent the formation of brain metastasis is essential to understand the

mechanisms involved in the metastatic invasion of the CNS. Importantly, patients with brain metastases exhibit an enhanced systemic hypercoagulability, which accounts for a notable percentage of the mortality and morbidity reported due to the high risk of thromboembolic complications (Caine et al. 2002).

1.2 Cancer and thrombosis

The association between cancer progression and thrombotic complications is well established since in 1865 the French physician Armand Trousseau described the correlation between gastric cancer and venous thromboembolism (VTE) (Trousseau 1865).

Indeed, it is estimated that 4-20% of the cancer patients suffer from VTEs at some stage of the disease (Abdol Razak et al. 2018). The highest incidences of VTE have been observed in patients with cancer of the brain, lung, uterus, pancreas, stomach, bladder and kidney (Sheth et al. 2017). The occurrence of VTEs is also related to the stage and aggressiveness of the disease. It has been shown that VTE incidence varies from 1% in some cancer entities and increases up to 20% in aggressive malignancies, such as pancreatic cancer and malignant gliomas (I. Pabinger and Ay 2012). Consistent with this, patients with an advanced stage of malignant melanoma are at high risk of suffering VTEs (incidence of 25% in stage IV) (Sparsa, et al. 2011) and this risk is particularly increased in patients bearing cerebral metastases (Alvarado et al. 2012). The incidence of VTE is often associated with a poor prognosis, due to an elevated risk of metastasis and decreased survival (Wun and White 2009). Indeed, it was reported that cancer patients with VTEs exhibit a significant lower survival in the first year (12%) compared to patients without VTEs (36%) (Sørensen et al. 2000). Based on these observations, it can be speculated that CTC interact with the coagulation system and vascular ECs, promoting hypercoagulation and favoring metastasis.

1.2.1 Melanoma and the activation of the plasmatic coagulation

Cancer-associated activation of the coagulation depends on the ability of tumor cells to interact with the components of the plasmatic coagulation system. (Lima and Monteiro 2013). The major initiator of the coagulation cascade is the transmembrane protein Tissue factor (TF) (Mackman 2009). Under normal circumstances, physiological active TF is not in contact with the blood components. However, when vascular damage occurs subendothelial TF is exposed to the coagulation factors in the blood (Butenas et al. 2005). Additionally, inflammatory

conditions induce the expression of active TF in neutrophils and monocytes contributing to the activation of the coagulation(Bode and Mackman 2014; Darbousset et al. 2012). Exposed TF initiates the extrinsic coagulation cascade by the formation of the extrinsic tenase complex with activated factor (F) VII (FVIIa). The extrinsic tenase complex activates FIX and FX. Then, FXa together with activated FV (FVa) cleave FII (prothrombin) generating FIIa (thrombin) (**Figure 6**). In turn, the serine protease thrombin is an important regulator of platelet/thrombocyte aggregation and EC activation by cleaving the protease-activated receptors (PARs) (Coughlin 2000).

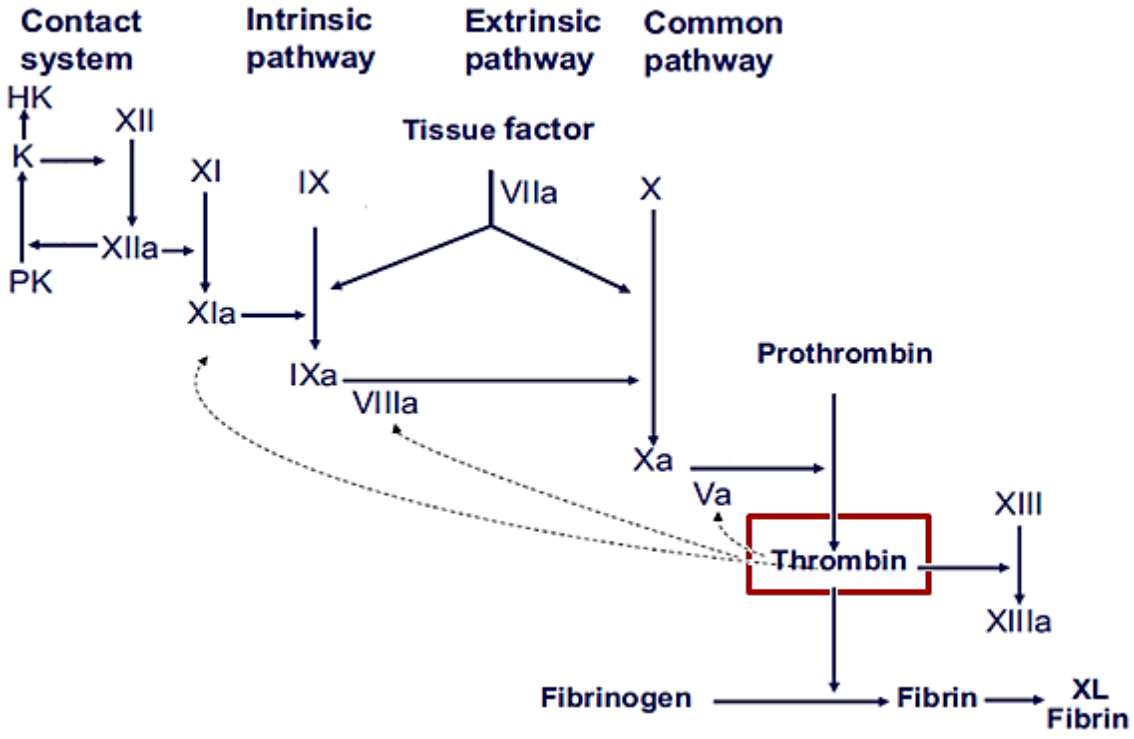

Figure 6. Plasmatic activation of thrombin. The coagulation factors in the blood circulate as zymogens. Their eventual activation triggers their serine protease activity which cleaves the next zymogen in the coagulation cascade generating more serine proteases which finally activate fibrinogen (Chaudhry and Babiker 2019). *Image adapted from Cugno and Tedeschi 2013*.

Interestingly, the expression of TF has been correlated with the aggressiveness of distinct tumor cell lines (Gerotziafas et al. 2012; Lima et al. 2011; Mueller et al. 1992) In line with this, TF is frequently overexpressed on the surface of melanoma

cells (Kerk et al. 2010). Moreover, the activation of the tenase complex is enhanced by the expression of phosphatidylserine molecules in the extracellular matrix of melanoma cells, which provides an optimal negatively charged surface for the assembly of coagulation factors (Spronk, ten Cate, and van der Meijden 2014). Many clinical studies have shown the relation between TF expression in tumor cells and the progression of the disease. It was shown that elevated levels of plasmatic tumor-derived TF is associated with a high incidence of thromboembolic complication and increased metastases (Tesselaar et al. 2009; Yokota et al. 2009; Zwicker et al. 2009). Consistent with this, Tinholt and colleagues showed that enhanced expression of TF pathway inhibitor (TFPI) in breast tumors correlates with a better prognosis for the patients. In contrast, they also showed that patients with large tumors exhibit decreased expression of TFPI associated with elevated levels of plasmatic TF and multiple metastases (Tinholt et al. 2015). These findings suggest a strong link between the activation of the coagulation cascade and tumor dissemination.

1.2.2 Interaction between tumor cells and the vascular endothelium

An indispensable condition for metastasis dissemination is the interaction between tumor cells and the vascular endothelium. The crosstalk between tumor cells and ECs triggers a series of intracellular signaling pathways which modulate the phenotype of ECs (Pober 2002). This process is known as *EC activation* and turns the endothelium into a procoagulant and proadhesive surface which facilitates cell adhesion and extravasation (Blann 2012).

Indeed, previous studies described how melanoma cells mediate EC activation. It was shown that the expression of TF on the surface of melanoma cells induces the generation of thrombin. This protease is not only involved in coagulation but also contributes to EC activation by cleaving the endothelial PAR-1 (Kerk et al. 2010). Additionally, melanoma cells secrete vascular endothelial growth factor A (VEGF-A), which binds to the endothelial VEGF receptor 2 (VEGFR-2) and activates ECs (Desch et al. 2012). It was shown that this mechanism is further amplified by the secretion of MMP-2, which enhances the expression of VEGF-A via interaction with αVβ5 integrin and MMP-14 (Desch et al. 2012) (**Figure 7**).

One of the consequences of EC activation is the massive influx of calcium ions into the cytoplasm (Andrikopoulos et al. 2015; Cudmore et al. 2012). The increase of intracellular calcium activates Rab GTPases (Parkinson et al. 2014). Activated Rab GTPase triggers a complex signaling pathway, which ends up with the exocytosis of Weibel-Palade body (WPB) organelles (Nightingale and Cutler 2013). WPBs contain many different biomolecules, such as P-selectin, interleukin-8 (IL-8),angiopoietin-2 (Ang-2) and von Willebrand factor (VWF), which are involved in angiogenesis, inflammation, coagulation and tissue repairing (Valentijn et al. 2011) (**Figure 7**).

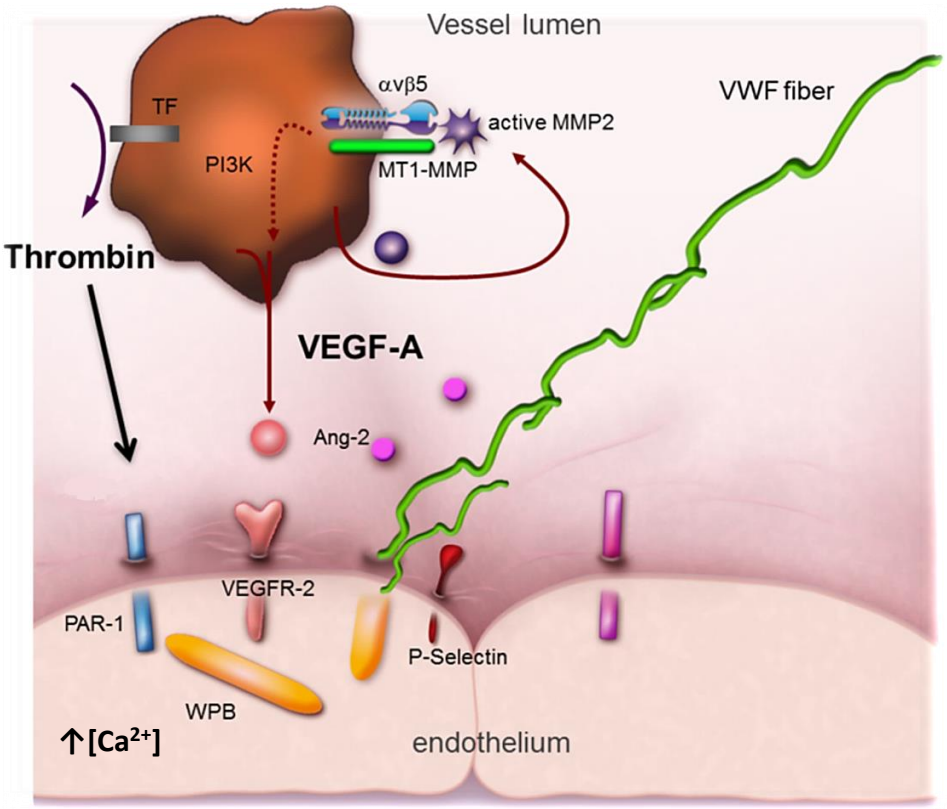

Figure 7. Mechanisms of endothelial cell activation. Indirect Activation: Melanoma cells activate the coagulation cascade by exposition of TF on their cell surface This interaction results in the generation of thrombin which cleaves PAR-1 on the surface of EC (Kerk et al. 2010). Direct activation: Melanoma cells secrete VEGF-A which activates endothelial cells via VEGF receptor-2. VEGF-A secretion is enhanced in an autocrine fashion via MMP-2-αvβ5 integrin interaction (Desch et al. 2012). Both pathways lead to the exocytosis of WPBs and luminal secretion of Ang-2, P-selectin and VWF. *Adapted from Desch et al., 2012.*

1.2.3 Von Willebrand factor

As it was described above, tumor-mediated EC activation triggers the exocytosis of WPBs. The most abundant constituent of WPBs is the prothrombotic glycoprotein VWF (Valentijn et al. 2011). This protein is principally stored by ECs in WPBs and by platelets in α-granules (Randi and Laffan 2017).

The VWF precursor protein (pre-po VWF) is composed of 5 distinct domain groups: The propeptide domains D1 and D2, the D'D3 domains, the A domains (-A1-A2-A3-), the D4 domain and the C domains (-C1-C2-C3-C4-C5-C6-CK) (Zhou et al. 2012). Each group of domains displays a specific binding site enabling VWF to bind several ligands simultaneously (Ruggeri 2003b) (**Figure 8**).

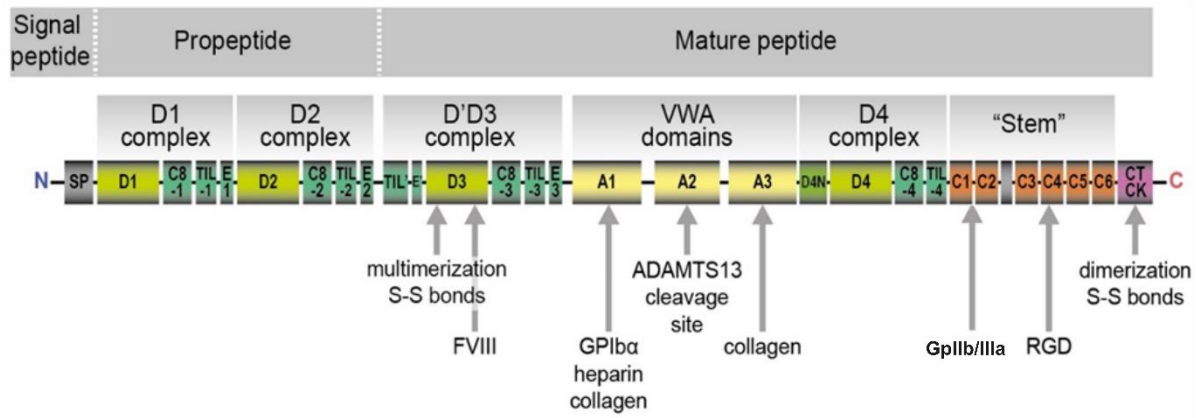

Figure 8. Structure and binding sites of VWF. The pre-pro VWF consists of a sequence of domains: (D1-2 group) - (D'D3 group) - (D4 group) -C1-C2-SS. In the Golgi apparatus the pro-pre VWF undergoes a maturation process by which the pro-peptide (D1 and D2 group) is cleaved and VWF peptide is glycosylated. Each domain of the mature VWF glycoprotein shows a specific binding sites: Platelet glycoproteins GpIb and GpIIb/IIIa interact with the A1 and C1-C2 domains respectively; the coagulation factor VIII (FVIII) binds to the D3 domain; collagen binds to VWF in the A1-3 domains; and ADAMTS13 cleaves VWF by the A2 domain *Adapted from* www.shenc.de

The synthesis of VWF is initiated in the rough endoplasmic reticulum where the pre-pro VWF is dimerized by disulfide bridges in the C-terminal CK domains. Pre-pro VWF dimers are then delivered to the Golgi apparatus where the propeptide D1-2 is cleaved. Then, the VWF peptide is glycosylated resulting in a mature VWF

glycoprotein. The mature VWF plays a central role in primary blood hemostasis (Gale 2011): Under physiological conditions VWF is secreted into the abluminal surface of the vessel (J. W. Wang et al. 2011). When the vascular endothelium is disrupted, subendothelial VWF is exposed to the blood components and mediates the accumulation of thrombocytes at the site of the injury, preventing bleedings and contributing to vessel repair (Brass 2001; Eming, Krieg, and Davidson 2007) (**Figure 9**).

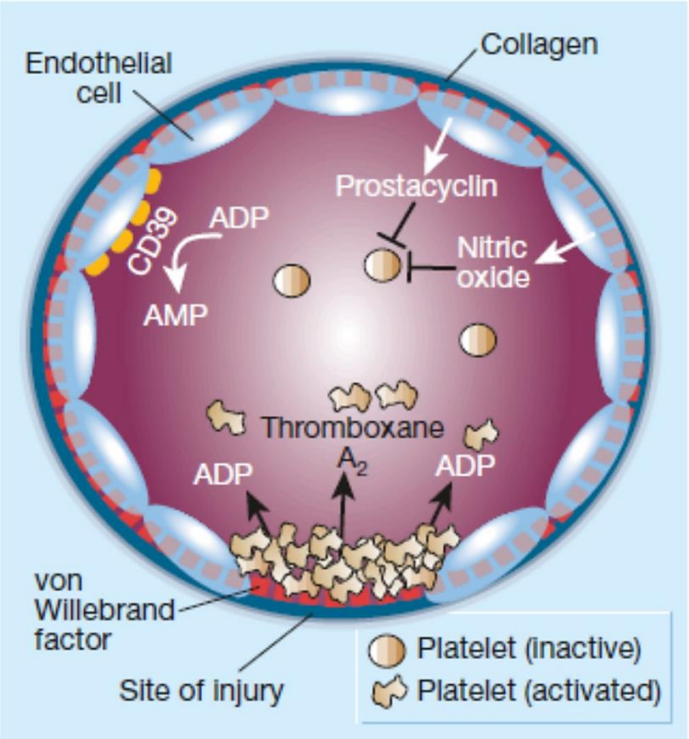

Figure 9. Role of von Willebrand factor in vessel repair. ECs-secreted prostacyclin and nitric oxide maintain platelets in a resting state. The enzyme CD39 expressed on the luminal surface of ECs hydrolyzes active ADP, impeding the activation of platelets by ADP. At sites of vascular injury, disruption of the endothelium exposes collagen fibrils and the subendothelial VWF. VWF exposition mediates the adhesion of platelets. Collagen activates platelets which secrete APD and thromboxane A into the lumen inducing the local formation of a platelets plug, which closes the gap in the vessel wall. Source: Brass 2001.

In parallel, VWF is constitutively secreted into the plasma(Peyvandi, Garagiola, and Baronciani 2011a). In the plasma VWF binds to FVIII and protects it against proteolytic degradation, thereby, FVIII is available for the completion of the plasmatic coagulation cascade (Schrenk et al. 2010). Circulating VWF shows an inactive globular conformation which hides its binding domain A2 (Gragnano et al. 2017). However, under certain conditions, such as high shear rates, globular VWF is rapidly elongated into a long string conformation becoming active (Crawley et al. 2011) (**Figure 10 A and B**).

In addition, mature VWF dimers are also polymerized and organized in helical VWF

tubules tightly packed in WPBs (Lenting, Christophe, and Denis 2015). Each WPB stores between 10,000 to 50,000 compacted tubular VWF multimers, which are responsible for the elongated shape of WPBs (Huck, Schneider, Gorzelanny, & Schneider, 2014). This “spring-loaded” structure of WPB-stored VWF facilitates the release of VWF towards the lumen when WPB exocytosis is promoted (Michaux et al. 2006). Under inflammatory conditions VWF is released from WPBs (KM et al. 2010). The exposition of densely packed multimeric VWF tubules to the luminal conditions triggers a rapid elongation of VWF tubules and the formation of ultra-large VWF (ULVWF) strings/fibers, a process favored by the hydrodynamic forces of the blood flow (Schneider et al., 2007). Still attached to the EC surface by interaction with P-selectin, integrin αVβ or membrane lipids ULVWF strings become activated by the exposure of their binding sites (Huck et al. 2014) (**Figure 10 A-C**).

Activated VWF strings mediate the recruitment of platelets and leukocytes, contributing to tissue repair, coagulation and inflammation (Petri et al., 2010; Ruggeri, 2003). This process is strongly regulated by a disintegrin and metalloproteinase with a thrombospondin type 1 motif, member 13 (ADAMTS13), which cleaves VWF in the A2 domain (Fujioka et al. 2010) and reduces the thrombogenic potential of an excessive formation of luminal ULVWF fibers (Lenting, Christophe, and Denis 2015) (**Figure 9 D**).

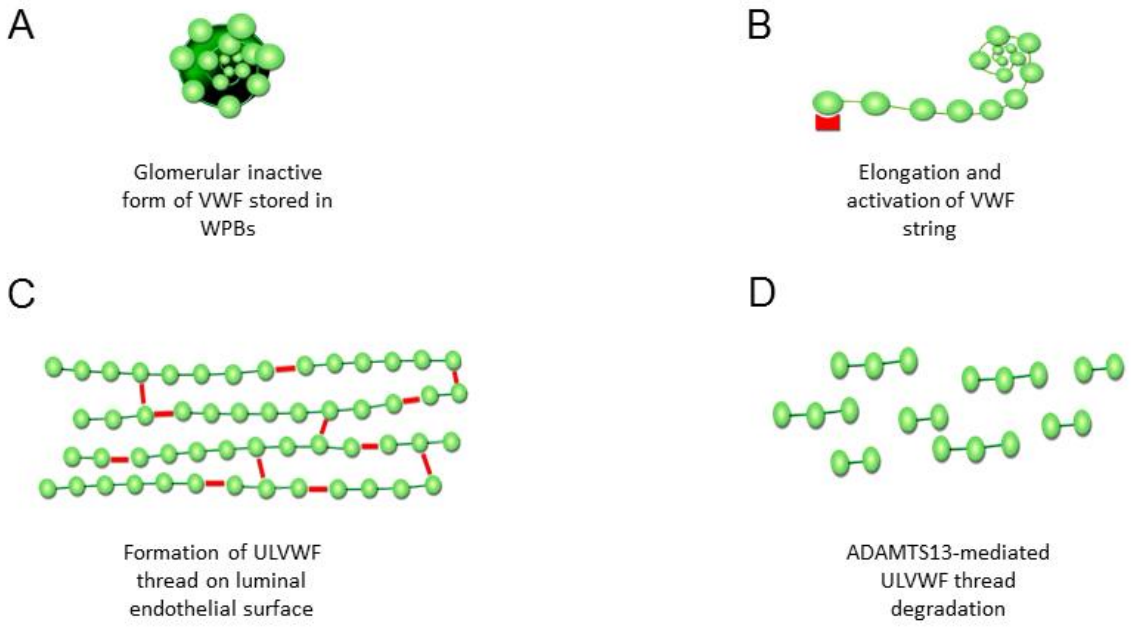

Figure 10. VWF activation and regulation. A. The globular VWF multimers are stored in WPBs of ECs. EC activation induces the release of VWF multimers into the vessel lumen. **B.** VWF multimers anchoraged to the endothelial surface are unfolded by the hydrodynamic forces of the bloodstream. **C.** Subsequently, the multimers crosslink and form intraluminal VWF threads on the endothelial surface. **D.** This process is regulated by the VWF-specific protease ADAMTS13 which cleaves VWF protein in the A2 domain.

1.2.4 Pathology of dysregulated von Willebrand factor activity

Due to the important contribution of VWF in the maintenance of blood hemostasis a deficient expression or dysregulated activation of VWF can lead to severe pathologies.

The most frequent bleeding disorder caused by a deficient expression of VWF is the inherited von Willebrand disease (VWD). VWD is classified in three subtypes: The VWD type 1 is characterized by low levels of VWF (Sadler et al. 2003). The VWD type 2 presents more severe symptoms, it is caused by the occurrence of mutations in distinct domains affecting VWF functionality, multimerization or binding capacity (Tosetto and Castaman 2015). The VWD type 3 consists of a complete absence of VWF resulting in life-threatening hemorrhages (Phillips, Lazarchick, and Bergmann 2016). Additionally, VWF deficiency can be acquired by the generation of autoantibodies against VWF which leads to the clearance of plasmatic VWF, this situation is defined as the acquired von Willebrand syndrome (AVWS) and is associated with severe bleedings (Federici 2006).

Conversely, a defective regulation of intraluminal VWF activity is related to thrombotic complications. This situation is depicted in the Thrombotic thrombocytopenic purpura (TTP) disease, characterized by a deficient ADAMTS13 activity (Mannucci and Peyvandi 2007). Two types of TTP have been described: the Moschcowitz syndrome associated with the generation of ADAMTS13 autoantibodies which dampen the activity of this enzyme in the plasma, and the inherited ADAMTS13 deficiency or Upshaw-Schulman syndrome (Tsai 2007). Both disorders are characterized by the accumulation of luminal ULVWF fibers mediating platelet aggregation and subsequent vascular occlusion. Additionally, this condition leads to a pathological consumption of platelets and consequently to thrombocytopenia which results in critical bleeding episodes (Ferrari, Rottensteiner,

and Scheiflinger 2013).

Furthermore, increased plasmatic levels of plasmatic VWF have been reported in several disorders associated with the occurrence of thrombotic events or microvascular damage. For instance, high levels of VWF were related to the incidence of thromboembolic strokes and myocardial infarctions (Conway et al. 2003; Morange et al. 2004). Additionally, this phenomenon has been also detected in patients suffering nephritis, pregnancy-induced hypertension, diabetic angiopathy and pulmonary hypertension (Müller et al. 2002a). Interestingly, elevated levels of plasmatic VWF haven been also detected in patients with various types of malignancies (Damin et al. 2002; Röhsig et al. 2001; W.-S. Wang et al. 2005a). Consistent with this, significant deficiencies of ADAMTS13 activity have been also detected in patients with metastasis (Garam et al. 2018; Page et al. 1992; Rieger et al. 2005), suggesting the contribution of VWF in cancer-associated thrombotic complications. In line with this, a recent publication of our group showed the impact of intraluminal VWF on to the development of cancer-associated thrombotic vessel occlusion in a mouse model of malignant melanoma (Bauer, et al. 2015). In addition, *in vitro* studies have demonstrated that VWF supports the adhesion of tumor cells (Floyd et al. 1992; Gomes, Legrand, and Lafeve 2005). These data suggest a pivotal role of VWF promoting cancer-associated thrombotic complications on the one hand and metastasis on the other.

1.2.5 Role of von Willebrand factor in cerebral pathologies

Little is known about the impact of VWF on pathophysiological processes in the CNS. However, an increasing body of evidence shows that elevated levels of plasmatic VWF are associated with diverse neuropathologies, such as ischemic strokes or intracranial endothelial injury (Folsom et al. 1999; Sandsmark et al. 2019; H. Yokota 2007). In line with this, O'regan and colleagues reported that VWF-mediated platelet and leukocyte recruitment in the brain compromises the integrity of the BBB and favors the progression of cerebral malaria (O'regan et al. 2016). Furthermore, it was shown that BBB stiffness is significantly enhanced in VWF-deficient mice showing low permeability upon hypoxia or seizure insults (Suidan et al. 2013). Furthermore, the absence of VWF in mice has been correlated with a

reduced disruption of the BBB and smaller edemas formation after ischemic insults (Kleinschnitz et al. 2009; Zhu et al. 2016). These studies indicate a role of VWF in increasing the permeability of the BBB in cerebral pathologies.

However, in an experimental model of pulmonary metastasis the absence of WPBs in VWF-deficient mice resulted in an increase of lung metastases (Terraube et al. 2006) a process which is correlated with an increase of vascular permeability (M.J. et al. 2012). This suggests different roles of VWF regulating the permeability in different vascular beds. Indeed, the vasculature is an organ that exhibits a strong heterogeneity. and it was shown that distinct vascular beds show different features and properties according to its location and function (Cines et al. 1998). This affects the expression of many EC-derived proteins, including VWF (Yamamoto et al. 1998). Given the specialized features of the CNS vasculature, characterized by a notable prothrombotic activity protecting the CNS from bleedings (Fisher 2013), the function and expression of VWF might be specifically regulated in the BBB to prevent pathological hypercoagulation.

Here we asked whether the specific function of VWF in the brain vasculature may have an impact on the hypercoagulable state related to brain metastasis.

2 Aim of the project

Hypercoagulability is a frequent complication in melanoma patients suffering from brain metastases. The aim of this project was to elucidate the relative contribution of endothelial cell-derived and platelet-derived von Willebrand factor in tumor-associated thrombosis and brain metastasis. To this end, we have applied high resolution microscopy techniques, microfluidic assays, *in vitro* models of the blood-brain-barrier and light transmission aggregometry assays. To confirm the clinical relevance of our findings, tissue samples from human metastatic brains were analyzed. Additionally, the *ret* transgenic mouse model of malignant melanoma with brain metastasis was implemented to study the contribution of VWF to brain metastasis *in vivo*. To examine the therapeutic impact of systemic anticoagulant on brain metastasis formation, the low molecular weight heparin Tinzaparin was evaluated in two different mouse models of brain metastasis. A better understanding of the mechanisms that contribute to the hypercoagulability associated with brain metastasis will lead to the discovering of potential targets for the development of novel therapeutic approaches.

3 Materials and methods

3.1 Materials

3.1.1 Laboratory equipment

Device	Product reference
Balance	CPA623S, Sartorius AG; Göttingen, Germany.
Centrifuge I	Heraeus® Megafuge 1.0R, DJB Labcare Ltd, Newport Pagnell, UK.
Centrifuge II	5910 R, Eppendorf AG, Hamburg, Germany.
Gel imaging system.	Intas Gel IX Imager, INTAS Science Imaging Instruments GmbH. Göttingen, Germany.
Electric Cell-substrate Impedance Sensing (ECIS) array	ECIS® 8W10E+ PET array Applied BioPhysics, NY 12180, USA.
Fluorescence Microscope	Z1 AxioObserver inverted fluorescence microscope, Carl Zeiss AG; Oberkochen, Germany.
ibidi Pump system: • ibidi Pump ibidi Perfusion Set ibidi Fluidic Unit	ibidi GmbH, Martinsried, Germany.
Cell culture incubators	Heraeus® CO2 Incubator. BBD6220, Thermo Fisher Scientific, Waltham, USA. MCO-17AIC CO2 Incubator. SANYO Electric Biomedical Co., Ltd. Panasonic, Osaka, Japan.

Light transmission aggregometer	CHRONO-LOG® Model 700, Chrono-log corporation, Harvertown, USA.
LightCycler®	LightCycler® 96 Sytem. Roche Life Sciences, Mannheim, Germany.
Magnetic stirrer	Mr 3001 Heidolph Instruments GmbH & CO. KG, Schwabach, Germany.
Microplate Readers	Power Wave XS2, BioTek Instruments, Inc; Winooski, VT, USA.
	Infinite® 200 PRO multiwell reader Life Sciences-Tecan Trading AG, Switzerland.
Microtome	Kryostat CM1900, Leica Microsystems; Wetzlar, Germany.
NanoDrop	NanoDrop™ 2000/2000c Spectrophotometer. Thermo Fisher Scientific, Waltham, USA.
Reflected light Microscope	Olympus CH2 Binocular Microscope, Olympus Europa SE & Co. KG, Hamburg, Germany.
Stereo Microscope	AF 90mm f/2.8, Tamron; Saitama, Japan.
Thermal Cycler	UNO Thermal Block, Biometra GmbH, Göttingen, Germany.
Ultrapure water system	PURELAB flex 3, ELGA LabWater,Hgh Wycombe, UK.
Vortexers	Vortex-Genie 2, Scientific Industries, Inc., NY, USA.
	Genius 3, IKA®-Werke GmbH & Co. KG; Staufen, Germany.
Water bath	TW20, Julabo GmbH; Seelbach, Germany.

3.1.2 Substances

Name	**Product reference**
1,4-Diazabicyclo Octane (DABCO)	Sigma-Aldrich Biochemie GmbH, Hamburg, Germany.
4,6-Diamidino-2-Phenylindole (DAPI)	Sigma-Aldrich Biochemie GmbH, Hamburg, Germany.
$CaCl_2$	Carl Roth GmbH & Co. KG, Karlsruhe, Germany
CellTrace™ Calcein Green, AM	Invitrogen, Darmstadt, Germany.
CellTrace™ Calcein Orange-red, AM	Invitrogen, Darmstadt, Germany.
D -Glucose (Dextrose)	Sigma-Aldrich Biochemie GmbH, Hamburg, Germany.
Dimethyl sulfoxide (DMSO)	Sigma-Aldrich Biochemie GmbH, Hamburg, Germany.
Ethanol (ETOH)	Carl Roth GmbH & Co. KG, Karlsruhe, Germany.
Bounding glue	Fixogum, Marabu GmbH & Co. KG; Bietigheim-Bissingen, Germany
Isoflurane	Abbvie GmbH & Co. KG, Ludwigshafen am Rhein, Germany.
KH_2PO	Carl Roth GmbH & Co. KG, Karlsruhe, Germany.
Methanol	Sigma-Aldrich Biochemie GmbH, Hamburg, Germany.
$MgCl_2$	Carl Roth GmbH & Co. KG, Karlsruhe, Germany
Mowiol mounting medium	Sigma-Aldrich Biochemie GmbH, Hamburg, Germany.
Na_2HPO_4	Sigma-Aldrich Biochemie GmbH, Hamburg, Germany.
NaCl	Sigma-Aldrich Biochemie GmbH, Hamburg, Germany.
Polysorbat 20	Tween® 20, Carl Roth GmbH & Co. KG; Karlsruhe, Germany.

Triton X-100	Sigma-Aldrich Biochemie GmbH, Hamburg, Germany.
Trypan blue	Sigma-Aldrich Biochemie GmbH, Hamburg, Germany.
Ultra-purified H_2O	
2-Mercaptoethanol	Sigma-Aldrich Biochemie GmbH, Hamburg, Germany.

3.1.3 Buffers and solutions

Name	**Composition**
4-(2-hydroxyethyl)-1-piperazineethanesulfonic acid (HEPES)	Sigma-Aldrich Biochemie GmbH, Hamburg, Germany.
Blocking buffer I	HEPES containing 0.3% TritonX-100 and 2% of BSA.
Blocking Buffer II	10% Goat Serum in PBS-T.
Citrated buffer	S-Monovette, SARSTETD AG &Co., Nümbrecht, Germany.
HEPES-buffered Ringer Solution (HBRS)	140 mM NaCl, 5 mM KCl, 1 mM MgCl2, 1 mM CaCl2, 5 mM Glucose, 10 mM HEPES.
Incubation Buffer	HEPES containing 0.3% TritonX-100
Phosphate Buffer Saline (PBS)	140 mM NaCl; 2.5 mM KCl; 6.5 mM Na_2HPO_4; 1.5 mM KH_2PO_4.
Phosphate Buffer Saline-Tween (PBS-T)	0.1% Tween® 20 in PBS.
Platelet resuspension buffer (PRB)	5% BSA in PWB (pH = 7.4.)
Platelet washing buffer (PWB)	103 mM NaCl, 5 mM KCl, 3 mM NaH_2PO_4* H_20, 5 mM HEPES, 5.5 mM Glucose (pH = 6.5)
Saline Solution	0.9% NaCl. B Braun AG, Melsungen, Germany.

3.1.4 Reagents and Kits

Reagents	**Product reference**
Adenosine 5'-diphosphate (ADP)	Sigma-Aldrich Biochemie GmbH, Hamburg, Germany.
Alexa 488-conjugated fibrinogen	Thermo Fisher Scientific, Waltham, USA.
Angiopoietin-2-ELISA-Kit	DuoSet® ELISA Development Systems, R&D Systems, Inc., Minneapolis, MN, USA.
Apyrase	Sigma-Aldrich, Inc.; St. Louis, USA.
Bevacizumab	Avastin, Roche Diagnos-tics GmbH, Mannheim, Germany.
Bovine serum albumin (BSA)	Sigma-Aldrich Biochemie GmbH, Hamburg, Germany.
Collagenase	Sigma-Aldrich, Inc.; St. Louis, USA.
Color Reagent A and Color Reagent B	R&D Systems, Wiesbaden, Germany.
Corning® Collagen type I	Corning Life Sciences, Amsterdam, The Nederland.
Fondaparinux	Arixtra®, Sanofi; Paris, France.
Goat serum	Dako Denmark A/S; Glostrup, Denmark.
Histamine	Sigma-Aldrich Biochemie GmbH, Hamburg, Germany.
Human Fibrinogen-Alexa Fluor™ 488	Thermo Fisher Scientific, Waltham, USA.
Protease inhibitor E-64	Calbiochem, Darmstadt, Germany.
Stop solution	2N H_2SO_4 ; Carl Roth GmbH & Co. KG, Karlsruhe, Germany
Thrombin (Human)	Sigma-Aldrich Biochemie GmbH, Hamburg, Germany.
Thrombin (Mouse)	Sigma-Aldrich Biochemie GmbH, Hamburg, Germany.

Tinzaparin	Innohep®, LEO Pharma A/S; Ballerup, Denmark.
Trypsin EDTA	Sigma-Aldrich Biochemie GmbH, Hamburg, Germany.
$VEGF_{165}$ (Human)	R&D Systems, Wiesbaden, Germany.

Kits

ADAMTS13 screening assay kit	Technoclone GmbH, Vienna, Austria
PCR-Kit	SYBR Green PCR Kit, Qiagen N.V.; Hilden, Germany.
Proteome Profiler-kit	Proteome Profiler Mouse Angiogenesis Array Kit, R&D Systems, Inc., Minneapolis, MN, USA.
Reverse Transcription Kit	QuantiTect Reverse Transcription Kit, Qiagen N.V.; Hilden, Germany.
RNA isolation-Kit	RNeasy Mini Kit, Qiagen N.V.; Hilden, Germany.
VEGF-A-ELISA-Kit	DuoSet® ELISA Development Systems, R&D Systems, Inc., Minneapolis, MN, USA.

3.1.5 Cell culture materials

Material	**Product reference**
12-well flat bottom with lid	Falcon®, Becton, Dickinson and Co. (BD), NJ, USA.
24-well flat bottom with lid	Falcon®, Becton, Dickinson and Co. (BD), NJ, USA.
Cell culture flask T75	Falcon®, Becton, Dickinson and Co. (BD), NJ, USA.
Cell culture flasks T25	Falcon®, Becton, Dickinson and Co. (BD), NJ, USA.
Cell culture inserts	ThinCert™ 24Well, Greiner Bio One International GmbH
Cell strainer (20 µm diameter)	Merck & Co., Inc., New Jersey, USA.
Coverslips Ø 20 mm	Menzel-Gläser, Thermo Fisher Scientific

	Gerhard Menzel B.V. & Co. KG; Braunschweig, Germany.
Cryovial (2 ml)	Thermo Fisher Scientific, Waltham, USA.
Dulbecco's Modified Eagle's Medium (DMEM)	Merck & Co., Inc., New Jersey, USA.
Endothelial Cell Growth Medium-2 (EGM™-2)	Lonza Group AG, Basel, Switzerland.
Endothelial Cell Medium (ECM)	ScienCell, Carlsbad, USA.
Fetal bovine serum (FBS)	Boehringer Mannheim, Mannheim, Germany.
Human Fibronectin	Sigma-Aldrich, Inc.; St. Louis, USA.
Medium 199 (M199)	Gibco-Thermo Sicentific, Waltham, USA.
Neubaur cell counter	Neubauer bright line, Paul Marienfeld GmbH & Co. KG, Lauda-Königshofen, Germany.
Porcine Gelatin	Sigma-Aldrich Biochemie GmbH, Hamburg, Germany.
Roswell Park Memorial Institute-Medium (RPMI)	Sigma-Aldrich Biochemie GmbH, Hamburg, Germany.
Trypsin EDTA	Sigma-Aldrich Biochemie GmbH, Hamburg, Germany.
µ-Slide 0.2 Luer	Ibidi GmbH, Munich, Germany

3.1.6 Primers

Targeted gene	**Sequence**	
VWF	Forward	5'-TGGTGCAGGATTACTGCGGC-3'
	Reverse	5'-GCTTTGCCCAGCAGCAGAAT-3'
PAR-1	Forward	5'-CCTGCTTCAGTCTGTGCGG-3'
	Reverse	5'-CTGGTCAAATATCCGGAGGCA-3'
VEGFR-1	Forward	5'-GCAAAGCCACAACCAGAAG-3'
	Reverse	5'-ACGTTCAGATGGTGGCCAAT-3'
VEGFR-2	Forward	5'-CGTGTCTTTGTGGTGCACTG-3'
	Reverse	5'-GGTTTCCTGTGATCGTGGGT-3'
P-Selectin	Forward	5'-CGTGGAATGCTTGGCTTCTG-3'
	Reverse	5'-TGAGCGGATGAACACAGTCC-3'
Ang-2	Forward	5'-CCTGTTGAACCAAACAGCGG-3'
	Reverse	5'-AACAGTGGGGTCCTTAGCTG-3'
ß-Actin	Forward	5'-AGAAAATCTGGCACCACACC-3'
	Reverse	5'-CCATCTCTTGCTCGAAGTCC-3'

3.1.7 Antibodies

Primary antibodies	**Working concentration**	**Incubation period**	**Product reference**
Mouse anti-Human CD 31	1:75	Overnight	M0823, Dako Denmark A/S; Glostrup, Denmark.
Mouse anti-Human TSP	1:75	120 minutes	Laboratory Vision/ Neomarkers
Rabbit anti-Human VWF	1:150	120 minutes	A0082, , Dako Denmark A/S; Glostrup, Denmark.
Rat anti-Mouse CD31	1:75	Overnight	550274, BD Pharmingen,
Rat anti-Mouse CD42b	1:75	120 minutes	M042-0, EMFRET Analytics,
Sheep FITC-conjugated anti-Human/Mouse	1:150	90 minutes	GTX28822, GeneTex, Inc, Irvin, USA
Secondary antibodies			
Alexa Fluor® 488 Donkey anti-Sheep IgG	1:200	60 minutes	A11015, Invitrogen, Darmstadt, Germany.
Alexa Fluor® 555 Goat anti-Mouse IgG	1:200	60 minutes	A21422, Invitrogen, Darmstadt, Germany.
Alexa Fluor® 555 Goat anti-Rabbit IgG	1:200	60 minutes	A21428, Invitrogen, Darmstadt, Germany.
Alexa Fluor® 555 Goat anti-Rat IgG	1:200	60 minutes	A21434, Invitrogen, Darmstadt, Germany.
FITC Goat anti-Rabbit IgG	1:200	60 minutes	554020, Becton, Dickinson and Company (BD), NJ, USA.

FITC Goat anti-Rat IgG	1:200	60 minutes	554016, Becton, Dickinson and Company (BD), NJ, USA.
Rabbit anti-Human VWF/HRP	1:200	60 minutes	P0226, Dako Denmark A/S; Glostrup, Denmark.

3.1.8 Consumables

Product description	**Product reference**
Cell strainer (20 µm diameter)	Merck & Co., Inc., New Jersey, USA.
ELISA-Microplate (96-Wells)	Nunc MaxiSorp®, Affymetrix, Inc.; Santa Clara, USA.
Filter tips: 10, 20, 200, 1000 µl	epTIPs Dualfilter, Eppendorf Research® plus, Eppendorf AG; Hamburg, Germany.
Needles (20G)	Falcon®, Becton, Dickinson and Co. (BD), NJ, USA.
Object slide 25 x 75 x 1 mm^3	Menzel-Gläser Superfrost Plus, Thermo Fisher Scientific Gerhard Menzel B.V. & Co. KG; Braunschweig, Germany
Polypropylene tubes 15 ml	Falcon®, Becton, Dickinson and Company (BD), Franklin Lakes, NJ, USA.
Polypropylene tubes 5 ml	Falcon®, Becton, Dickinson and Company (BD), Franklin Lakes, NJ, USA.
Polypropylene tubes 50 ml	Falcon®, Becton, Dickinson and Company (BD), Franklin Lakes, NJ, USA.
Safe lock tubes: 0.5, 1.5 and 2 ml	Eppendorf Research® plus, Eppendorf AG; Hamburg, Germany.
Serological pipettes (5, 10 and 25 ml)	SARSTEDT AG & Co. KG, Nümbrecht, Germany.
Syringes (1 ml and 20 ml)	Becton Dickinson (BD) and Co., New Jersey, USA.
Tips 10, 20, 200, 1000 µl	epT.I.P.S®, Eppendorf AG; Hamburg, Germany.

3.1.9 Software

Product description	**Source**
Fiji/ImageJ	NIH, USA
GraphPAd Prism	GraphPad Software, Inc. USA
Inkscape vector graphic editor	Inkscape. Open source. inkscape.org
Light Cycler ® 96 Software 1.1	Roche Life Sciences, Mannheim, Germany.
Mendeley	Mendeley Ltd.,UK
Microplate Software Gen 5 V1.3	BioTek Instruments, Inc; Winooski, VT, USA.
Microsoft Ofice™	Microsoft Corporation, Washington, USA.
Nano drop 2000	Thermo Fisher Scientific, Waltham, USA.
PlateletWeb	Systems Biology Workbench. University of Würzburg
Zeiss Zen Microscope Software	Zeiss, Jena, Germany

3.1.10 Cell lines

HUVEC: Primary human umbilical vein endothelial cells (HUVECs) were isolated from umbilical cords as it was previously described (Kerk et al. 2010).

HBMEC: Primary human microvascular endothelial cells (HBMECs) were purchased from ScienCell #1000 (USA).

bEND3: The murine immortalized brain endothelial cell line bEND3 was purchased from ATCC Genuine Cultures® CRL-2299™ (USA).

Ret cells: Ret melanoma cells (Ret cells) kindly provided by Prof. Viktor Umansky, from the Skin Cancer Unit, German Cancer Research Center (DKFZ), Heidelberg, Germany. Ret cells were originally isolated from skin tumors from *ret* transgenic mice (Zhao et al. 2009)

3.1.11 Animals

Our animals were maintained under specific pathogen-free conditions and all experiments were performed according to a protocol approved by the governmental animal care authorities. **Permission numbers for animal experimentation:** AZ: 35-9185.81/G-206/16 and G-220/16.

The Wild type C57BL/6J (**Wt**) mice were purchased from the Jackson Laboratory (USA).

VWF deficient (**VWF KO**) mice with C57BL/6 background were originally purchased from the Jackson Laboratory (USA) and maintained in our own breeding facility.

The ***ret* transgenic mouse** (***ret***) was kindly provided by Prof. Viktor Umansky from Skin Cancer Unit, German Cancer Research Center (DKFZ), Heidelberg, Germany. These animals with a C57BL/6 background overexpress the human ret transgene in melanocytes. Its expression is regulated by mouse metallothionein-I promotor-enhancer (Kato et al. 1998). The *ret* mice develop spontaneously cutaneous melanoma with metastases in different organs such as lymph nodes, lungs, liver, brain and the bone marrow (Umansky and Sevko 2013), resembling the malignant melanoma disease in humans.

3.2 Methodology

3.2.1 Cell culture

3.2.1.1 Culture initiation

All cells were seeded in T25 or T75 flasks as monocultures and maintained under culture conditions, in a humidified atmosphere at 37°C and 5% CO_2. All the work involving cellular material was carried out under strict sterile conditions. To this end, all cells were manipulated within a laminar flow bench previously decontaminated with 70% ETOH. Cell monitoring was performed daily and the nutrient medium was changed every two days:

HUVECs were grown in a 0.5% Gelatin (Sigma-Aldrich) coated surface in a complete culture medium containing two thirds of M199 (Life Technologies), supplemented with 2% of fetal bovine serum (FBS), hydrocortisone (200 ng/ml culture medium solution), 0.5 ng/ml VEGF, 10 ng/ml human FGF-2, 5 ng/ml human epidermal growth factor (EGF), 20 ng/ml human IGF-1, and 1 µg/ml ascorbic acid and one third of EGM2 (LONZA). HUVECs were daily monitored and maintained under culture conditions (95% humidity, 37° C, and 5% CO_2). Only passages lower than 6 were used for all experiments.

HBMECs were grown in a 10 µg/ml Fibronectin (Sigma-Aldrich) coated surface in Endothelial Cell Medium (ECM) (ScienCell) supplemented with 5% FBS (ScienCell), 1% endothelial cell growth supplements and 1% penicillin/streptomycin solution (ScienCell). HBMECs were daily monitored and maintained under culture conditions (95% humidity, 37° C, and 5% CO_2). Only passages lower than 5 were used for all experiments.

The murine brain endothelial cell line **bEND3** was grown in a 0.5% Gelatin coated surface in Dulbecco's Modified Eagle's Medium (DMEM) (Merck) supplemented with 10% FBS. bEND3 were daily monitored and maintained under culture conditions (95% humidity, 37° C, and 5% CO_2). Only passages lower than 20 were used for all experiments

The murine melanoma **Ret** cells were grown in RPMI (Sigma-Aldrich) containing 10% FBS, 2 mM L-glutamine, 1% nonessential amino acids and 1% Penicillin-Streptomycin. Ret cells were daily monitored and maintained under culture conditions (95% humidity, 37° C, and 5% CO_2). Only passages lower than 20 were used for all experiments.

3.2.1.2 Cell passaging

After reaching a confluency of 80-90% they were either passaged, transferred to the assay systems or cryopreserved.

For cell detachment cell monolayers were firstly rinsed with 5 ml of PBS and then incubated with 1 ml of Trypsin-EDTA solution (Sigma-Aldrich) under culture conditions (95% humidity, 37° C, and 5% CO_2) for 2-5 minutes. Cell detachment was confirmed under the microscope, when more than 90% of the cells were detached 5 ml of complete medium was added to stop the trypsin. Cell suspension was then transferred into a 15 ml conical bottom tube and cell density was determined using a Neubauer counting chamber (to discern between living and dead cells 1:10 Trypan blue was added into a 10 µl cell suspension and living cells were colorized in blue). The total number of cells per milliliter was calculated by this formula:

*(Counted living cell number / number of counted chambers) * 10^4 * dilution factor.*

Then, the cell suspension was centrifuged at 300 x *g* for 5 minutes. After centrifugation, the supernatant was discarded and the cell pellet resuspended in the corresponding volume with complete medium or in complete medium supplemented with 10% DMSO and 10% FBS for cryopreservation.

3.2.1.3 Ret melanoma cell supernatant

For the generation of Ret cell supernatant (Ret Sn), Ret cells were grown in a T75 flask with complete RPMI medium. When the confluence was reached, the medium was removed and cell monolayer rinsed three times with 10 ml of PBS. Then Ret cells were incubated for 8 hours with 5 ml of HRBS under culture conditions (95% humidity, 37° C, and 5% CO_2). After the starvation, cell supernatant was transferred

into a 15 mL conical bottom tube and centrifuged at 300 x *g* for 5 minutes. Next, the supernatant was collected and transferred into 1.5 ml tubes. Ret Sn was then stored at -20° C and used within the following 3 months.

3.2.1.4 Endothelial cell stimulation

Endothelial cells (ECs) were seeded on coated coverslips in a 12-well plate. 500 µl of complete medium with $100*10^3$ cells was added in each well. Next day, medium was substituted with fresh complete medium and cells were grown until confluence under culture conditions (95% humidity, 37° C, and 5% CO_2).

Before stimulation, each well was washed once with 500 µl of HBRS. As a negative control, endothelial cells were incubated with 500 µl HBRS (Vehicle). As positive controls, ECs were incubated with 0.5 U/ml of thrombin or with 2500 pg/ml Vascular endothelial growth factor-165 ($VEGF_{165}$) diluted in HBRS as it was described in Desch et al. 2012. Additionally, cells were also incubated with 500 µl Ret Sn. To examine the inhibitory effect of distinct molecules, preincubation with Tinzaparin (100U/ml), Fondaparinux (50 µg/ml) or Bevacizumab (0.65 mg/mL) was applied for 30 minutes before the administration.

After 15 minutes of incubation under culture conditions (95% humidity, 37° C, and 5% CO_2) 450 µl of the supernatant was collected and transferred into 1.5 ml Tubes coated with 50 µl of 4% BSA. Supernatants were analyzed directly by ELISA or stored at -20°C for their analysis in the following days.

3.2.1.5 Enzyme-linked Immunoabsorbent Assay (ELISA)

ELISAs for VWF were performed to quantify the release of VWF in the supernatant of stimulated ECs and in the plasma of cancer patients.

96-well ELISA microplate was coated with the capture antibody Rabbit anti-human VWF (Dako) diluted in PBS (1:500) and incubated overnight at 4° C. Next day, coated wells were washed with PBS-T and incubated with 4% BSA for one hour at 37° C in order to block the unspecific binding sites. In the meantime, the samples were thawed at room temperature (RT) and the standard samples prepared by serial

dilutions of human plasma pool with a determine VWF content. After blocking, the microplate was washed three times with PBS-T and samples were loaded (100µl per well) and incubated for 1 hour at 37°C. Next, the microplate was washed three times with PBS-T and incubated for 1 hour at 37°C with the secondary antibody, HRP-rabbit anti-human VWF (Dako) in PBS-T (1:4000). After the incubation, microplate was washed three times with PBS-T. Next, microplate was loaded with the Substrate solution (1:1 mixture of Color Reagent A and Color Reagent B, R&D System) and incubated for 20 minutes. Then, the reaction was stopped by using the Stop solution (2N H_2SO_4).The optical changes were determined in each well at 450 and 540 nm using a microplate reader (BioteK PowerWave XS2 photometer).

3.2.1.6 Immunofluorescence staining

Cells seeded on 20 mm coverslip were washed twice with HEPES and, depending on the antibodies, cells were fixed with methanol for 30 minutes at -20°C or with 4% PFA for 30 minutes at 4°C. After fixation, cells were washed three times with HEPES and incubated for 1 hour with Blocking buffer I (HEPES containing 0.3% TritonX-100 (Sigma) and 2% of BSA). After the blocking, cells were washed with Incubation buffer (HEPES containing 0.3% TritonX-100) and incubated with the primary antibody diluted in Incubation buffer. After primary antibody incubation, cells were washed three times with Incubation buffer and secondary antibody incubation was performed as it was described before. Working concentrations of the antibodies and the incubation times were implemented following the instructions of the manufacturers (**3.1.7 Antibodies**). Whether a secondary antigen was required to be stained, the cells were blocked again for 30 minutes and the staining procedure was repeated as before. To stain the nuclei, cells were incubated with DAPI diluted in PBS (1: 1000). Coverslips were then thoroughly washed twice with PBS and once distilled water. Finally, coverslips were mounted on object slides with 30 µl of DABCO-Mowiol and stored overnight at 4°C.

Images from the staining were obtained by using the Z1 AxioObserver inverted fluorescence microscope (Carl Zeiss).

3.2.1.7 Quantitative real-time polymerase chain reaction

To examine the genetic signature of ECs quantitative real-time polymerase chain reactions (qRT-PCR) technique was applied as follows:

RNA was isolated from confluent EC cultures using the RNeasy Mini Kit (Qiagen). The procedure was performed following the instructions provided by the manufacturers. Briefly, ECs were lysed with RLT lysis buffer (Qiagen) containing 1 % of 2-Mercaptoethanol. The cell lysate was transferred to an RNeasy column, where RNA was purified after being washed and treated with DNases. The purified-RNA was eluted and its purity was calculated with a NanoDrop™ 2000/2000c Spectrophotometer. For long term storage RNA was stored at -20°C.

Next, cDNA was generated using the Qiagen´s QuantiTect Reverse Transcription Kit. In accordance to the instructions of the manufacturers 500 ng of isolated RNA was incubated with a master mix (1µl of Quantiscript Reverse Transcriptase, 4µl of Quantiscript RT buffer 5X and 1µl of RT Primer Mix) for 15 min at 42° C. To inactivate the reverse transcriptase a second incubation for 3 minutes at 95°C was performed. The resulting cDNA was diluted 1:10 in RNase-free water and stored at -20° C.

Finally polymerase chain reaction (PCR) was carried out in accordance to the Qiagen's QuantiFast SYBR Green PCR Kit protocol. Primers described in the section **3.1.6** were used to amplify the targeted genes. The reaction took place in a 96-well PCR plate loaded as follows:

Components	**Volume/well**
RNase-free water	Variable (up to 25 µl)
Primers (Forward + Reverse)	5 µg
cDNA	100 ng (volume depends on sample concentration)
QuanitFast SYBR Green PCR Master Mix	12.5 µl
Total volume	**25 µl**

The PCR cycles took place in a thermocycler under the following conditions:

Step 1.	**Time**	**Temperature**
PCR initial activation step	5 min	95° C
Step 2.*Two-step cycle*		
Denaturation	10 seconds	95° C
Combined/annealing/extension	30 seconds	60° C
Number of cycles	Between 30-40 depending in the amount of template DNA)	

3.2.2 *Ex vivo* examination of platelets

3.2.2.1 Platelet and erythrocytes isolation

Blood was drawn from a forearm vein of healthy donors or from the inferior cava vein of mice as was previously described (Parasuraman, Raveendran, and Kesavan 2010). The blood was anticoagulated with 3.2% of sodium citrate buffer (SARSTETD AG& Co.) and kept for 30 minutes at room temperature (RT). Then, citrated blood was centrifuged at 180 x *g* for 15 minutes without break. Upon centrifugation the resultant blood was stratified in three phases: The first one, formed by the platelet rich plasma (PRP) which contains plasmatic proteins and platelets. Secondly an interphase identified as the “buffy coat” where leukocytes are deposited. The third phase is composed by erythrocytes.

PRP was then gently transferred into a 15 ml conical bottom tube containing of 1:1 Washing Buffer supplemented with 1 U/ml of the platelet inhibitor Apyrase. Importantly, the pH of the Washing Buffer was previously stablished at 6.6 to avoid platelet activation (Scharbert et al. 2011).Then, platelet suspension was centrifuged at 1200 x g; 15 minutes; without breaks. The resulting supernatant was discarded and the platelet-pellet was resuspended in Resuspension buffer with a physiological pH of 7.4 (Scharbert et al. 2011). Note that either the Washing or the resuspension buffers lack of calcium (**3.1.3 Buffers and solutions**). For an adequate activation of the internal signalling calcium ions must be provided, thus $CaCl_2$ was added to a final

concentration of 1 mM (Paniccia et al. 2015).

To obtain a physiological haematocrit for our *in vitro* perfusion assays, erythrocytes from citrated blood were also isolated. The erythrocyte pellet obtained from the citrated blood was transferred into a 50 ml conical tube and washed with PBS (1:1). Then erythrocytes were centrifuged at 800 x *g* for 10 minutes. The supernatant and buffy coat was aspirated and the same procedure was repeated. In a final washing step erythrocytes were washed with HEPES (1:1) and centrifuged at 800 x *g* for 10 minutes. The resulting supernatant was aspirated obtaining a pure pellet of washed erythrocytes.

3.2.2.2 Light transmission aggregometry

The light transmission aggregometry (LTA) technique was used to study the effect of different platelet agonists on platelet aggregation *in vitro*. In our experiments stirred suspensions of washed platelets (**3.2.2.1**) were exposed to collagen type I (50 µg/ml), histamine (100 µM) or thrombin (0.5 U/ml) and subsequent formation of platelet aggregates was monitored by a CHRONO-LOG® Model 700 (Chrono-log Corporation, Hawertown, USA).

To test the impact of different drugs on platelet aggregation, preincubation of platelets with Tinzaparin (100 U/ml) or Fondaparinux (50 µg/ml) was implemented before the addition of the agonists.

3.2.2.3 Generation of platelet-derived supernatant

Platelets secrete many proinflamatory and procoagulatory factors stored in *α granules* and dense granules (Golebiewska and Poole 2015) To analyze the platelet secretome, we induced the activation of platelets and harvested the resulting platelet releasates.

Washed platelets, isolated as described before in the section **3.2.2.1**, were activated by the addition of the platelet agonists thrombin (0.5 U/ml) or collagen type I (50 µg/ml) for 15 minutes. Next, platelet activation was stopped by adding 1:1000 prostaglandin-1 (PGE-1) and platelets were centrifuged at 1200 x *g* for 15 minutes

without brakes. The supernatant was carefully harvested avoiding the contact with the platelet-pellet. Platelet supernatant was used directly or stored at -20°C. To test the effect of different inhibitors on the platelet secretome, washed platelets were incubated for 30 minutes with Tinzaparin (100 U/ml), Fondaparinux (50 µg/ml) or Bevacizumab (0.65 mg/mL) prior their activation.

3.2.2.4 Platelet-derived vascular endothelial growth factor A secretion

ELISAs for vascular endothelial growth factor A (VEGF-A) secretion in platelet releasates was performed by using the Quantikine® ELISA kits (R&D Systems). The assay procedures were carried out in accordance to the instructions provided by the manufacturers.

3.2.2.5 *In vitro* perfusion assays

Microfluidic assays (ibidi GmbH) were implemented to study in real time and under specific flow conditions the formation of a micro-thrombus..

A µ-Slide 0.2 Luer channel was coated with 0.5% Gelatin. Then, 0.4 x 10^6 ECs (HUVECs, HBMECs or bEND3) were homogeneously dispensed along the microchannel. The microfluidic slides containing ECs were maintained under culture conditions (95% humidity, 37° C, and 5% CO_2) and the medium was replaced every with fresh equilibrated medium (37° C and 5% CO_2). The formation of a confluent monolayer within the microchannel was monitored under the microscope every day; usually confluence was achieved two days after the seeding.

When the monolayer was formed, the Perfusion Set was mounted onto the Microfluidic slide and both were placed together in the Microscope incubation chamber which maintains the cells under cell culture conditions (95% humidity, 37° C, and 5% CO_2). Then the microfluidic slide was perfused with a 4 ml mixture buffer containing HBRS, 25% hematocrit and 15% platelets. Shear rate was set at 2.5 dyn/cm^2 to mimic the shear stress of brain microvessel (Nicolay et al. 2018).

In order to examine the impact of EC activation on platelet adhesion 100 µM histamine was added through the Perfusion Set. In a second step, platelet activation

was induced by addition of the platelet agonist collagen type I (50 µg/ml) in combination with a FITC-conjugated sheep anti-mouse VWF antibody (1:100; GeneTex Inc) for the visualization of VWF. Platelet attachment and aggregation was recorded in real time using using a Zeiss AxioObserver Z1 equipped with an AxioCam MRc (Carl Zeiss AG, Oberkochen, Germany).

3.2.2.6 Transmigration assay

A transwell migration assay was performed to test the migratory response of Ret cells in presence of platelet-derived supernatant.

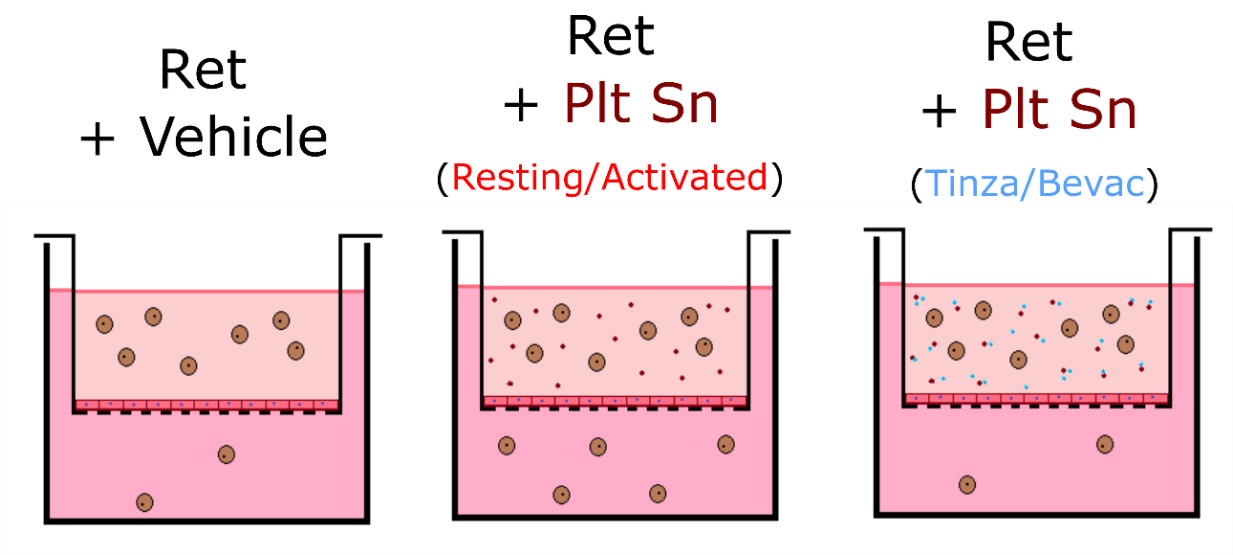

Figure 11. Schematic diagram of the transmigration assay: Ret melanoma cells were co-incubated for 8 hours with the supernatant of resting platelets (rest Plt Sn) or collagen type I-activated platelets (act Plt Sn) with or without incubation with Tinzaparin (100 U/ml) or Bevacizumab (0.65 mg/mL) (act Plt Sn +Tinza/Bevac). Then, upper chambers were removed and transmigrated tumor cells counted after 24 hours.

To this end $0.12x10^6$ HBMECs were seeded in the inner well of a Transwell system and grown for 72 hours under cell culture conditions (95% humidity, 37° C, and 5% CO_2). Then, Ret cells were harvested and labeled with 1:1000 CellTrace™ Calcein Green (Invitrogen) for 10 minutes. After labeling, Ret cells were centrifuged at 500 x *g* for 5 minutes, and resuspended in RPMI without supplements (Harvesting

medium). Then inner wells were loaded with $20*10^3$ labeled Ret cells supplemented with 200µl of platelet supernatant. After 8 hours of coincubation, inner wells were removed and transmigrated Ret cells adhered to the bottom of the outer well were counted after 24 hours.

3.2.2.7 Transendothelial electrical resistance

The transendothelial electrical resistance (TEER) is the measurement of the electrical resistance across a cellular monolayer and is considered a reliable indicator of the integrity and permeability of a cellular barrier (Srinivasan et al. 2015). To examine the impact of platelet activation on the integrity of brain endothelium, we monitoring the impact of platelet releasates on the TEER of a HBMEC monolayer by using Endothelial Substrate Impedance Sensing (ECIS) arrays (Applied BioPhysics Inc., NY USA).

HBMECs were seeded into coated 8-well ECIS slides (8W1E PET; Applied BioPhysics Inc., NY, USA) at a concentration of $1x10^5$ cells/ well. The electrical resistance at a frequency of 4,000 Hertz was measured every 48 seconds by ECIS-zeta system software (Applied BioPhysics Inc., NY, USA) while cells grew under cell culture conditions (95% humidity, 37° C, and 5% CO_2). After 72 hours ECs reached their confluence, reflected by the stabilization of TEER values. The impact of the supernatant of resting platelets or platelets activated with collagen type I (50 µg/ml) with or without preincubation with Tinzaparin (100 U/ml) or Bevacizumab (0.65 mg/mL) on TEER was measured for 24 hours.

3.2.3 Human samples

In accordance with the Declaration of Helsinki and the International Conference on Harmonization of Technical Requirements for Registration of Pharmaceuticals for Human Use (ICH) guidelines an informed written consent was obtained from all participants

3.2.3.1 Human blood samples

Blood samples from cancer patients were anticoagulated with 3.2% of sodium citrate buffer (SARSTETD AG& Co.) and kept for 30 minutes at room temperature (RT). Then, samples were centrifuged at 1000 x *g* for 5 minutes and the citrate plasma was collected in 2 ml Tubes and stored at -70°C.

3.2.3.2 ADAMTS13 activity measurements

ADAMTS13 activity was evaluated in the citrate plasma of cancer patients by a commercially available kit according to the instructions of the manufacturer (TechnocloneGmbH).

3.2.3.3 Concentration of plasmatic von Willebrand factor in cancer patients

Plasmatic levels of VWF was quantified using a sandwich enzyme-linked immuno-sorbent assay (ELISA) technique as described before (**section 3.2.1.5**)

3.2.3.4 Tissue samples

Tissue samples from human metastatic brains were obtained from the Neurosurgery department of the Medical Faculty of Mannheim.

Tissue was directly embed in Tissue-Tek® (Sakura Finetek) and placed on dry ice for freezing. Frozen tissue samples were stored in -80° C until they were cryosectioned as is explained afterwards (**section 3.2.4.3**)

3.2.4 Animal models

3.2.4.1 Impact of anticoagulant therapy with Tinzaparin on platelet activation

To determine the effect of Tinzaparin on platelet activation in the context of brain metastasis, 8- to 12-weeks *ret* mice were subcutaneously treated for 100 days with 0.6 U/g of Tinzaparin (innohep; Leo Pharma) or saline solution (NaCl) as it was described before (Bauer, Suckau, Frank, Desch, Goertz, Wagner, Hecker, Goerge, Umansky, Beckhove, Utikal, Gorzelanny, Diaz-valdes, et al. 2015)

3.2.4.2 Impact of anticoagulant therapy with Tinzaparin on brain metastasis formation

In order to confirm the direct impact of Tinzaparin on brain metastasis formation an alternative mouse model of brain metastasis was applied by Prof. Winkler's group from Experimental Neurooncology, German Cancer Research Center (DKFZ), Heidelberg, Germany. This model consisted on the injection of $5x10^5$ A2058 (ATCC® CRL11147™) melanoma cells in 100 µl of PBS into the left cardiac ventricle of 8- to 12-week-old male NMRI-nu/nu mice (≥20 g, Charles River Germany) previously anesthetized with ketamine/xylazine. A group of animals received daily a subcutaneous injection of 0.6 U/g of tinzaparin (innohep; Leo Pharma) from day -2 (before tumor cell intracardiac injection) until day +31 (after tumor cell intracardiac injection).

3.2.4.3 Brain cryosectioning

When the *in vivo* experiments were terminated mouse brains were rapidly harvested under sterile conditions:

Head skin was pulled away and exposed skull was disinfected with 70% ETOH. Then, using sterile surgical scissors the skull was open by a scission from the *foramen magnum* along the midline until the end of the *frontal* bone. Thereafter, the *parietal* bones were removed and the brain was harvested after cutting the brain

steam at the base of the brain. Then, brains were immediately embedded in Tissue-Tek and placed on dry ice for freezing.

Frozen tissue embedded in Tissue-Tek ® was cryosectioned (10 µm coronal sections) at -20°C using the high precision microtome (Kryostat CM 1900). Sections were picked up on object slides and dried out for 1 hour at RT and stored at -20°C.

3.2.4.4 Immunohistochemistry

For immunohistochemical analyses cerebral coronal cryosections of 10 µm of thickness were 130 µm apart to avoid extensive overlapping of metastases over several slices. Plain hematoxylin and eosin (H&E) staining was used to analyze cerebral metastases. Image acquisition was performed via slide scanner (Axio Scan.Z1; ZEISS) in brightfield configuration with a 20x/0.8 Plan-Apochromat objective (ZEISS) and a Hitachi HV-F202SCL camera.

3.2.4.5 Immunofluorescence

Tissue cryosections were dried for 30 minutes at room temperature (RT). Then, they were fixed for 30 minutes with methanol at -20° C or with 4% PFA at 4° C, depending on the specifications provided by the manufacturers. Next, sections edges were delimited with FixoGum (Marabu Fixogum®) and washed three times with PBS. Thereafter, the tissue sections were blocked with Blocking buffer II (10% goat serum in PBS-T) for 90 minutes. After the blocking, the sections were washed once with PBS and incubated with the primary antibody diluted in PBS-T (working concentration as well as incubation time was performed according to the instructions of the manufactures). In order to reveal whether the secondary antibody may show non-specific bindings, negative control sections were incubated only with PBS-T. After washing three times with PBS-T, sections were incubated with the secondary antibody diluted in the Blocking buffer II (working concentration as well as incubation time was performed according to the instructions of the manufacturers; **3.1.7 Antibodies**). From now on, all steps were performed under dark conditions to prevent bleaching. When a second structure was required to be stained, the cells

were blocked again for 30 minutes and the same staining procedure was repeated. For nuclei staining, sections were incubated with 1: 1000 DAPI in PBS. Finally, the tissue sections were washed thoroughly with PBS and distilled water, then sections were capped with 40 µl of DABCO-Mowiol and covered by 24x60 mm coverslip. Slides were stored at 4°C for a short term and at -20°C for long storage.

Images from the staining were obtained by using the Z1 AxioObserver inverted fluorescence microscope (Carl Zeiss).

3.2.4.6 Fibrinogen binding assay

To identify activated platelets in tissue sections, an *in situ* fibrinogen binding assay was performed. Tissue sections were incubated with 100µl (20µg/ml) of Alexa 488-conjugated fibrinogen (Thermo Fisher Scientific) for two hours at RT, in a humidified atmosphere.

Next, sections were washed with PBS and fixed with 4% PFA for 30 minutes at 4°C. Thereafter, tissue sections were stained for the platelet marker CD42 (EMFRET) following the procedure previously described in the section **3.2.3.7**.

Images from the fibrinogen binding assay were obtained by using the Z1 AxioObserver inverted fluorescence microscope (Carl Zeiss).

3.3 Statistical analysis

Data are presented as the mean ± standard deviation (SD) of a number of independent experiments specified in each section. *GraphPad Prism. Version 8.1.0.* was used to determine the significance of the results. To compare the differences between two groups of data Two-Tailed, Student T-test was implemented. When more than two groups were compared, Two way ANOVA, Bonferroni post-test was implemented. And F-test was used to analyze the differences among linear results. Significance was assumed only when *, $P < 0.05$, **, $P < 0.01$.

4. Results

4.1 Distinct expression of von Willebrand factor in brain microvascular endothelial cells

4.1.1 Brain microvascular endothelial cells express low amounts of VWF

In order to characterize the expression of VWF in macro- and microvascular endothelial cell (ECs) systems an immunofluorescence staining for VWF and the endothelial cell marker CD31 was performed on primary human umbilical vein endothelial cells (HUVECs) and primary human brain microvascular ECs (HBMECs).

HUVECs, as well as HBMECs exhibited the characteristic distribution of CD31 at the lateral borders of ECs (Cheung et al. 2015). Besides, both cell types exhibited the typical punctuate distribution of VWF within intracellular storage granules, indicative of quiescent ECs storing VWF in Weibel-Palade bodies (WPBs) (**Figure 12 A and B**). However, clear differences in the abundance of VWF were detected between HUVECs and HBMECs. The percentage of VWF positive cells was significantly lower in HBMECs (26.22 ± 3.12%) compared to HUVECs (76.80 ± 19.55%) (**Figure 12 C**). Additionally, the mean number of intracellular VWF storage granules (WPBs) per cell was calculated by using ImageJ/Fiji Software (NIH) and the corresponding quantification showed that compared to HUVECs (123 ± 27) the number of WPBs was notably reduced in HBMECs (70 ± 15) (**Figure 12 D**). This finding suggests that VWF is heterogeneously expressed among the different EC populations.

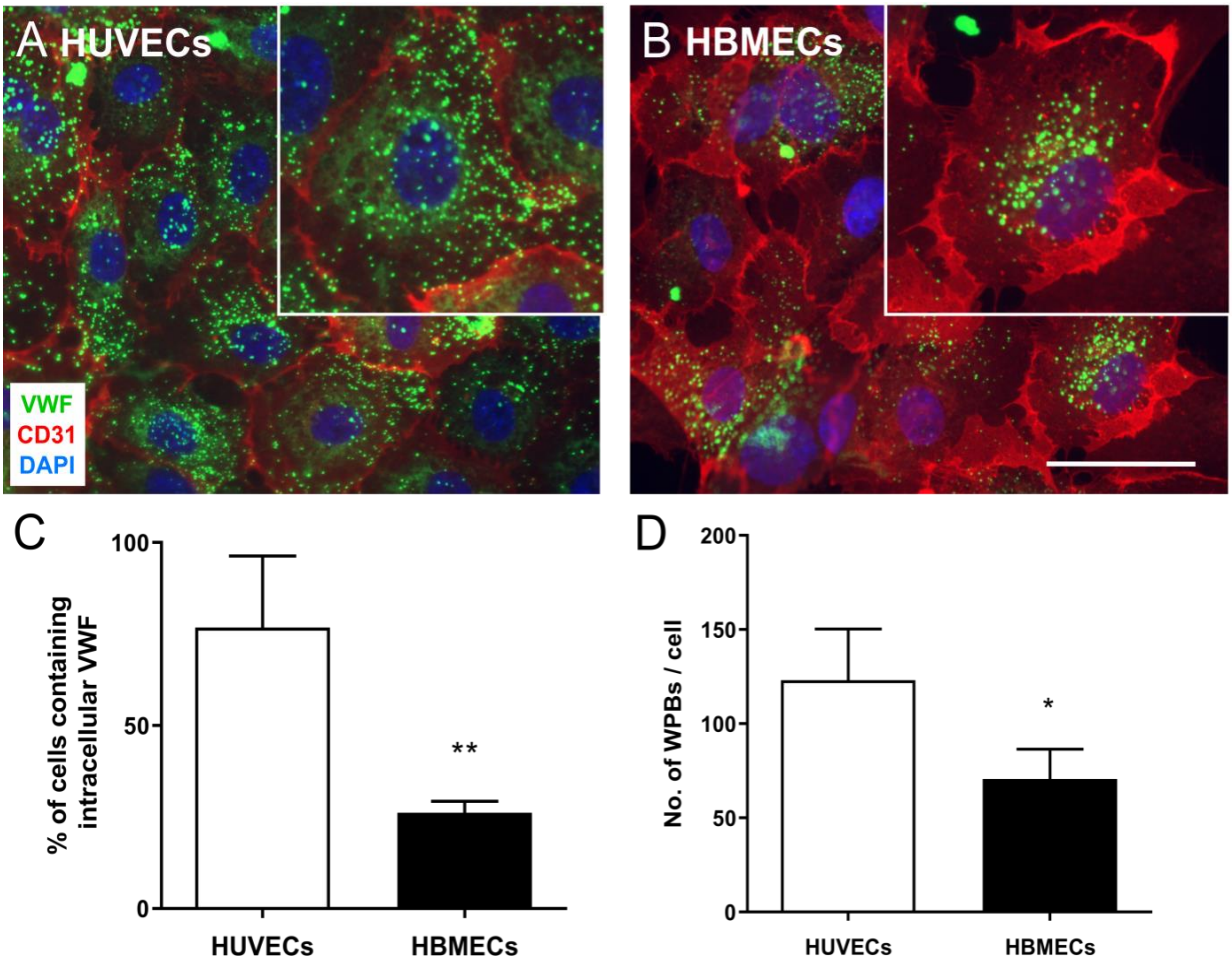

Figure 12. Distinct abundance of VWF in HUVECs and HBMECs. **A and B**. Confluent HUVECs (**A**) and HBMECs (**B**) were stained for VWF (green), the endothelial cell marker CD31 (red) and DAPI (blue) for nuclei. Both cell types exhibit a regular distribution of EC markers: CD31 is concentrated at the cell borders and VWF shows a punctuate distribution in ECs, depicted by green rod-shaped structures in the cytosol. C and D. The percentage of cells containing intracellular VWF (**C**) and the number of VWF storage granules (WPBs) per cell (**D**) were quantified in HUVECs and HBMECs by using ImageJ/Fiji Software (NIH) (n = 1000-2000 cells/group from 3 independent experiments); *, $P < 0.05$, **, $P < 0.01$ (two tailed, Student's t-test). Data are presented as mean ± SD. Scale bar: 50 µm.

4.1.2 Heterogeneous distribution of VWF in brain microvasculature

For an *in vivo* validation of the previous findings, VWF expression was analyzed in the brain vasculature of wild type mice (Wt). For this purpose brain cryosections of Wt mice were stained for VWF (green), CD31 (red) and DAPI (blue).

The analysis of immunofluorescence staining reactivity revealed that VWF was almost absent in vessels with small diameter (< 10 µm) (**Figure 13 A**). In bigger

vessels (10-50 µm), VWF reactivity increases considerably, but still showed an incomplete mosaic-like VWF staining pattern (**Figure 13 B**). Only in vessels with large diameter (> 50 µm) a clear and strong VWF staining was detected in the vessel walls (**Figure 13 C**). These observations suggested a marked regulation of VWF expression with regard to the vessel diameter. To confirm this, the abundance of VWF was quantified by using ImageJ/Fiji in more than 500 brains vessel grouped by their diameter. The correlation analysis demonstrated a positive correlation between VWF abundance and vessel diameter (**Figure 13 D)** and significant differences among the groups (**Table 2**).

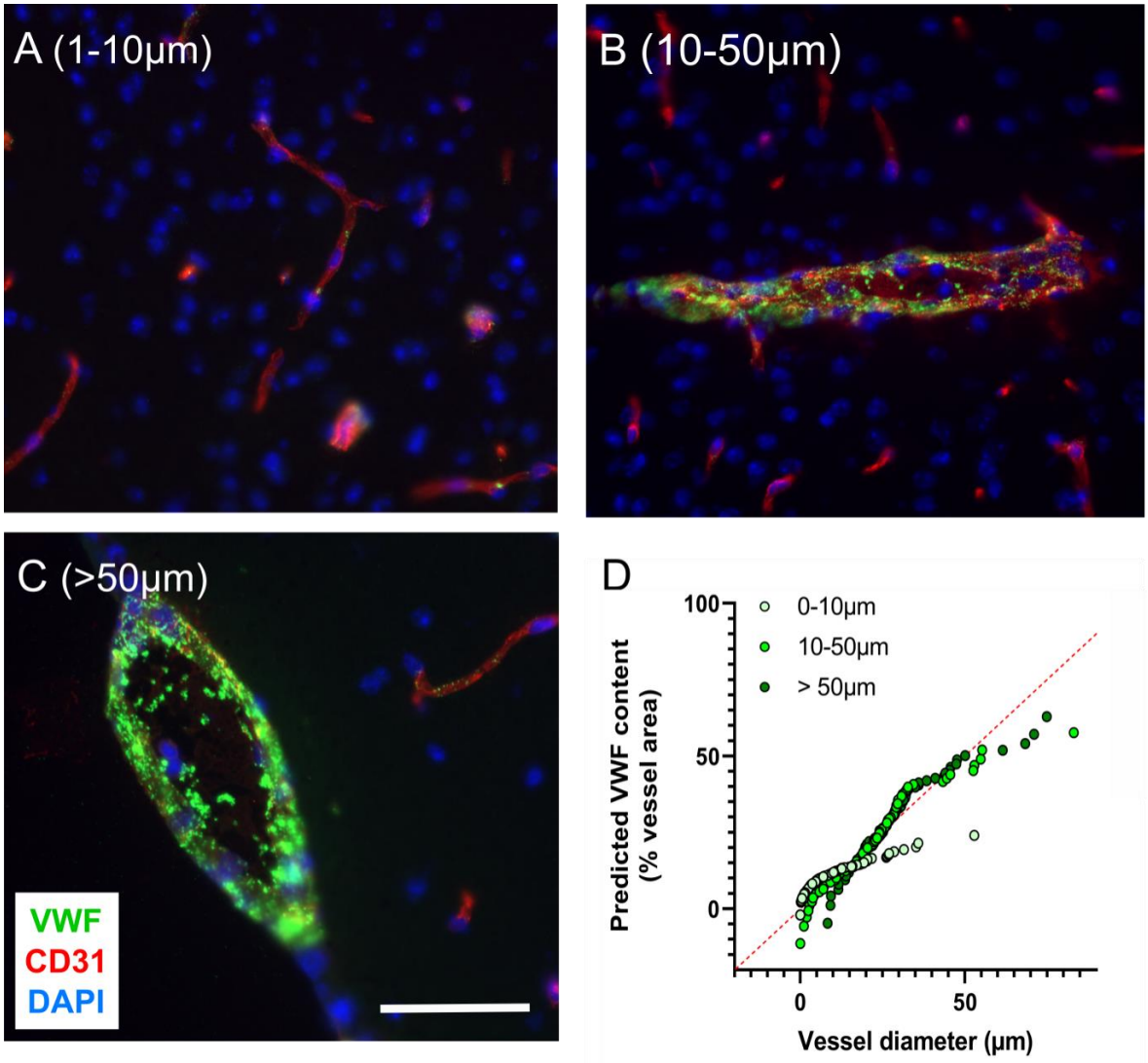

Figure 13. Immunofluorescence staining of VWF in the brain vasculature. Brain cryosections of Wt mice were stained for VWF (green), CD31 (red) and DAPI (blue). **A-C.** Representative images of distinct brain vessels showing the heterogeneity in VWF expression based on their diameter: Small size vessel (6 µm ø) (**A**); intermediate size vessel (29 µm ø) (**B**) and large vessel (84 µm ø) (**C**). **D.** Correlation between the vessel diameter and the percentage of VWF area per vessel. (n = 504 vessels from 3 mouse brains). Scale bar: 50 µm.

Table 2. VWF content in brain vessels according to their diameter

	VWF content (% endothelial area)		
Vessel Diameter (µm)	***Mean***	***SD***	***No. of vessels***
0-10	3.6	6.97	289
10-50	23.3	13.29	106
>50	29.4	13.84	109

Note: VWF content differs significantly among each group of vessels; **, P<0.01. Anova.

These results confirm the heterogeneous regulation of VWF expression in the brain vasculature.

4.1.3 Molecular mechanisms of melanoma-mediated brain microvascular endothelial cell activation

As it was previously shown, melanoma-induced activation of HUVECs is driven by two main pathways: indirectly via the generation of thrombin by TF-expressing melanoma cells or directly, via secretion of vascular endothelial growth factor A (VEGF-A). This interaction results in the exocytosis of WPBs containing VWF and the formation of luminal VWF strings (Desch et al. 2012; Kerk et al. 2010).

In order to assess whether the same molecular mechanisms are involved in the crosstalk between melanoma cells and microvascular ECs of the blood-brain barrier (BBB), we compared the secretion of VWF in HUVECs and HBMECs upon stimulation with, thrombin (0.5 U/ml), VEGF-A_{165} (2500 pg/ml), the supernatant of Ret melanoma cells and HEPES Buffered Ringer's Solution (HBRS), used as negative control.

The secretion of VWF in the supernatant of ECs was quantified by an enzyme-linked immunosorbent assay (ELISA). As expected, the release of VWF by HUVECs was significantly increased by thrombin (91.97 ± 30.33 ng/ml) and VEGF-A_{165} (91.46 ± 31.62 ng/ml) compared to HBRS-treated cells (42.35 ± 19.38 ng/ml). The addition of

the VEGF-A_{165} antibody Bevacizumab (0.65 mg/mL) blocked the impact of VEGF-A_{165} (64.97 ± 21.50 ng/ml). Similarly, Ret supernatant also induced a significant release of VWF (97.252 ± 30.877 ng/ml), which was abrogated by addition of Bevacizumab (40.90 ± 2.91 ng/ml) (**Figure 14 HUVECs**).

Next, HBMEC stimulation was performed under the same conditions. In line with our previous findings in **section 4.1.1**, the resulting concentration of secreted VWF by HBMECs was notably low compared to HUVECs (approximately 5-fold decreased). Interestingly, in contrast to the strong effect observed in thrombin-induced activation of macrovascular HUVECs, thrombin did not induce a notably increase of VWF release in HBMECs (11.29 ± 4.915 ng/ml). By contrast, exposure to VEGF-A_{165} (21.76 ± 7.25 ng/ml) and Ret Sn (18.02 ± 8.58 ng/ml) significantly increased the release of VWF in HBMECs compared to cells treated with HBRS (8.21 ± 6.86 ng/ml). Bevacizumab reduced the secretion of VWF mediated by VEGF-A_{165} (13.68 ± 7.25 ng/ml) and Ret Sn (8.56 ± 2.08 ng/ml) to levels similar to those obtained with HBRS (p=0.6645; p>0.999, respectively) (**Figure 14 HBMECs**).

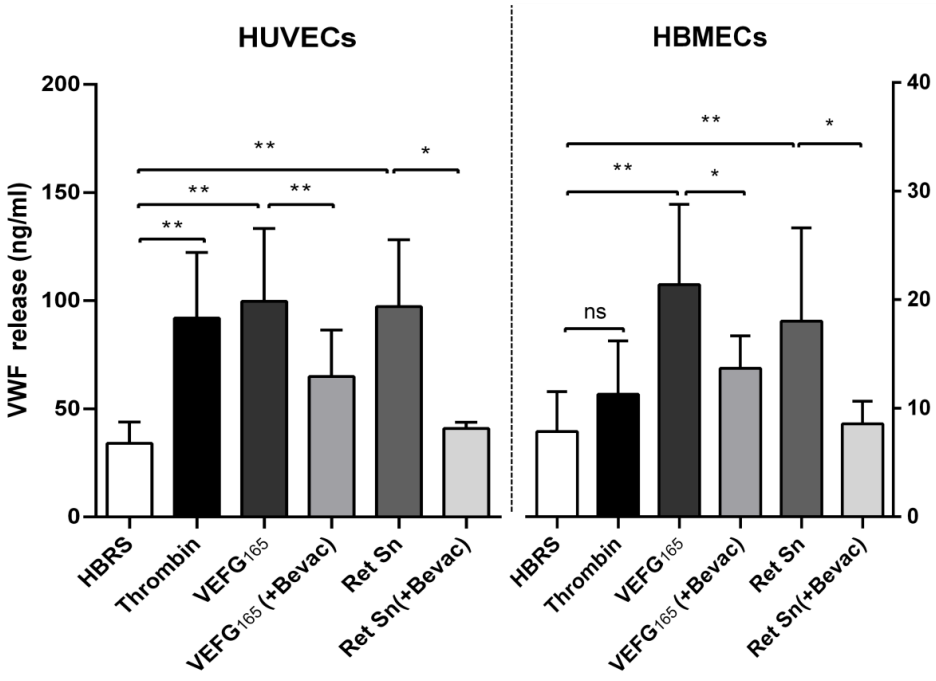

Figure 14. The molecular mechanisms of EC activation. To evaluate the molecular mechanisms involved in the activation of HUVECs and HBMECs, ECs were stimulated for 15 minutes with HBRS (Control), thrombin (0.5 U/ml), VEGF-A_{165} (2500 pg/ml) or Ret Sn. Additionally, the effect of the VEGF-A_{165} inhibition with the antibody Bevacizumab (Bevac) (0.65 mg/mL) was tested in VEGF-A_{165} and Ret Sn stimulatory conditions. The concentration of VWF in cell supernatants was analyzed by ELISA (n = 9 of 3 independent experiments); ns, no significant, *, P < 0.05, **, P < 0.01 (One-way Anova).

To investigate the differences in the regulation of HUVECs and HBMECs activation, the relative gene expression of EC receptors protease-activated receptor 1 (PAR-1) and VEGF receptors 1 and 2 (VEGFR-1,2) were analyzed by qRT-PCR. The results of the analysis revealed that the expression of PAR-1 mRNA was relative lower in HBMECs compared to HUVECs. By contrast, the expression of VEGFR-2 was significantly increased in HBMECs (**Figure 15**). These findings could explain the results obtained in the ELISAs where stimulation of HBMEC with thrombin had no effect on VWF secretion, while VEGF-A induced a significant increase of secreted VWF outlining the relevance of the VEGF-A/VEGFR-2 signaling axis in the specific activation of brain ECs. Additionally, the expression of VWF mRNA was analyzed in this assay. The data showed that in HBMECs VWF is expressed in lower degree than in HUVECs confirming our immunofluorescence analysis.

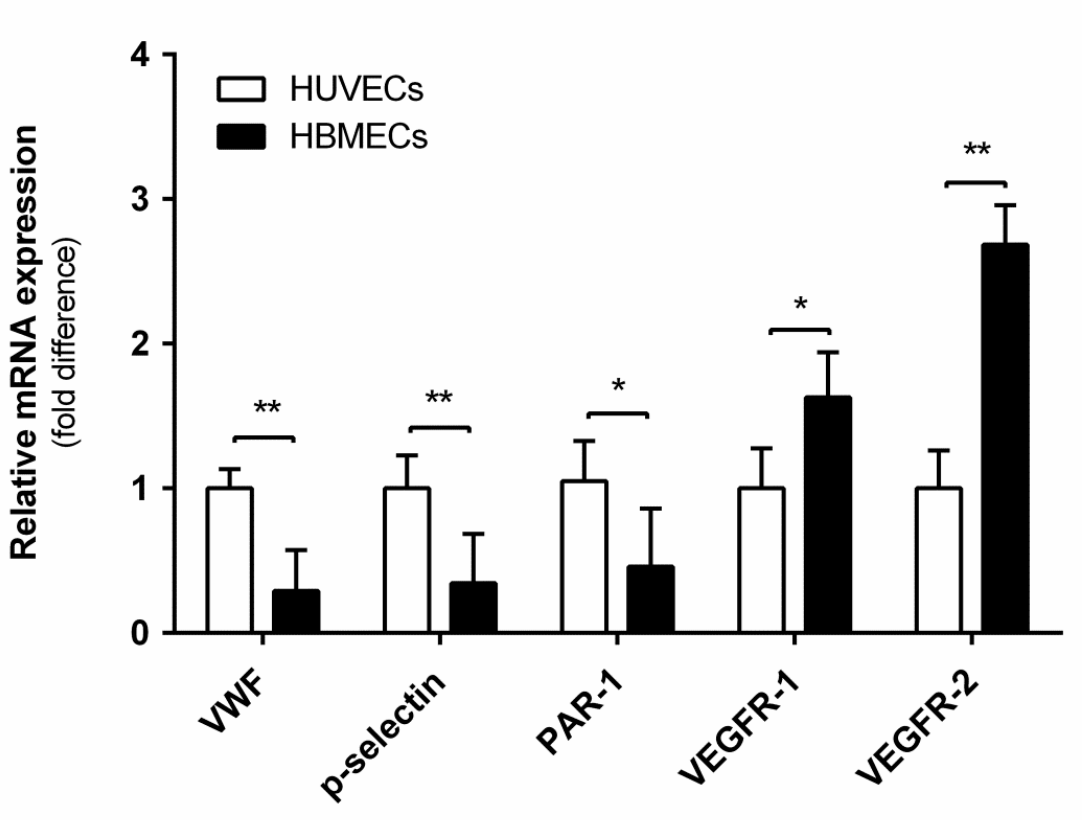

Figure 15. Regulation of EC activation. The gene expression of endothelial receptors (PAR-1, VEGFR-1 and VEGFR-2), as well as WPBs markers (VWF and P-Selectin) were analyzed in HUVECs and HBMECs by q-PCR. The expression of these genes was normalized to β -actin. (n = 3 independent experiments); ns, not significant *, $P < 0.05$, **, $P < 0.01$, (Two-way Anova). Data are presented as mean ± SD.

4.1.4 Brain microvascular endothelial cells show a limited capacity to form luminal VWF fibers

To further analyze the differences in VWF secretion between macro- and microvascular ECs, the formation of luminal VWF fibers was evaluated on HUVECs and HBMECs after stimulation.

The immunofluorescence-based analyses showed that HBRS-treated (control) HUVECs, as well as HBMEC, exhibited the characteristic intracellular punctuate VWF distribution of quiescent endothelium (**Figure 16;** HUVECs and HBMECs [control]). As expected, stimulation with thrombin (0.5 U/ml), VEGF-A_{165} (2500 pg/ml) and Ret melanoma cell supernatant had a distinct impact on the activation of macorvascular HUVECs and HBMECs: in HUVECs thrombin, VEGF-A_{165} and Ret supernatant induced a profound EC activation reflected by the formation of large VWF fibers on the apical surface of the EC monolayers (**Figure 16;** HUVECs). In contrast, the effect of the same stimuli on HBMECs was considerably limited: on the one hand, as expected thrombin had not effect on the formation of VWF strings in HBMECs. On the other, VWF strings were barely visualized upon incubation with VEGF-A and Ret supernatant compared to HUVECs (**Figure 16** HBMECs, magnifications).

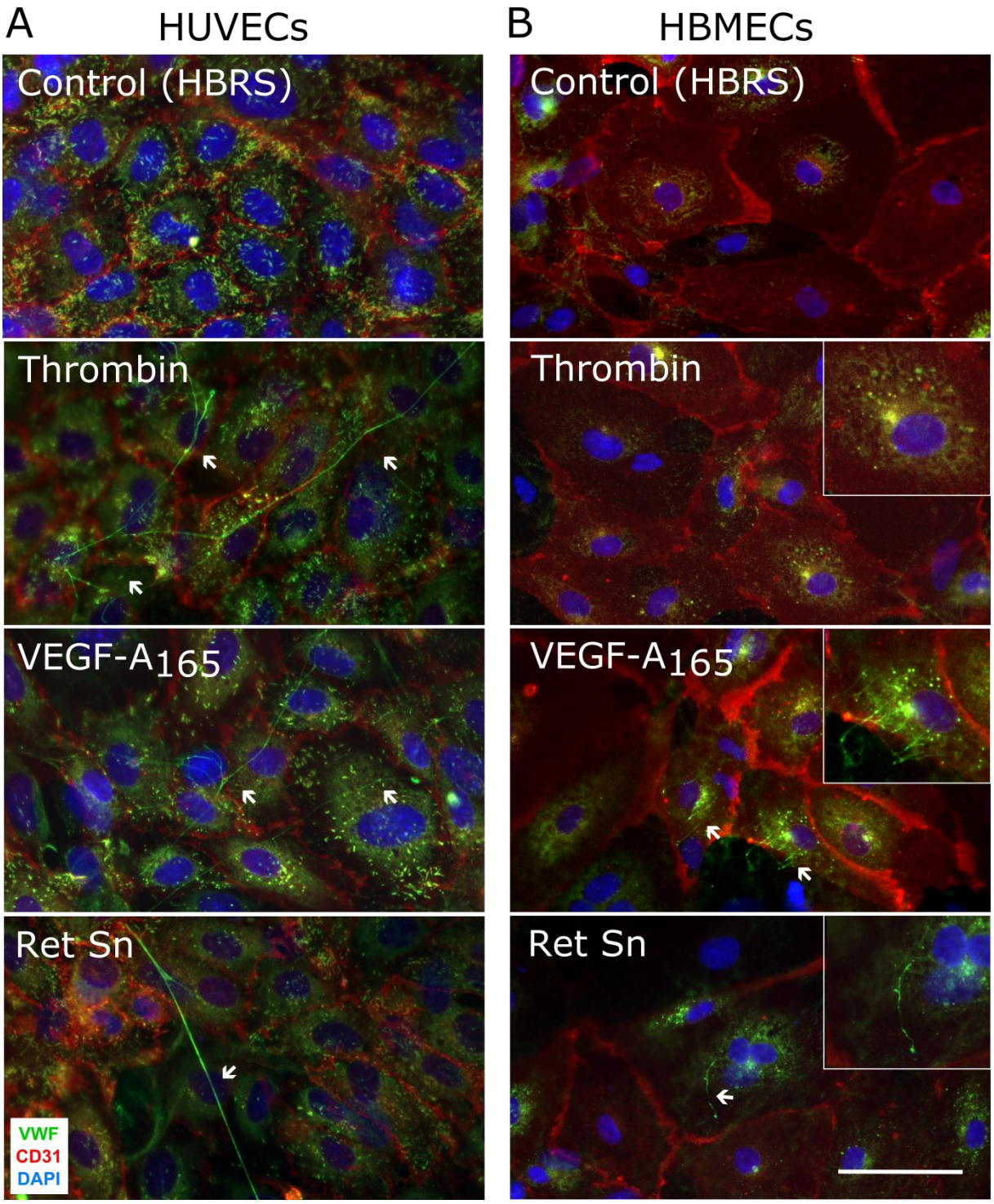

Figure 16. Formation of apical VWF strings upon EC activation. HUVECs and HBMECs were exposed to HBRS (Control), thrombin (0.5 U/ml), VEGF165 (2500 pg/ml), Ret Sn for 15 minutes and then fixated with methanol at -20°C. **A and B**. Next, immunofluorescence staining for VWF (green), CD31 (red) and DAPI (blue) was performed. Representative images of HUVECs (**A**) and HBMECs (**B**) showing the differences in VWF string formation. Scale bar: 50 µm.

Furthermore, the length of luminal VWF fibers derived from HUVECs or HBMECs was measured. The data showed that mean length of HUVEC-derived strings (> 100 µm) were significantly longer than HBMEC-derived strings (< 50 µm) (**Figure 17**) indicating that the decreased expression of VWF in microvascular ECs limits the generation of VWF fibers.

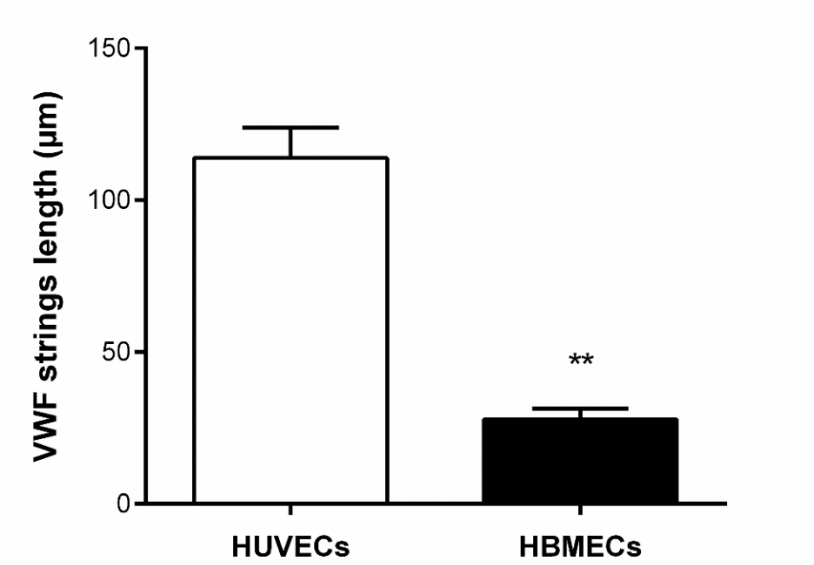

Figure 17. Immunofluorescence analysis confirm the formation of VWF strings *in vitro.* The formation of VWF strings was analyzed in HUVECs and HBMECs upon stimulation with Ret Sn. Then, ECs were fixated with methanol at -20°C and stained for VWF (green), CD31 (red) and DAPI (blue). The mean length of apical VWF strings was measured in HUVECs and in HBMECs by using Fiji/ImageJ (n= 3 independent experiment; > 15 images analyzed per experiment); **, P < 0.01 (two tailed, Student's t-test).

Taken together, these results suggest in the first place, strong differences in the expression of VWF between the macro- and the microvascular ECs (**Figure 12**). Differences in the VWF abundance were also confirmed *in vivo*, showing a specific regulation of VWF expression in brain vessels depending on their size (**Figure 13**). Additionally, here we revealed the contribution of the VEGF-A/VEGFR-2 axis in tumor cell-mediated activation of brain microvascular ECs (**Figure 14-17**).

4.2 Formation of luminal von Willebrand factor fibers is associated with brain metastasis

4.2.1 Luminal VWF fibers are detected in human brain metastases

Based on a previous study from our group showing that malignant melanoma patients in stage IV exhibit elevated levels of plasmatic VWF (24,239 ± 11,544 ng/mL) compared to healthy controls (14, 077 ± 4,910 ng/ml) (Bauer, et al. 2015), we assessed if a systemic increase of plasmatic VWF concentration was also associated with the development of brain metastasis. To confirm this, the concentration of VWF was measured in the plasma of 8 patients suffering from brain metastasis of different origins. Compared to the plasmatic concentration of VWF in patients with semi-malignant basal cell carcinoma (BCC) (20,877.50 ± 12,161.63 ng/ml), used as control, patients bearing cerebral metastasis showed a significant increase of plasmatic VWF (33,518.05 ± 11,095.65 ng/ml) (**Figure 18 A**).

Then, we asked whether the increase of plasmatic VWF was due to a systemic loss of the activity of a disintegrin and metalloproteinase with a thrombospondin type 1 motif, member 13 (ADAMTS13). To answer this question we quantified the activity of ADAMTS13 in patients' serum. In control samples, the measured activity of ADAMTS13 showed a regular activity (112.2 ± 7.58%). Interestingly, in patients suffering from brain metastasis the activity of ADAMTS13 remained unaltered (108 ±7.188%) (**Figure 18 B**).

To assess if the increase of plasmatic VWF in patients with brain metastasis is reflected by the formation of luminal VWF fibers in cerebral vessels, an immunofluorescence analysis was performed on cryosections of brain metastatic tissue. CD31 (red) and VWF (green) staining revealed a strong formation of intraluminal VWF networks in the vessels of the brain metastatic tissue. (**Figure 18 C**). A second immunofluorescence staining for human platelet marker thrombospodin (TSP) (red) and VWF (green) confirmed a strong association between luminal VWF and platelet aggregates, resulting in the occlusion of cerebral vessels (**Figure 18 D**). Interestingly, this finding indicates an association between brain metastasis and the formation of luminal VWF fibers despite the regular activity of ADAMTS13.

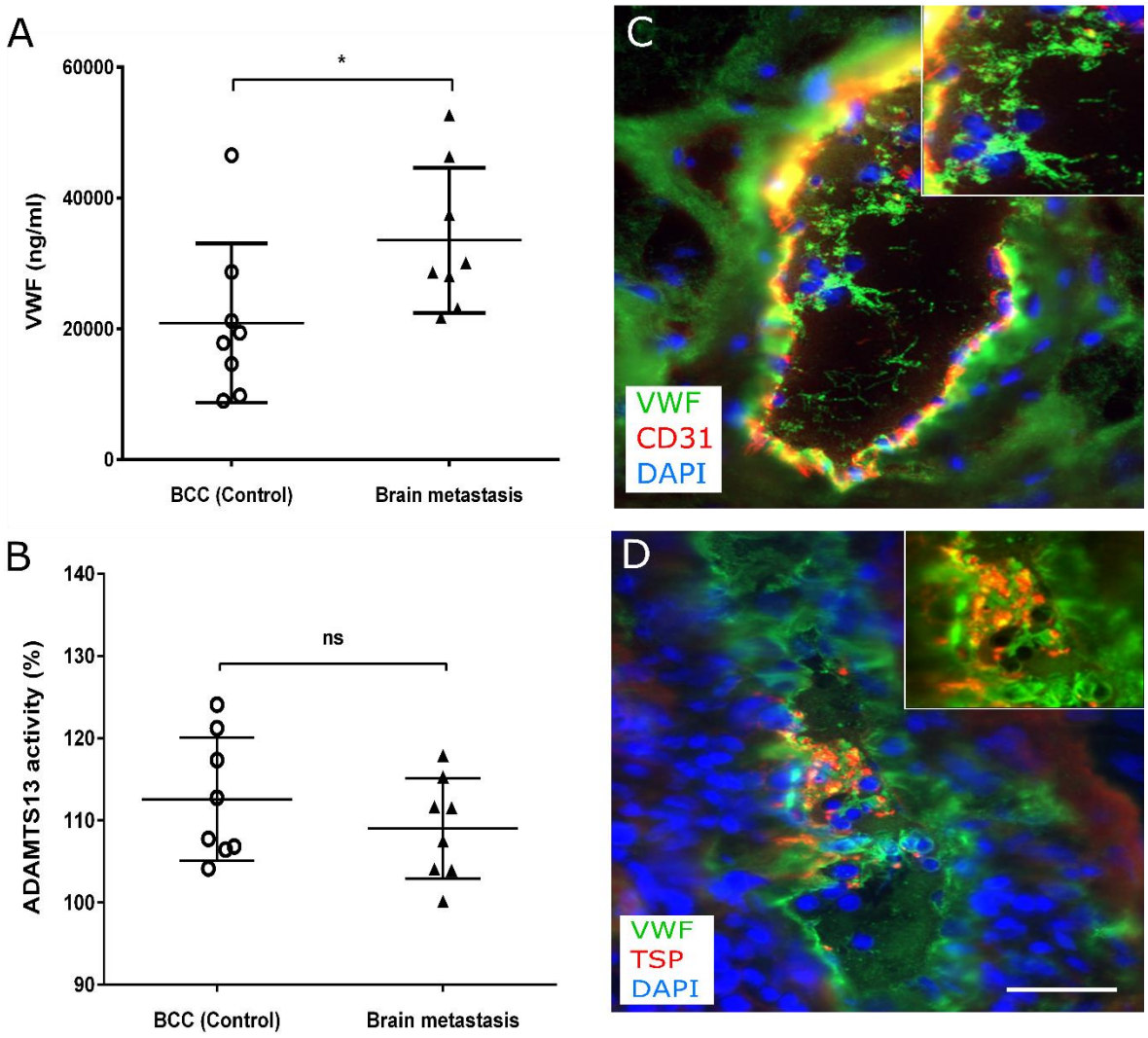

Figure 18. Brain metastasis is associated with increased levels of plasmatic VWF and the formation of luminal VWF fibers. A and B. Concentration of plasmatic VWF (**A**) as well as ADAMTS13 activity (**B**) was analyzed in blood samples of patients with BCC (Control) and brain metastasis. (n = 8 patients/group); ns, not significant *, *P* < 0.05, (Two-tailed, t-Student). Data are presented as mean ± SD. **C and D.** Cryosections of metastatic brain tissue were analyzed by immunofluorescence staining for VWF (green) and CD31 (red) (**C**) or thrombospondin (TSP) (red) (**D**). Nuclei were stained with DAPI (blue). (n = 8 patients). Scale bar: 50 µm.

4.2.2 Brain vessels from *ret* transgenic mice exhibit luminal VWF fibers

To further investigate, if VWF is involved in the hypercoagulability associated with brain metastasis, the *ret* transgenic mouse model (*ret* mouse) was used. According to the literature, after a short period of latency (20 to 70 day of age) *ret* mice spontaneously develop melanocytic tumors (Kimpfler et al. 2009). Then, the animals

start to suffer aggressive metastatic processes which initially affect the lymphatic nodes and later distant organs as the liver, the lung and the brain (Kato et al. 1998), resembling the clinical progression of malignant melanoma in humans.

To represent malignant melanoma in advanced stage of the disease, 40 *ret* mice were maintained for 100 days (14 weeks) under specific pathogen-free conditions (**Figure 19 A**). Then, brains were harvested and longitudinally cryosectioned to evaluate the occurrence of brain metastases. Sections every 100 µm were selected to represent the whole brain. In total 32 brains were screened by H&E staining and we found that more than 30% of the *ret* mice developed macroscopic brain metastases (**Figure 19 B and C**).

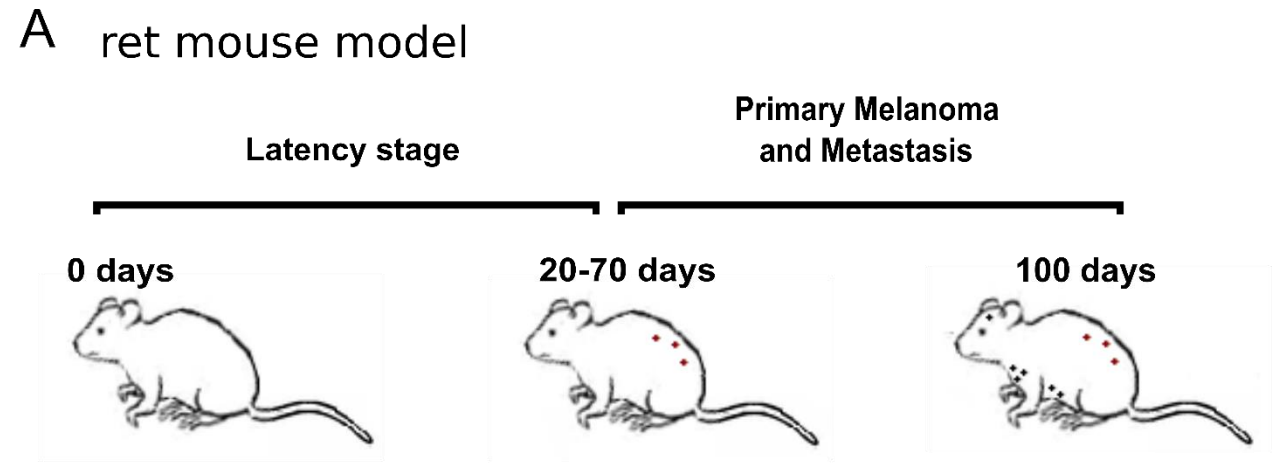

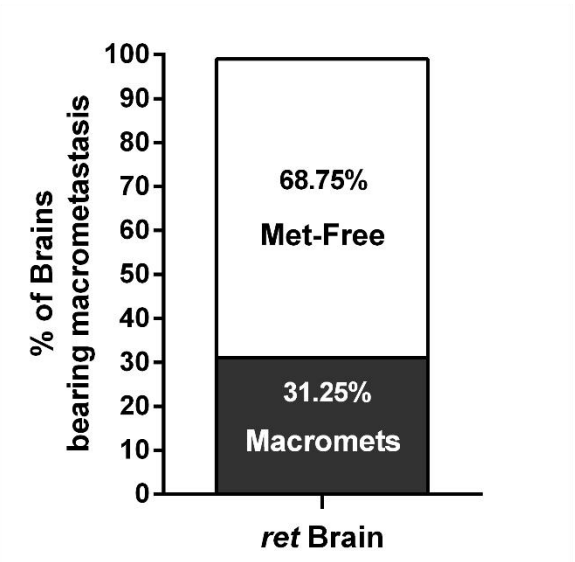

Figure 19. The *ret* transgenic mouse model A. Schematic overview of our experimental settings. *Ret* mice were maintained under controlled conditions for a maximum of 150 days with daily monitoring. **A.** *Ret* mice show a tumor-free stage of 20 to 70 days before the spontaneous development of primary melanocytic tumors with metastases in the lung, the liver and the brain. **B.** Brain metastasis formation was detected by H&E staining (dashed line). **C.** Corresponding quantification of *ret* mouse brains showing the percentage of brains with detectable metastasis (n = 32 mice). Scale bar: 500 µm.

Based on these results, we distinguished 4 different types of brain tissue: Brain tissue from healthy wild type mice (**Wt**). Brain tissue from *ret* mice without visible metastases (**Met-free**). Peripheral brain tissue from *ret* mice with macroscopic metastases (**Peri-Met**). And cerebral intra-metastatic tissue (**Intra-Met**) of *ret* mice (**Figure 20**).

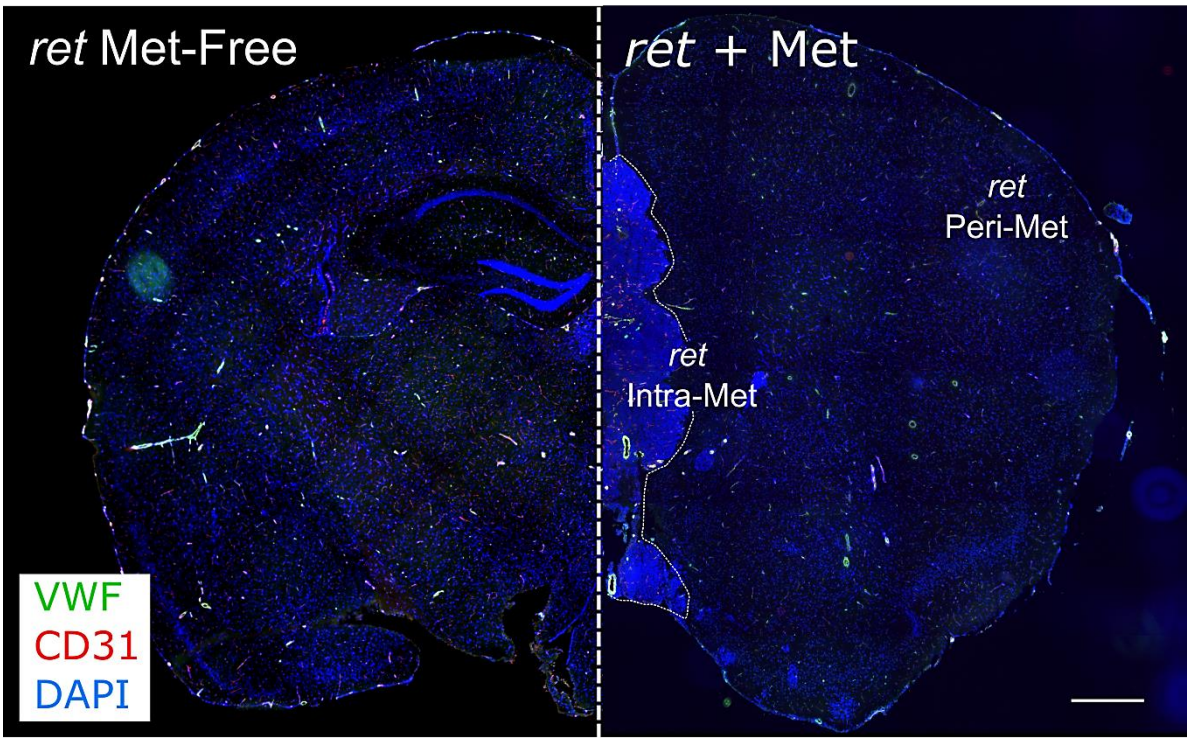

Figure 20. Analysis of *ret* mouse brain tissue. Brain sections from wild type (Wt) (Control) and ret mice were stained for VWF (green), CD31 (red) and DAPI (blue). To examine the formation of luminal VWF fibers we distinguished vessels from Wt brains (Wt), *ret* brains without macroscopic metastasis (Met-free) and vessels from *ret* brains with macrometastasis, either from the peripheral tissue (Peri-Met) or from the intra-metastatic tissue (Intra-Met). Scale bar: 500 µm.

Next, the formation of luminal VWF fibers was quantified in healthy (Wt) and *ret* mouse brain vessels by immunofluorescence staining for VWF (green), the endothelial cell marker CD31 (red) and DAPI (blue) for nuclei. The corresponding quantification showed that in healthy Wt brains, VWF was mostly distributed in the vessel wall, indicating the storage of VWF in WPBs, and only some vessels exhibited intraluminal VWF fibers (22.28% ± 8.49%). By contrast, the formation of luminal VWF fibers was notably enhanced in the vessels of all analyzed groups in *ret* brain tissues (44.11% ± 3.02%) (**Figure 21 E**).

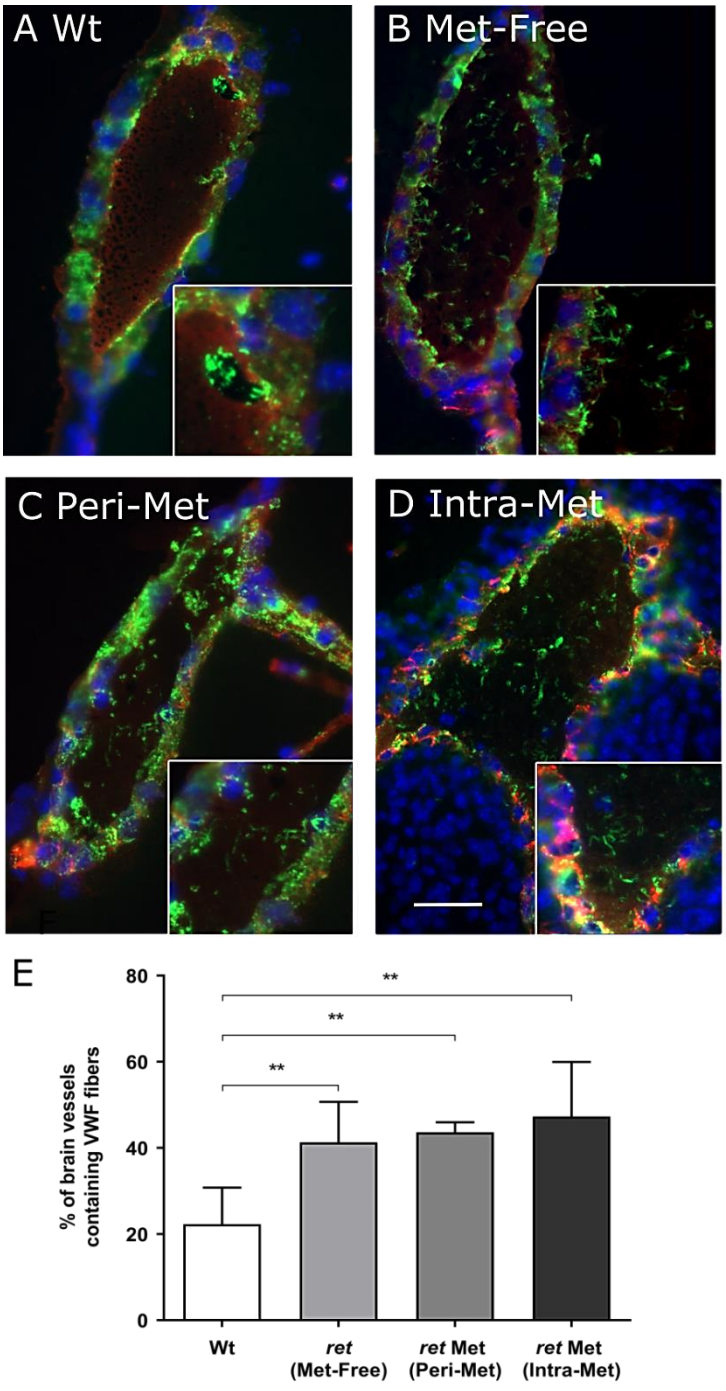

Figure 21. Formation of luminal VWF fibers is associated with brain metastasis. To investigate the involvement of VWF in the development of brain metastasis brain sections from Wt and *ret* mice were stained for VWF (green), CD31 (red) and DAPI (blue). **A-D.** We compared the formation of luminal VWF fibers in vessels from Wt brains (**Wt**) (**A**), *ret* brains without macroscopic metastasis (**Met-free**) (**B**) and vessels from *ret* brains with metastasis, either from the peripheral tissue (**Peri-Met**) (**C**) or from the intra-metastatic tissue (**Intra-Met**) (**D**). **E.** Shown is the percentage of cerebral vessels containing luminal VWF fibers in each group (n = 4-6 animals per group); **, $P < 0.01$ (One-way Anova). Data are presented as mean ± SD. Scale bars: 50 µm.

In line with our previous results showing intraluminal VWF strings in human brain metastatic tissue (**section 4.2.1**), these findings confirmed the presence of luminal VWF fibers in *ret* mouse bearing brain metastasis. Importantly, the formation of VWF networks was already significantly increased in metastasis-free brains (41.33% ± 9.37%).

4.2.3 Endothelial cells are not the main source for VWF fibers in the brain vasculature

Quiescent/non-activated endothelium is characterized by the typical punctate VWF staining in the vessel wall and virtually no VWF within the vessel lumen. In contrast, activation of the endothelium is associated with a clear decrease of VWF abundance in the vessel wall, indicative of the exocytosis of WPB-stored VWF. This is usually reflected by the formation of ULVWF fibers within the lumen of the activated vessel (Bauer, et al. 2015). Interestingly, we observed that the formation of luminal VWF strings in *ret* mouse brain vessels did not correlate with this distribution (**Figure 21 B-D**). Therefore, we wondered if the secretion of VWF from activated endothelium is involved in the formation of luminal VWF fibers detected in *ret* brains.

To address this question we quantified the VWF within the vessel wall and within the lumen of brain vessels from healthy (Wt) and *ret* mice. As controls, vessels from healthy skin and primary malignant melanoma tumors were used to represent non-activated and activated vessels respectively.

In healthy skin vessels, VWF was strongly located in the vessel wall with little presence of VWF within the lumen (**Figure 22 A-I and C**). This distribution is characteristic of non-activated endothelium, with VWF stored in endothelial WPBs. By contrast, the amount of VWF in the endothelium of primary tumor vessels was importantly reduced, correlating with a strong generation of intraluminal VWF fibers (**Figure 22 A-II and C**) indicative of activated endothelium with subsequent secretion of VWF into the vessel lumen. In the brain, vessels from healthy Wt mouse exhibited a distribution of VWF similar to non-activated vessels in healthy skin, with VWF stored in the vessel wall and almost no luminal VWF fibers. (**Figure 22 B-I and C**). Moreover, and in line with the observations from the primary tumor (**Figure 22 A-II**),

vessels of *ret* Intra-Met brain tissue exhibited a pronounced formation of luminal VWF fibers associated with a significant decrease of endothelial VWF (**Figure 22 B-IV and C**). Luminal VWF networks were also found in *ret* Peri-Met brains vessels. However, these vessels also showed a strong VWF signal in the wall, indicative of non-activated endothelium (**Figure 22 B-II and C**). Interestingly, the same distribution was detected in the vessels from *ret* Met-Free brain tissue (**Figure 22 B-III and C**).

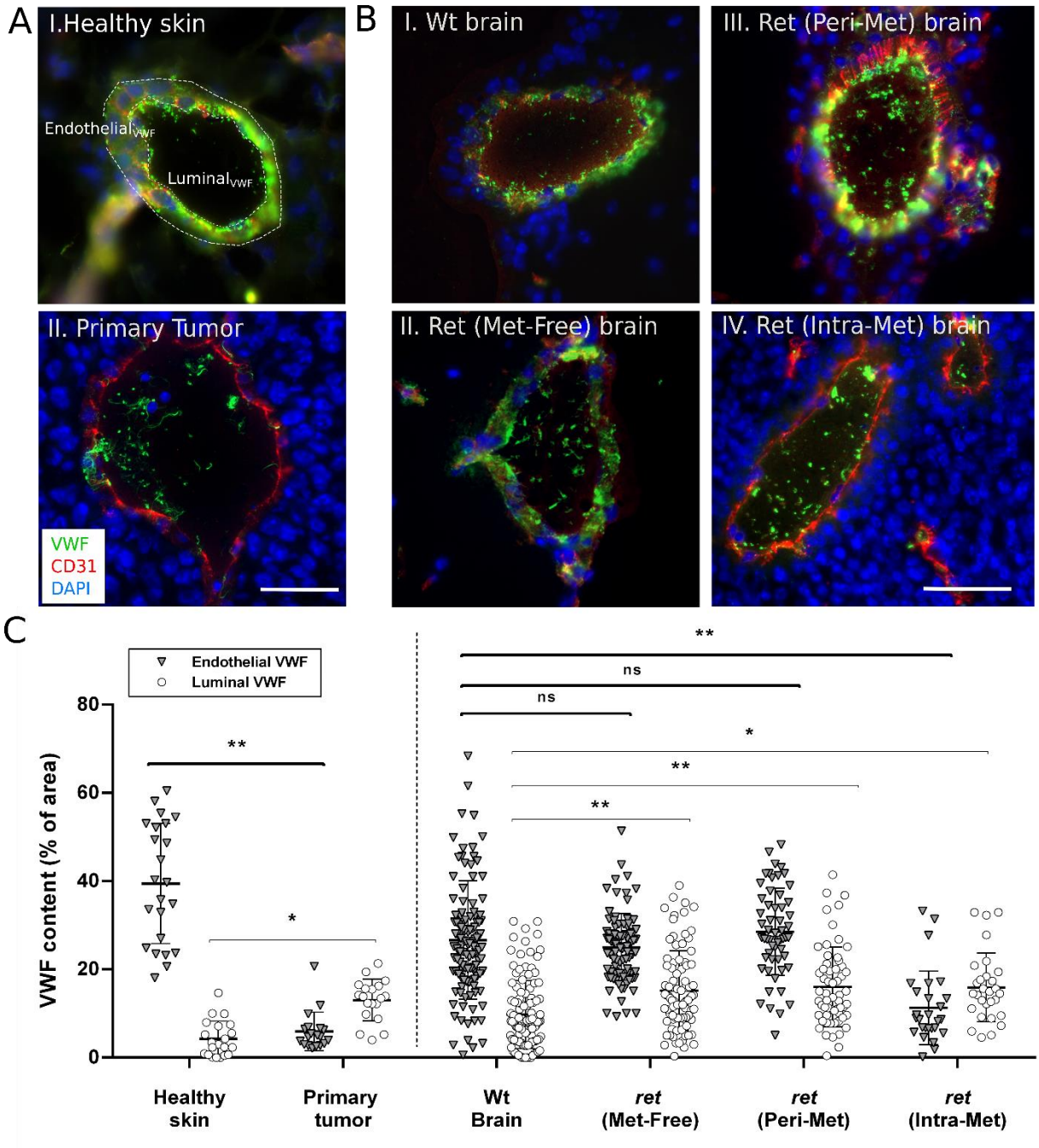

Figure 22. Luminal VWF fiber formation is not associated with a decrease of endothelial VWF in the brain vasculature. A. Representative examples of non-activated vessels (I Healthy skin vessel) and activated vessel (II Primary tumor vessel). **B.** The distribution of VWF was analyzed in brain vessels from Wt brains (I), ret Met-Free (II), *ret* Peri-Met (III) and *ret* Intra-Met (IV). **C.** The percentage of the area occupied by VWF in the endothelium (Endothelial VWF) and within the lumen (Luminal VWF) was quantified by using Fiji/ImageJ (n = 24-117 vessels per group); ns, not significant *, P< 0.05, **, P<0.001, (Two way Anova). Data are presented as mean ± SD. Scale bars: 50 µm.

These results indicate that endothelial VWF could not be the major source for the observed VWF network formation in brain vessels and suggests the contribution of plasmatic VWF multimers or platelet-derived VWF.

4.2.4 Platelet-derived VWF contributes to the formation of luminal VWF fibers in brain vessels

Next to ECs, platelets store VWF in α-granules (Garam et al. 2018). Platelet-derived VWF represents an important source of VWF providing about 20% of plasmatic VWF within the blood (Peyvandi, Garagiola, and Baronciani 2011b). Given the heterogeneous distribution of VWF in the brain vasculature and the restricted secretion of VWF by brain vessels, we asked whether platelet activation and secretion of α-granule might be responsible for the luminal VWF fibers in *ret* transgenic mouse brains.

To answer this question, we first evaluated the activation of platelets in *ret* brains with or without metastasis. Because activated thrombocytes bind to fibrinogen via the active GpIIb/IIIa (or αIIbβ3) integrin complex (Nieswandt, Varga-Szabo, and Elvers 2009), an *in situ* fribinogen binding assay was performed. To this end, brain sections were incubated with Alexa Fluor® 488-conjugated fibrinogen and later were stained for the platelet marker CD42 (or GpIbα) (red) and DAPI (blue) for nuclei.

In **Figure 23,** representative images of brain vessels show the differences on of platelet-fibrinogen interaction in healthy Wt versus *ret* brains. Platelet-fibrinogen interaction was measured by the t-Mander's coefficient of colocalization (Fiji/Image J). Our analyses revealed that in brain vessels from healthy Wt mice intraluminal platelet-fibrinogen interaction was a minor event. In contrast, in *ret* mice the colocalization of intraluminal platelets and fibrinogen was significantly enhanced in *ret*

Met-Free brains (2.95-fold), *ret* Peri-Met (2.79-fold) and *ret* Intra-Met (2.96-fold). (**Figure 23 B**). This result suggests that platelet activation may be enhanced during brain metastasis. It is important to note that in line with our previous result showing an increased formation of luminal VWF fibers in *ret* Met-Free brains (**section 4.2.3**), enhanced fibrinogen-CD42 colocalization was also detected in metastasis-free brains.

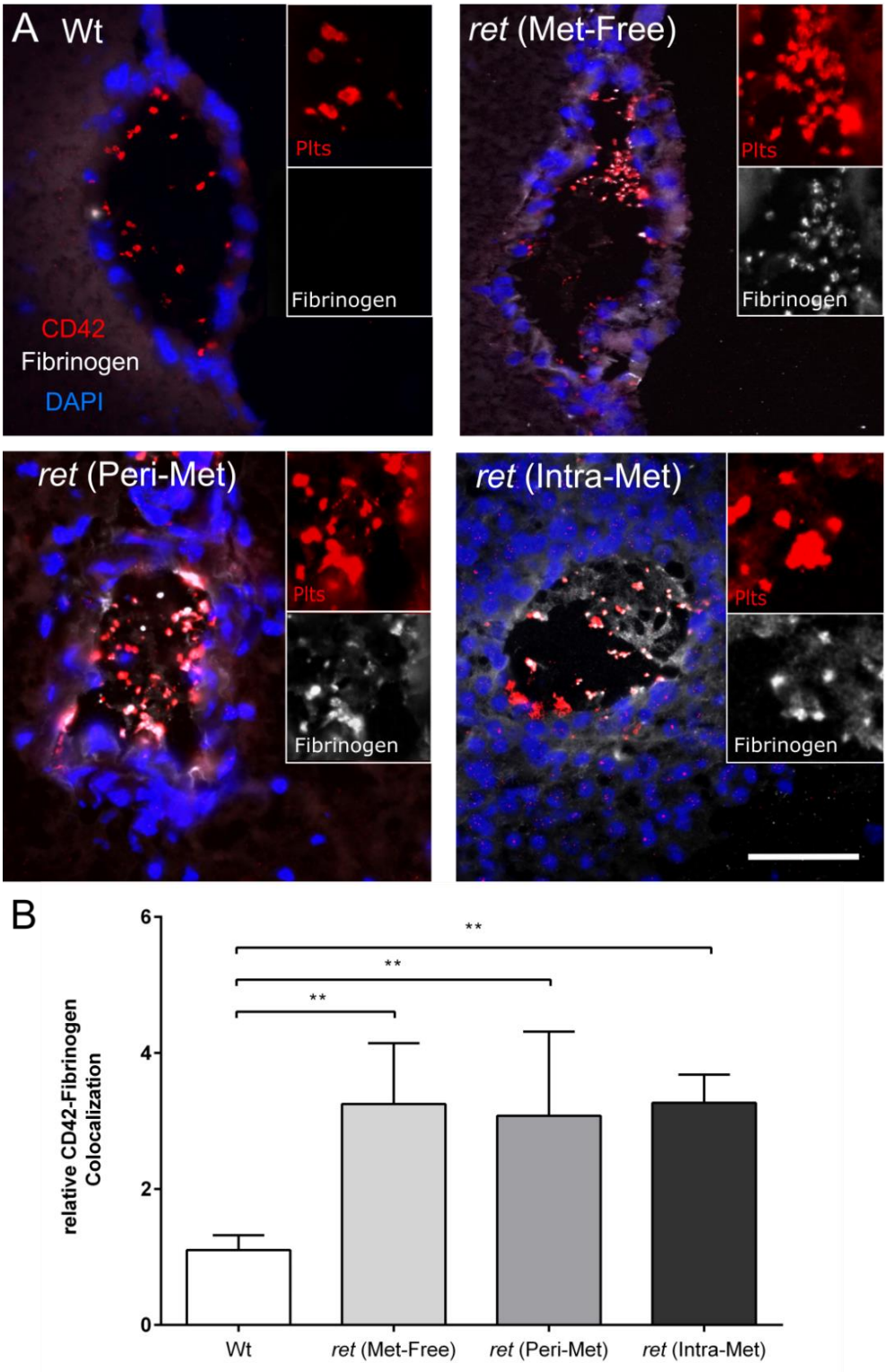

Figure 23. Platelet-fibrinogen interaction is enhanced in brain metastasis. To identify activated platelets *in situ*, a fibrinogen binding assay was performed. Tissue sections were incubated with Alexa Fluor®488-conjugated fibrinogen (white) and stained for CD42 (red) and DAPI (blue). **A.** Representative images show the interaction between fibrinogen and platelets in wild type (Wt) and ret transgenic (ret) mouse brain vessels. **B.** CD42-Fibrinogen interaction was quantified by the Mander's colocalization coefficient (Fiji/Image J). Values in each group were normalized to the results obtained in Wt brains. (n= 4-6 mice per group); **, P < 0.01, (One-way Anova). Data are presented as mean ± SD. Scale bar: 50 µm.

In addition, an immunofluorescence analysis for VWF (green) and CD42 (red) was performed in brain cryosections of Wt and *ret* brains, to determine whether the secretion of VWF stored in platelet α-granules was associated with the formation of luminal fibers. Platelets identified in the lumen of healthy Wt brain vessels exhibited a discoid morphology with a intracellular punctuate distribution of VWF indicative of resting platelets storing VWF in α-granules (**Figure 24 A**). By contrast, in *ret* brain vessels an enhanced number of platelets showed pseudopodial projections, which are considered a feature of activated platelets (Modic et al. 2014). Additionally, platelets with pseudopodia were found in a strong association with VWF fibers suggesting the secretion of VWF stored in α-granules. In addition, EC-derived VWF remained in the vessel wall (**Figure 24 B and C**) excepting in the vessel walls of intratumoral vessels were endothelial staining for VWF was not clearly detected (**Figure 24 D**). In conclusion, pronounced fibrinogen binding in combination with the strong association of platelets with luminal VWF fibers, indicate that platelet activation related to the brain metastatic cascade.

In line with this, platelet activation in *ret* brain correlated with an increase in thrombocyte aggregation. To quantify the formation of platelet aggregates, the mean area of CD42 positive individual platelets was measured by ImageJ/Fiji (NIH). With this value, the number of platelets involved in each luminal CD42-positive aggregate was stimated. Thereby, we could distinguish between single platelets (1-2 platelets) and platelet aggregates (>2 platelets). The corresponding quantification showed that the mean number of single platelets in each vessel did not differ significantly among the groups. Nevertheless, the number of platelet aggregates per vessel significantly increased in the vessels of *ret* Met-Free (9.41 ± 3.01 aggregates/vessel), in *ret* Peri-Met (11.13 ± 2.66 aggregates/vessel) and in *ret* Intra-Met (8.16 ±1.09 aggregates/vessel) brains compared to Wt brain vessels (4.75 ± 1.41

aggregates/vessel) (**Figure 24 E**). These results confirm that platelet-secreted VWF contributes to the formation of platelet-rich thrombi.

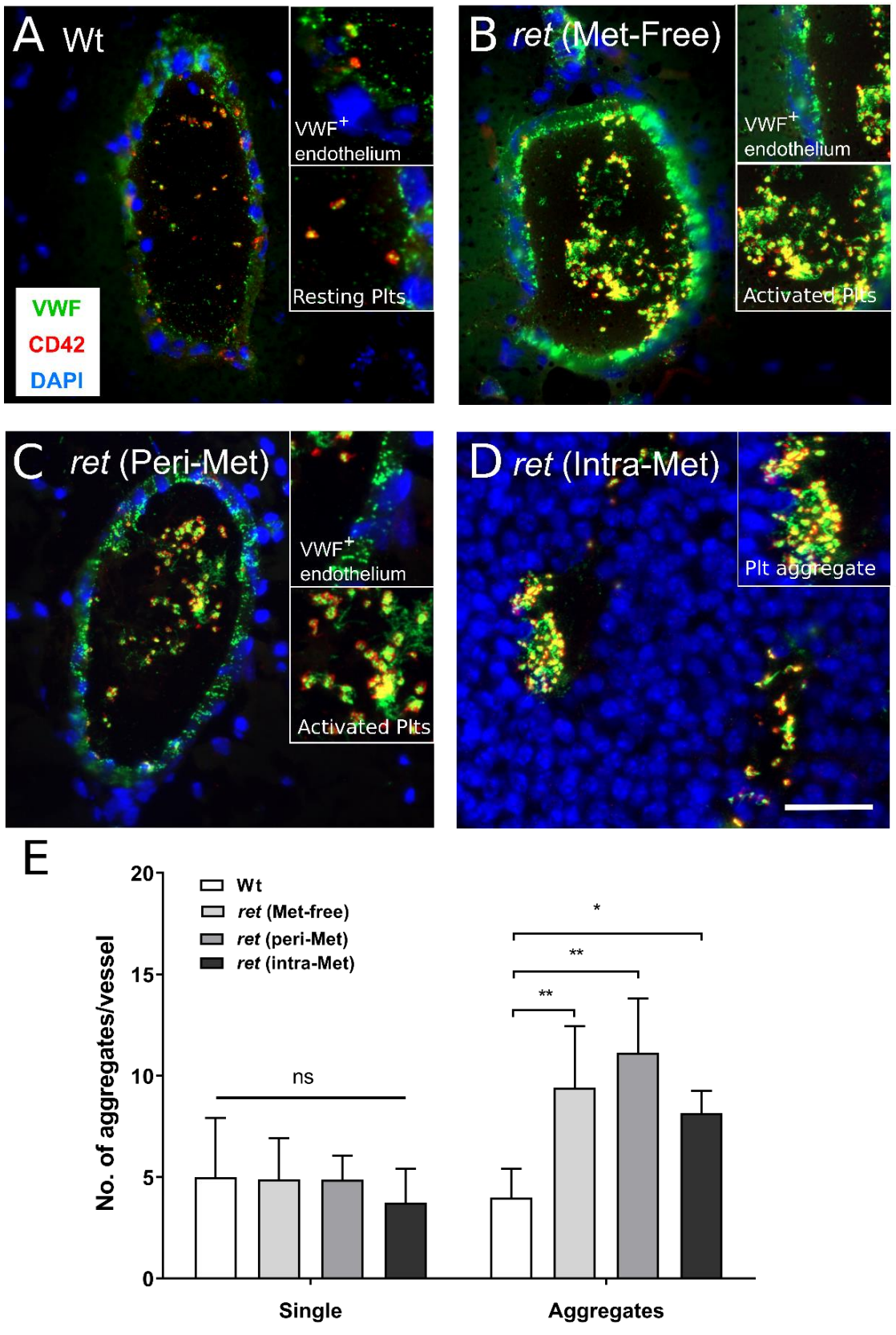

Figure 24. VWF-Platelet aggregates are increased in brain metastasis. Brain sections were stained for VWF (green), for CD42 (red), and DAPI (blue). **A-D.** Images show the differences between endothelial-derived VWF and platelet-derived VWF secretion between healthy (Wt) (**A**) and *ret* brains (**B-D**). **E.** Luminal platelet area was measured to analyze the formation of platelet-rich thrombi in brain vessels (n=4-6 brains per group); ns, not significant *, $P < 0.05$, **, $P < 0.01$ (One-way Anova).

4.3 Platelet-derived von Willebrand factor and thrombus formation

4.3.1 Platelet-secreted VWF contributes to platelet aggregation

To determine if the contribution of endothelial-derived and platelet-derived VWF differs in the occlusion of cerebral microvessels, we investigated the mechanisms underlying the formation of platelet-rich microthrobi *in vitro*.

First, we studied the impact of different agonists on the activation of ECs and platelets. For this purpose, macrovascular HUVECs and brain murine microvascular bEND3 were exposed to thrombin (0.5 U/ml), histamine (10 µM) or collagen type I (50 µg/ml). The effect of thrombin-mediated VWF release was detected only in HUVECs but not in bEND3. Moreover, histamine induced a significant increase of VWF secretion in both HUVECs and bEND3. By contrast, collagen type I had no effect neither on HUVECs nor on bEND3 (**Figure 25 A and B**). In parallel, the aggregation of platelets was examined after incubation of isolated thrombocytes with the same agonists. Light transmission aggregometry (LTA) assays revealed a strong aggregation of platelets mediated by thrombin and collagen type I but not by histamine (**Figure 25 C**). In conclusion, our experiments revealed that histamine is an important agonist of EC activation but has no effect on platelet aggregation. In contrast, collagen type I mediates platelet aggregation without any effect on VWF secretion by ECs.

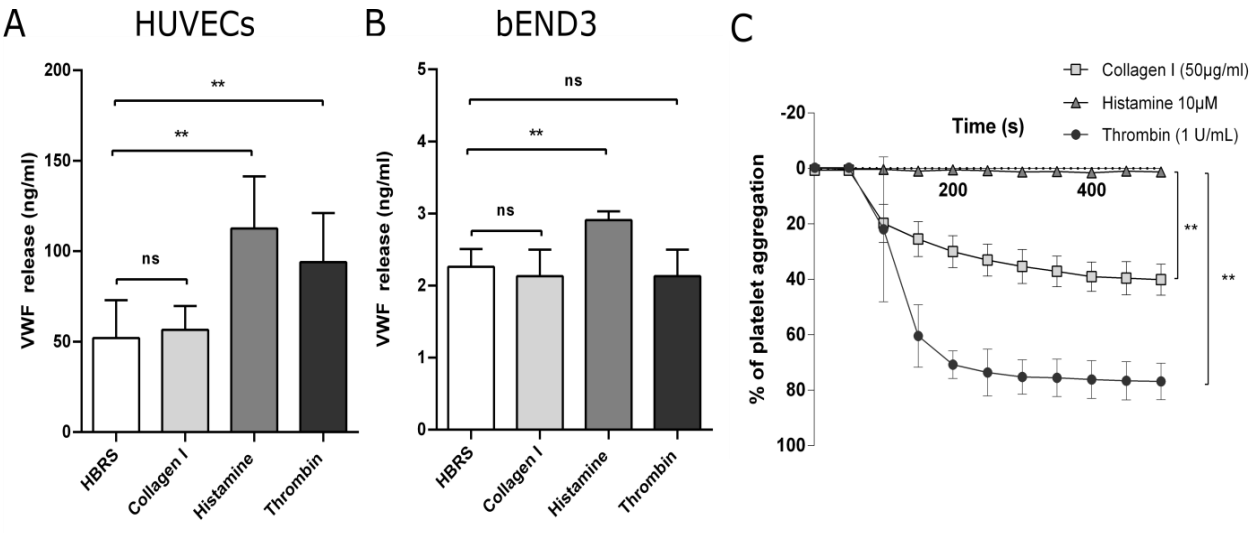

Figure 25. Different agonists are required for EC andr platelet activation. A and B. HUVECs (**A**) and bEND3 (**B**) were stimulated with HBRS (Control), collagen I (50 µg/ml), histamine (10 µM) and thrombin (0.5 U/ml) and the supernatant was analyzed for VWF release by ELISA (n = 3 independent experiments); ns, no significant, **, *P* < 0.01 (Student's t-test). **C.** The impact of these agonists was evaluated on platelet aggregation by LTA. (n = 4 independent experiments); **, P < 0.01 (F-test).

The different steps in the formation of a platelet-rich thrombus were studied by implementation of an *in vitro* microfluidic system that mimics the conditions within the vasculature. HUVECs and HBMECs were seeded in separated microfluidic slides and perfused with washed human platelets in absence of plasmatic factors. Based on the previous results EC activation was induced by histamine addition (100 µM). The formation of luminal VWF strings was visualized by the formation of the so-called “platelets on a string” structures, indicative of the initial platelet adhesion. At this point, platelet coverage was measured and the results showed that in HUVEC layers (1650 ± 501.8 µm^2) thrombocyte adhesion was notably greater than in HBMECs (683 ± 269.60 µm^2) (**Figure 26 A and C** [platelet adhesion]). In a second step, the addition of collagen type I (50 µg/ml) evoked the activation of platelets leading to their aggregation and the subsequent formation of thrombocyte plugs (**Figure 26 B**). The corresponding quantification showed that platelet coverage increased significantly both in HUVECs (7923 ± 1800.1 µm^2) and in HBMECs (2238 ± 600.9 µm^2) (**Figure 26 C** [platelet aggregation]). Interestingly, despite the differences in the initial adhesion of platelets between HUVECs and HBMEC, the relative increase of platelet coverage after collagen I addition was similar on HUVEC and HBMEC monolayers, showing approximately 4-fold increase of platelet deposition. This indicates that whereas theinitial adhesion of thrombocytes is mediated by endothelial derived VWF

strings, platelet aggregation is induced mainly by the specific activation of thrombocytes. Additionally, these data suggests that the restricted secretion of VWF in brain ECs may protect against an excessive deposition of thrombocytes in the brain vasculature preventing the potential occlusion of brain microvessels.

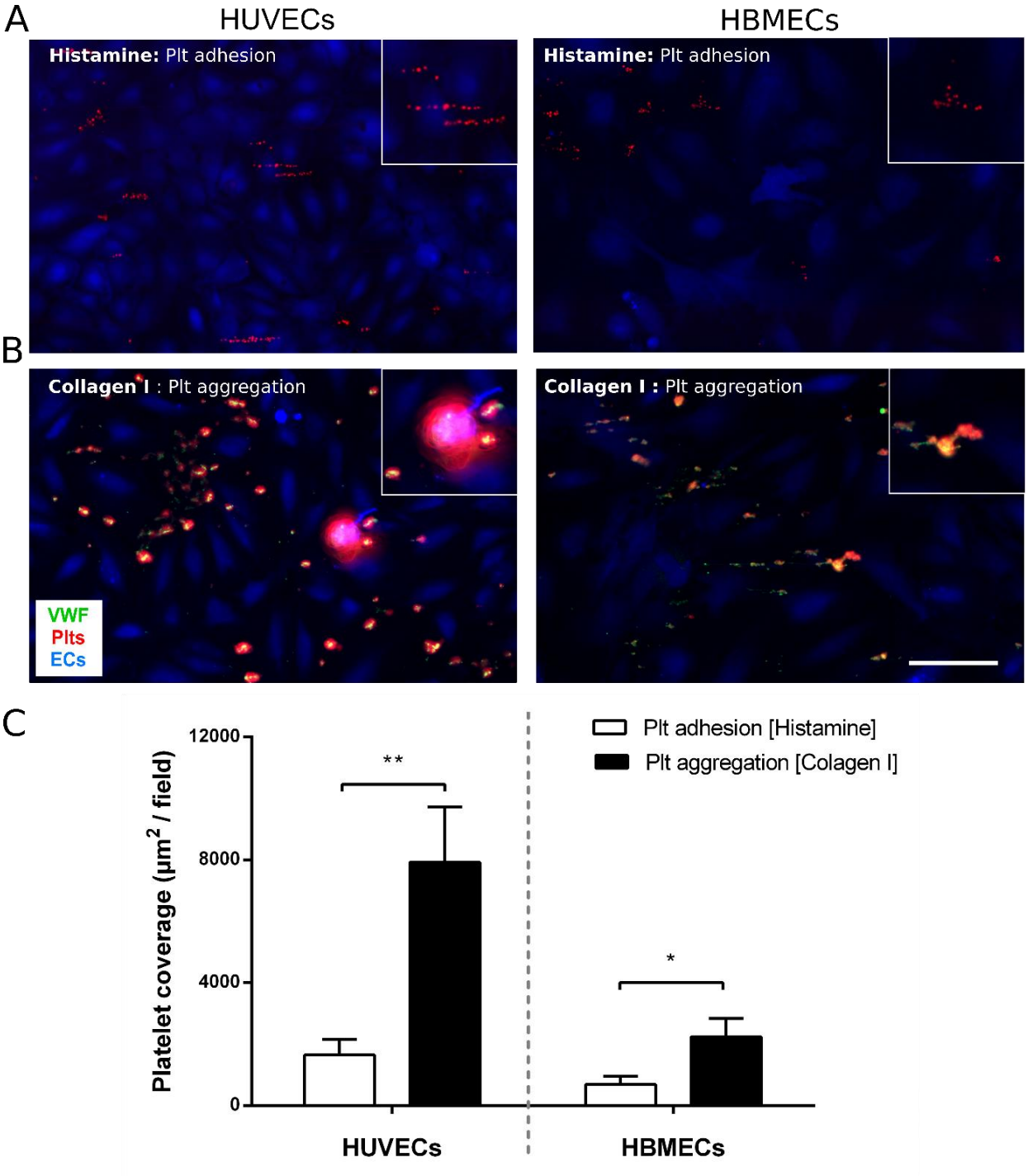

Figure 26. Platelet binding and aggregation in distinct vascular beds. The effect of the low VWF abundance in brain microvascular ECs was evaluated on the formation of platelet-rich thrombi under flow conditions. **A and B**. HUVEC and HBMEC monolayers were perfused with human labeled-platelets. EC activation was induced by histamine (1 U/ml) mediating platelet adhesion (**A**). In a second step, platelet activation and subsequent aggregation was induced by collagen type I (50 µg/ml) (**B**). **C.** Platelet coverage was quantified at the initial adhesion of platelets and after aggregation in 12 independent fields per experiment (n = 3 experiments); *, P < 0.05, **, P < 0.01 (two tailed, Student's t-test).Scale bar: 50 µm.

To proof that platelet-derived VWF plays a critical role in thrombus formation within the brain vasculature, isolated platelets from Wt or $VWF^{-/-}$ mice were perfused over murine bEND3 monolayers. The initial adhesion of platelets was mediated by histamine addition (100 µM). No significant differences were found in the formation of thrombocyte strings between Wt (132.72± 38.19 μm^2) and $VWF^{-/-}$ platelets (57.43 ± 51.09 μm^2) (**Figure 27 A and C**). Next, the formation of platelet plugs was evaluated after addition of collagen type I (50 µg/ml). Wt platelets exhibited a regular response to collagen, forming platelet aggregates and increasing the platelet coverage (311.55 ± 121.32 μm^2). However, $VWF^{-/-}$ platelets showed a defective aggregation upon collagen addition, resulting in a non-significant increase of thrombocyte surface coverage (74.59 ± 42.51 μm^2) (**Figure 27 A and C**). These findingsindicate the importance of α-granule-secreted VWF in the aggregation of platelets. To confirm this, aggregation of purified Wt and $VWF^{-/-}$ platelets was evaluated by LTA in absence of plasmatic factors (including plasmatic VWF). In line with our previous results, LTA showed that the formation of platelet aggregates was significantly reduced in platelets lacking VWF (59%) in comparison with Wt platelets (72%), highlighting the important contribution of platelet-derived VWF in the formation of platelet aggregates. (**Figure 27 D**). These results provide a new insight into the mechanism of thrombus formation and confirmed that platelet-derived VWF plays a critical role in the aggregation of activated platelets in the vasculature of the brain.

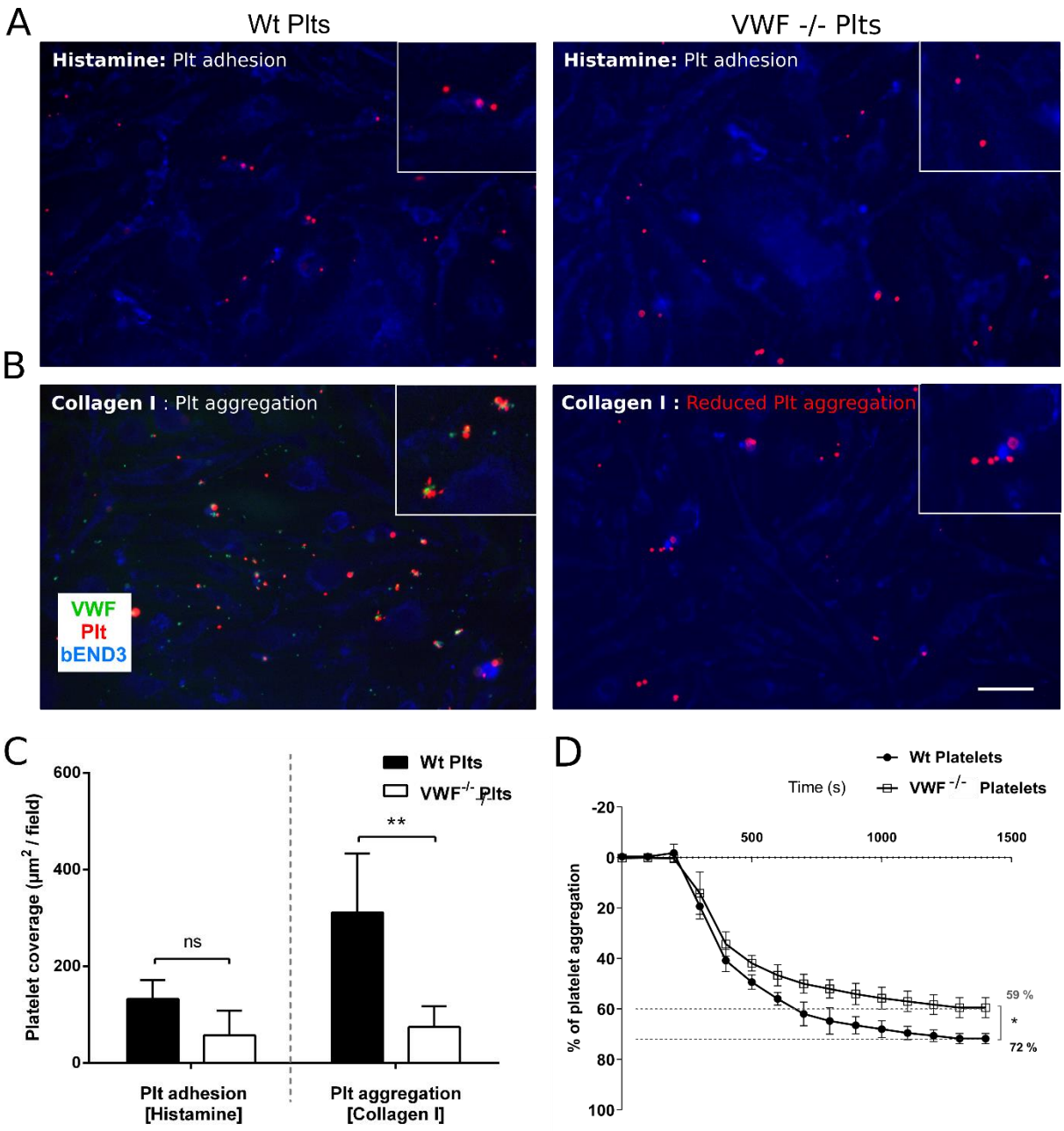

Figure 27. Platelet-derived VWF mediates the formation of platelet aggregates. The contribution of platelet-derived VWF on thrombus formation was analyzed by using microfluidic devices. The murine bEND3 cells were perfused with platelets from Wt or VWF knockout (VWF KO) mice. **A and B.** The murine bEND3 cells were perfused with platelets from Wt or VWF knockout (VWF KO) mice. bEND3 activation was induced by histamine (1 U/ml) mediating platelet adhesion (**A**). In a second step, platelet activation and subsequent aggregation was induced by collagen type I (50 µg/ml) (**B**). **C.** Size of platelet coverage at the initial adhesion of platelets and after aggregation was quantified in 12 independent fields per experiment (n = 4-6 experiments); *, P < 0.05, **, P < 0.01 (two tailed, Student's t-test). **D.** The capacity of Wt and VWF KO platelets to form aggregates was determined by light transmission aggregometry (LTA) after activation with collagen type I (50 µg/ml) (n = 4 independent experiments); *, *P* < 0.05. (F-test). Data are presented as mean ± SD. Scale bar: 50 µm.

4.3.2 Impact of distinct anticoagulants on platelet activation

Besides its involvement in thrombocyte aggregation, the secretion of platelet α-granules is also involved in the modulation of vascular permeability (Leblanc and Peyruchaud 2016). One of the major regulators of vascular integrity and development is VEGF, which includes VEGF-A, VEGF-B and placental growth factor (Greenberg and Jin 2013). Importantly, platelet α-granules are an prominent source of VEGF-A (Cloutier et al. 2012).

To ensure whether the activation of platelets results in the secretion of α-granules, the supernatant of activated thrombocytes was analyzed for VEGF-A secretion. Our analyses demonstrated that in the absence of plasmatic factors, collagen type I (50 µg/ml) and thrombin (0.5 U/ml) induce the activation and the subsequent aggregation of platelets correlated with a significant increase of secreted VEGF-A in platelet supernatant compared to non-activated platelet (**Figure 28 A and B**).Because it is known that anticoagulant heparins interfere in the communication between tumor cells and thrombocytes (Ponert et al. 2018), the impact on platelet activation and VEGF-A secretion of the low molecular weight heparin (LMWH) Tinzaparin and the pentasaccharide Fondaparinux was evaluated. Our analyses revealed that the aggregation of platelets was abrogated by Tinzaparin (100 U/ml) and this correlated with a strong reduction of platelet-derived VEGF-A secretion (12.54 ± 6.42 pg/ml). (**Figure 28 A and B**). In contrast, preincubation with Fondaparinux did not show any effect on platelet aggregation and only induced a partial reduction of VEGF-A secretion in platelet releasates (33.56 ± 19.38 pg/ml).

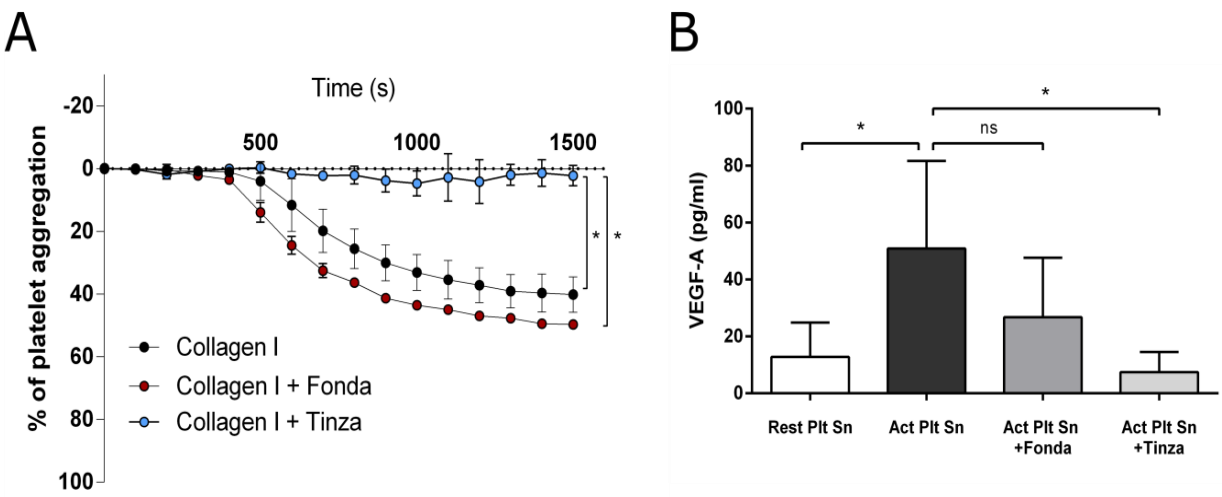

Figure 28. Tinzaparin blocks platelet activation and platelet-derived VEGF-A. The impact of distinct anticoagulants on platelet aggregation was examined by LTA. **A.** Platelets were preincubated for 30 minutes with 100 U/ml of Tinzaparin (Tinza) or 50 µg/ml of Fondaparinux (Fonda) and then, collagen type I (50 µg/ml) and thrombin (0.5 U/ml) was used as platelet agonist (n = 4 independent experiments); *, $P < 0.05$ (F-test). **B.** Supernatants of platelets were analyzed by ELISA for VEGF-A (n = 3 independent experiments); ns, non-significant, *, $P < 0.05$ (One-way Anova).

4.3.3 Tinzaparin reduces platelet-mediated endothelial permeability and tumor cell transmigration

Platelet-secreted VEGF-A is known to promote vascular permeability and tumor cell extravasation (Meikle et al. 2016). Therefore, we tested the impact of platelet-derived VEGF-A on the transendothelial permeability of brain EC monolayers and tumor cell transmigration.

First, we examined the effect of platelet activation on the transendothelial electrical resistance (TEER) of HBMEC monolayers. HBMECs seeded on an electric cell-substrate impedance sensing (ECIS) array (Applied BioPhysics Inc., NY, USA) were coincubated with platelet releasates for 24 hours and changes in the TEER were measured every 48 seconds (**Figure 29 A**). The results revealed that collagen type I (50µg/ml)-activated platelet releasates induced a significant decrease of HBMECs TEER (-426.6 ± 101.1 Ωcm^2) compared to resting platelet releasates (-246.6 ± 107.8 Ωcm^2) (**Figure 29 B**). In contrast, preincubation of platelets with Tinzaparin (100 U/ml) before activation significantly reduced the effect of platelet releasates on TEER (-317.4 ± 45.25 Ωcm^2). Similarly, Bevacizumab (0.65 mg/mL), an antibody against

VEGF-A, strongly inhibited the impact of platelet-supernatant on TEER (-247 ± 95.85 Ωcm^2) highlighting the role of platelet-secreted VEGF-A in the disruption of brain endothelial barrier.

The impact of platelet supernatant on Ret melanoma cell transmigration was evaluated in a trans-well system seeded with HBMECs (**Figure 29 C**). Incubation with the supernatant of collagen type I-activated platelets increased the number of transmigrated Ret cells through the endothelial barrier (68.58 ± 12.39 Ret cells/field) compared to Ret cells incubated with the supernatant of resting platelets (38.22 ± 16.89 Ret cells/field). By contrast, the number of transmigrated tumor cells was significantly reduced by the preincubation of platelets with Tinzaparin (37.23 ± 8.21 Ret cells/field). This effect was also detected after incubation of platelets with Bevacizumab (43.28 ± 12.90 Ret cells/field) (**Figure 29 D**).

In summary, these data suggest that the activation of arrested platelets may generate a local increase of VEGF-A in the microvasculature of the brain, promoting local permeability changes and tumor cell extravasation.

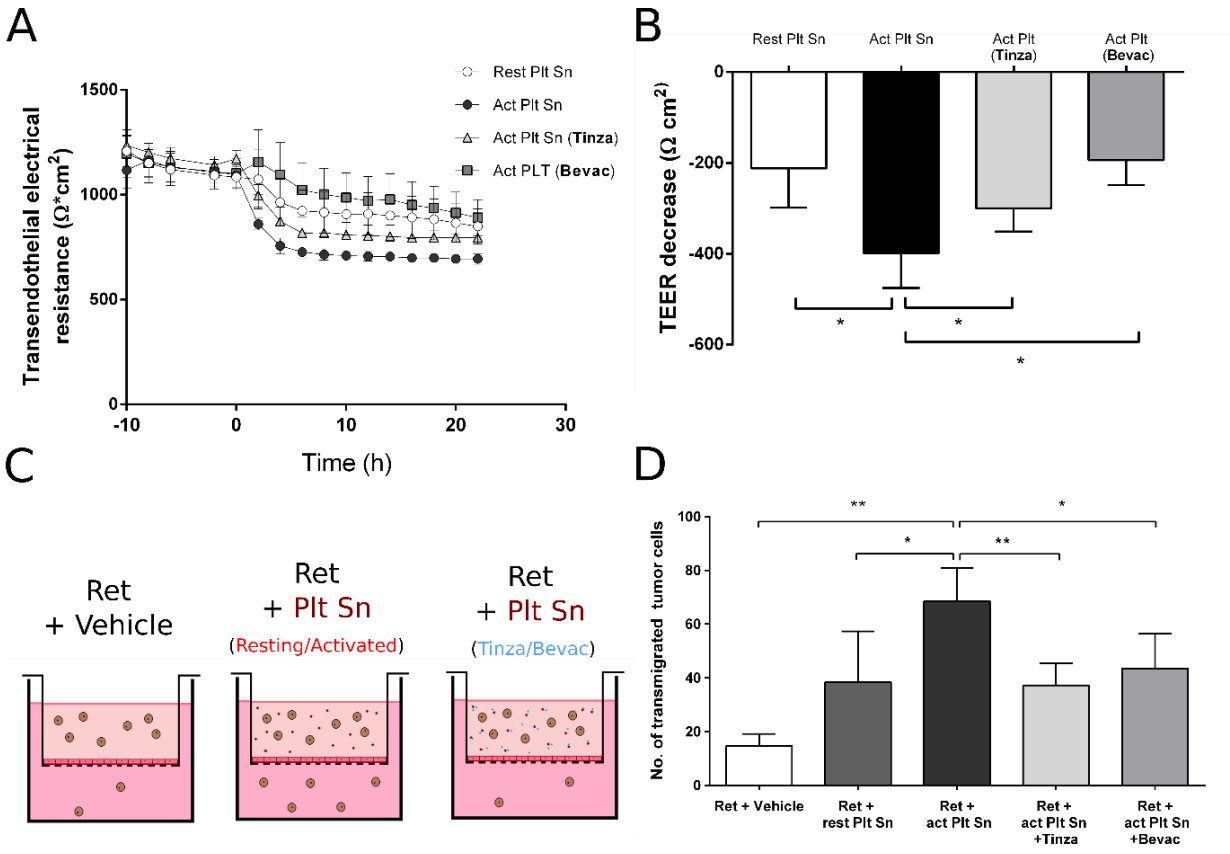

Figure 29.Tinzaparin attenuates platelet-mediated brain EC permeability and tumor cell transmigration. A. HBMEC monolayers were incubated with the supernatants of resting platelets (Rest Plt Sn) or with the supernatant of collagen type I (50 µg/ml)-activated platelets (Act Plt Sn), with or without a preincubation with Tinzaparin (100 U/ml; Act Plt Sn [Tinza]) or Bevacizumab (0.65 mg/ml; Act Plt Sn [Bevac]). Transendothelial electrical resistance (TEER) was used to evaluate endothelial integrity (n = 6 of 3 independent experiment per group). **B.** Bars show the absolute decrease of TEER in each group after incubation with platelet releasates. Data are presented as mean ± SD. *, P< 0.05, **, P<0.01 (Student's t-test).**C.** Schematic diagram of the tumor cell transmigration assay: Ret melanoma cells were co-incubated for 8 hours with the supernatant of resting platelets (rest Plt Sn), activated platelets (act Plt Sn) and activated platelets preincubated with Tinzaparin (100 U/ml) or Bevacizumab (0.65 mg/mL) (act Plt Sn +Tinza/Bevac). Then, upper chambers were removed and transmigrated tumor cells counted after 24 hours. **D.** shown is the corresponding quantification of transmigrated tumor cells (n = 6 of 3 independent experiments); *, P < 0.05, **, P < 0.01 (One-way Anova). Data are presented as mean ± SD.

4.4 Effect of anticoagulation with Tinzaparin on brain metastasis formation

Our *in vitro* results demonstrated the inhibitory effect of Tinzaparin on platelet activation and subsequent VEGF-A secretion. Besides, our results showed Tinzaparin reduced the effect of platelet-derived VEGF-A on transendothelial permeability and tumor cell transmigration through a brain EC monolayer. These findings suggest potential benefits of Tinzaparin in the prevention of cerebral metastasis.

4.4.1 Tinzaparin reduces platelet activation *in vivo*

To examine the impact of Tinzaparin on platelet activation *in vivo, ret* mice were subcutaneous injected with Tinzaparin for 100 days (0.6 U/kg daily) (n = 20 mice). As control, a group of mice received a daily injection of a saline solution (NaCl) (n = 20).

First, we investigated of the impact of Tinzaparin on platelet activation in *ret* mouse brains. To this end, an *in situ* fibrinogen binding assay was performed as described before (**section 4.2.4**). Briefly, brain cryosections of *ret* mice treated with Tinzaparin or with NaCl were incubated with fluorescently labeled fibrinogen and later stained with CD42 antibody for platelets. If platelet activation occurs, active GpIIIb/IIa is exposed on the surface of activated platelets and is able to bind fibrinogen. Images of *ret* brain vessels in **Figure 30 A and B** show how the colocalization between fibrinogen (white) and platelets (red) is enhanced in a *ret* mouse treated with NaCl compared to a *ret* mouse treated with Tinzaparin. This interaction was quantified as it is described before (**section 4.2.4**) and the results were normalized to the values obtained from the control group (NaCl). The analysis showed that in all the groups analyzed the interaction between fibrinogen and platelets was reduced by 50% in Tinzaparin-treated mice compared to the control group treated with NaCl (**Figure 30 B**).

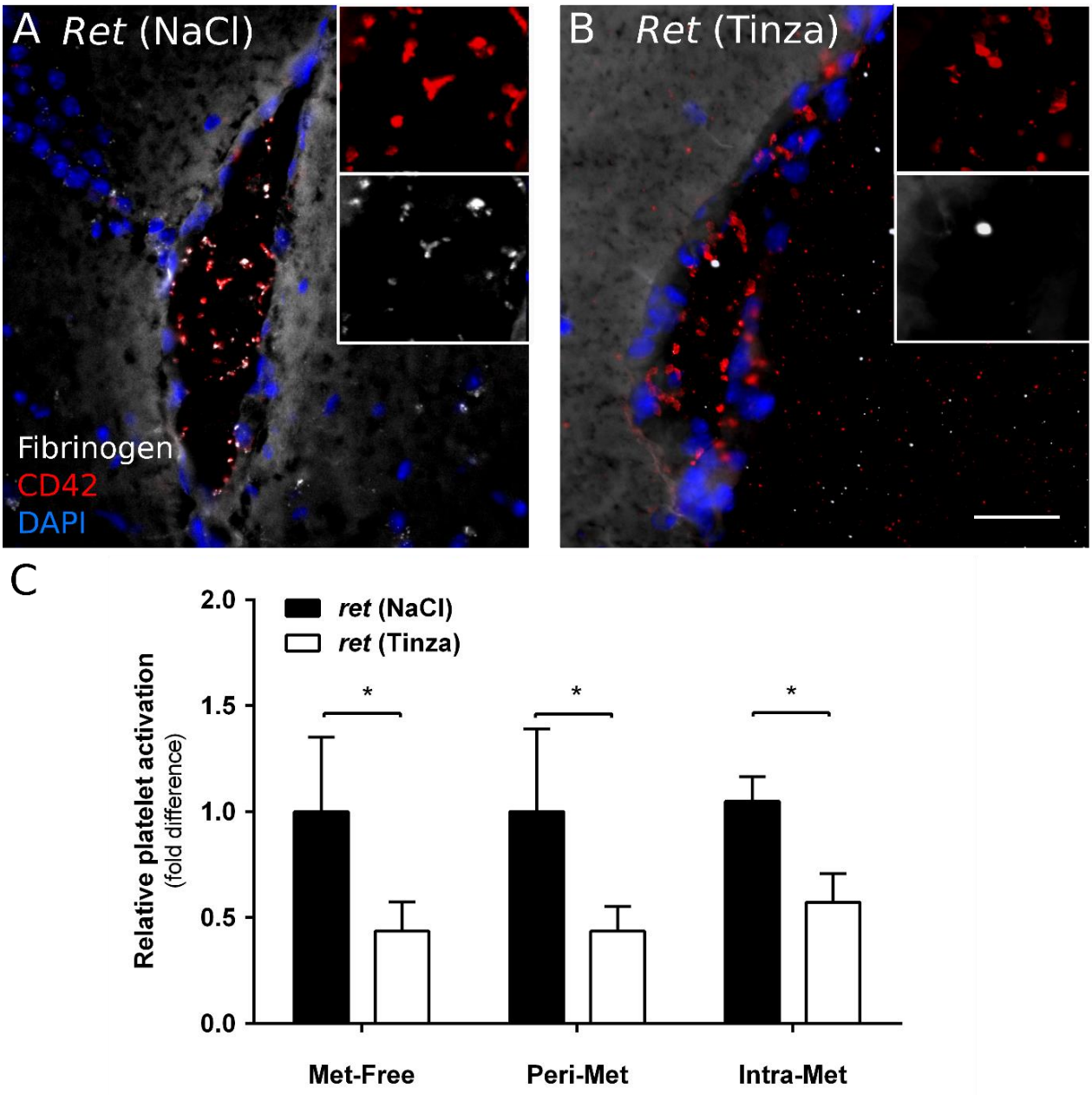

Figure 30. Tinzaparin attenuates platelet activation *in vivo*. To identify activated platelets *in situ*, a fibrinogen binding assay was performed. Tissue sections were incubated with Alexa Fluor®488-conjugated Fibrinogen (white) and stained for CD42 (red) and DAPI (blue).**A-B.** The activation of platelets was analyzed in brains of *ret* mice treated with NaCl (control group) (**A**) or Tinzaparin (Tinza) (0.6 IU/g) (**B**) for 100 days. **C.** CD42-Fibrinogen t-Manders coefficient of colocalization (Fiji/Image J) was calculated in each vessel and normalized to the results obtained in the control group. (n= 3-6 mice per group); *, $P < 0.05$, (two-way Anova). Scale bar: 50 µm.

4.4.2 Inhibition of platelet activation by Tinzaparin reduces the formation of luminal VWF fibers

Whether Tinzaparin reduces the activation of platelets *in vivo,* this phenomenon should be reflected by a decrease of α-granules secretion and, thus, a reduction of intraluminal VWF fibers. To prove this, an immunofluorescence staining for VWF (green), the endothelial cell marker CD31 (red) and DAPI (blue) for nuclei was performed on brain cryosections of *ret* mice treated with Tinzaparin or with NaCl (control).

Immunofluorescence analyses revealed that the generation of intraluminal VWF fibers was strongly reduced in *ret* mice treated with Tinzaparin compared to the control group (**Figure 31 A and B**). The corresponding quantification confirmed that the formation of circulating VWF strings was approximately reduced by 50% in *ret* mice treated with Tinzaparin compared to NaCl-treated control mice (**Figure 31 C**). This is in line with the previous result showing similar a decrease of platelet-fibrinogen interaction.

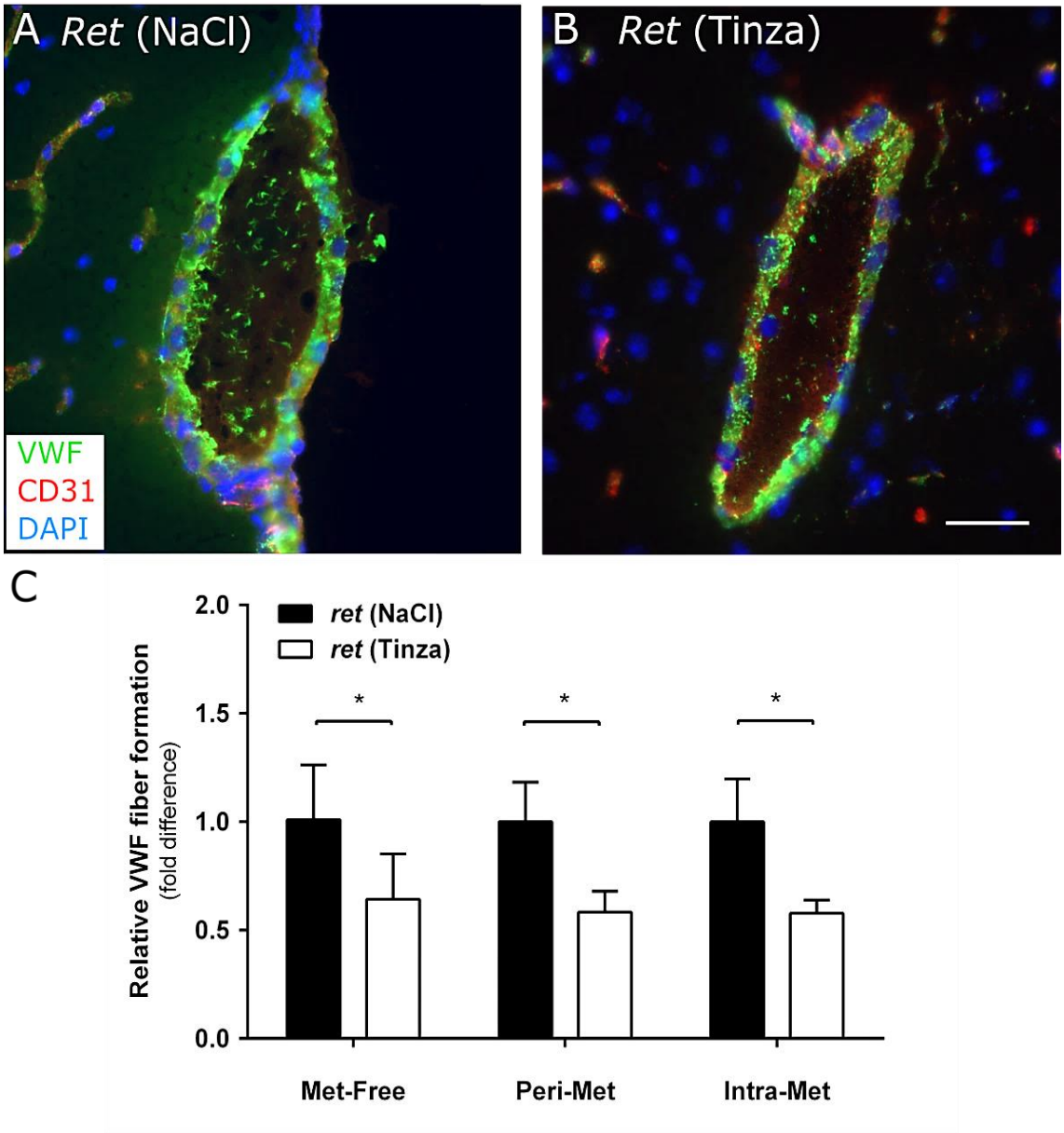

Figure 31. Platelet-derived VWF secretion is inhibited by Tinzaparin *in vivo*. To investigate the impact on the formation of luminal VWF fibers, brain sections from *ret* mice treated with NaCl (control group) or Tinzaparin (0.6 U/kg daily) were stained for VWF (green), CD31 (red) and DAPI (blue). **A and B.** Representative images showing the differences in the formation of luminal VWF fibers in brain vessels of a NaCl-treated *ret* mouse (**A**) and Tinzaparin-treated *ret* mouse(**B**). **C.** The number of vessels containing VWF fibers within the lumen of cerebral vessels was quantified in both groups and normalized to the results seen in the control group (n = 5-6 animals per group); *, $P < 0.01$ (Two-way Anova). Data are presented as mean ± SD. Scale bar: 50 µm.

4.4.3 Tinzaparin treatment reduces platelet aggregation in the the cerebral vasculature of *ret* mice

Based on our previous *in vitro* assays showing the relevance of platelet-derived VWF in platelet aggregation, we analyzed if the inhibition of platelet-derived VWF fiber formation by Tinzaparin interfered in the aggregation of thrombocytes *in vivo*. Therefore, an immunofluorescence staining for VWF (green) and CD42 (red) was performed in brain cryosections of *ret* mice treated with Tinzaparin or with NaCl (control).

The staining revealed notable differences in the morphology of circulating platelets ndicating differences in the activation state of these cells. In the control group treated with NaCl, platelets exhibiting pseudopodia protrusions were localized in close contact with luminal VWF fibers, mediating the formation of thrombocyte aggregates (**Figure 32 A**; magnifications). By contrast, Tinzaparin-treated mice showed circulating single platelets with the characteristic morphology of inactive state, characterized by a discoid-like shape and cytoplasmic storage of VWF (**Figure 32 B**; magnifications). These findings together with the observations described before (**section 4.4.1 and 4.4.2**) suggest a strong inhibitory effect of Tinzaparin on platelet activation *in vivo*. Indeed, compared to NaCl-treated *ret* mice, the number of intravascular thrombocyte aggregates was significantly reduced by 50% in Tinzaparin-treated mice in all the groups analyzed (**Figure 32 C**).

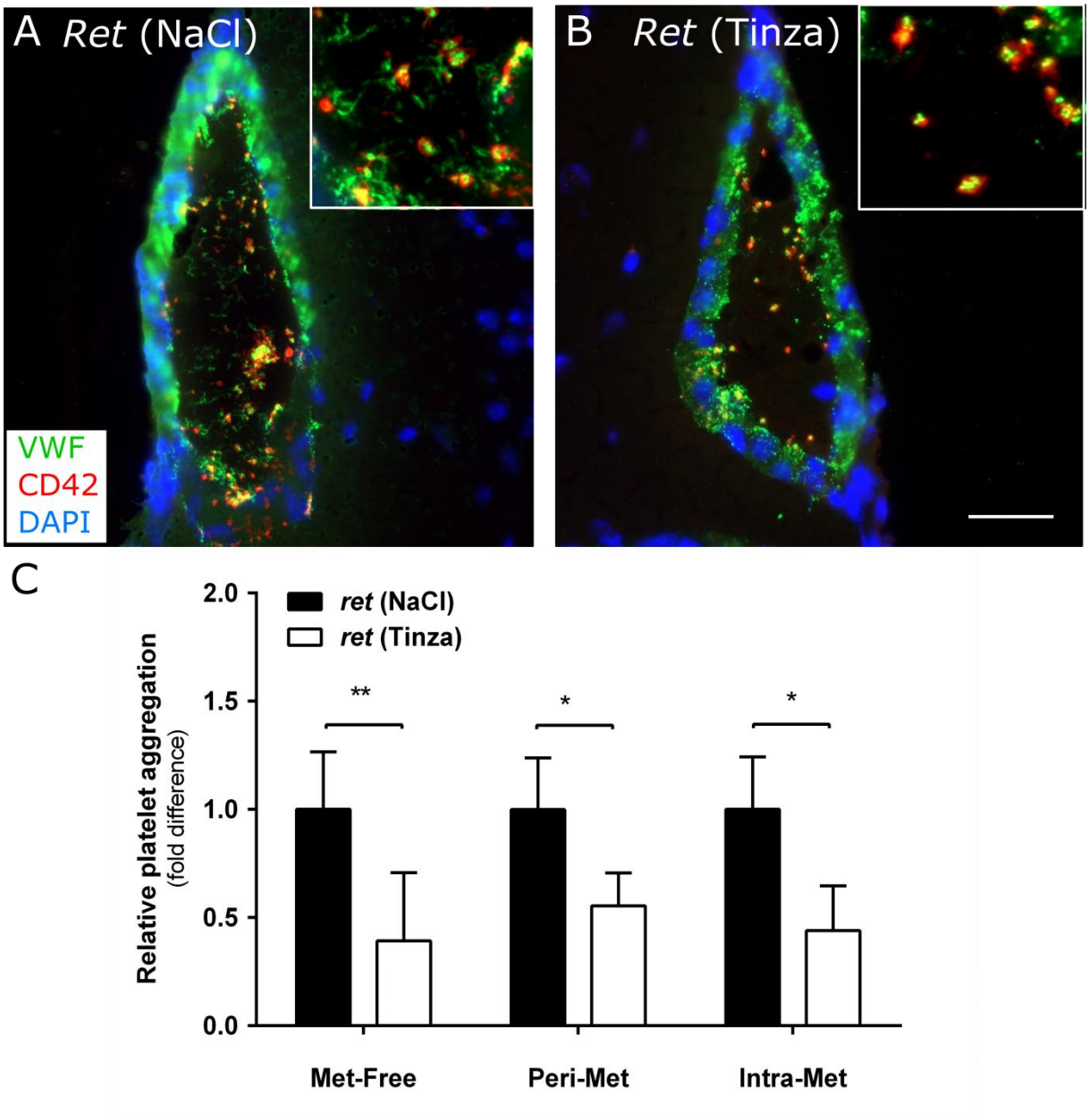

Figure 32. Tinzaparin reduces platelet aggregation *in vivo*. The impact of Tinzaparin on platelet aggregation was examined by immunofluorescence staining for VWF (green), CD42 (red), and DAPI (blue) on brain sections from *ret* mice treated with NaCl (control) or Tinzaparin (0.6 U/kg daily). **A and B.** Images represent the differences in platelet aggregation between ret mice treated with NaCl (**A**) or Tinzaparin (**B**). **C.** Luminal platelet area was measured to analyze the formation of platelet aggregates. The corresponding quantification shows the mean number of aggregates per vessels normalized to the results in the control group (n=4-6 brains per group); ns, not significant *, $P < 0.05$, **, $P < 0.01$ (two-way Anova). Scale bar: 50 µm.

4.4.4 Anticoagulation with Tinzaparin reduces the metastatic load in the brain

In close collaboration with the group of Prof. Dr. Winkler in the DKFZ in Heidelberg, the direct impact of Tinzaparin on metastasis formation was evaluated in amouse model for brain metastasis formation based on the intracardial (i.c.) injection of melanoma cells (**section 3.2.3**).

The i.c. injection of A2058 human melanoma cells was performed in 8-12 weeks old male NMRI-nu/nu mice. Treatment with the anticoagulant LMWH Tinzaparin (0.6 U/kg) was started two days prior IC injection and continued daily until day 10 after IC injection. Mice were maintained under specific pathogen-free conditions until the ultimate endpoint on day 31 after the IC injection (**Figure 33 A**). Then, brains were sectioned coronally (10 µm thick sections) and H&E staining was performed to determine the size of the metastatic lesions (**Figure 33 B**). As shown in **Figure 33 C**, the area of the metastatic lesions was significantly reduced in Tinzaparin-treated mice in comparison to non-treated control mice. This result highlights the therapeutic effect of Tinzaparin attenuating the metastatic load in the brain.

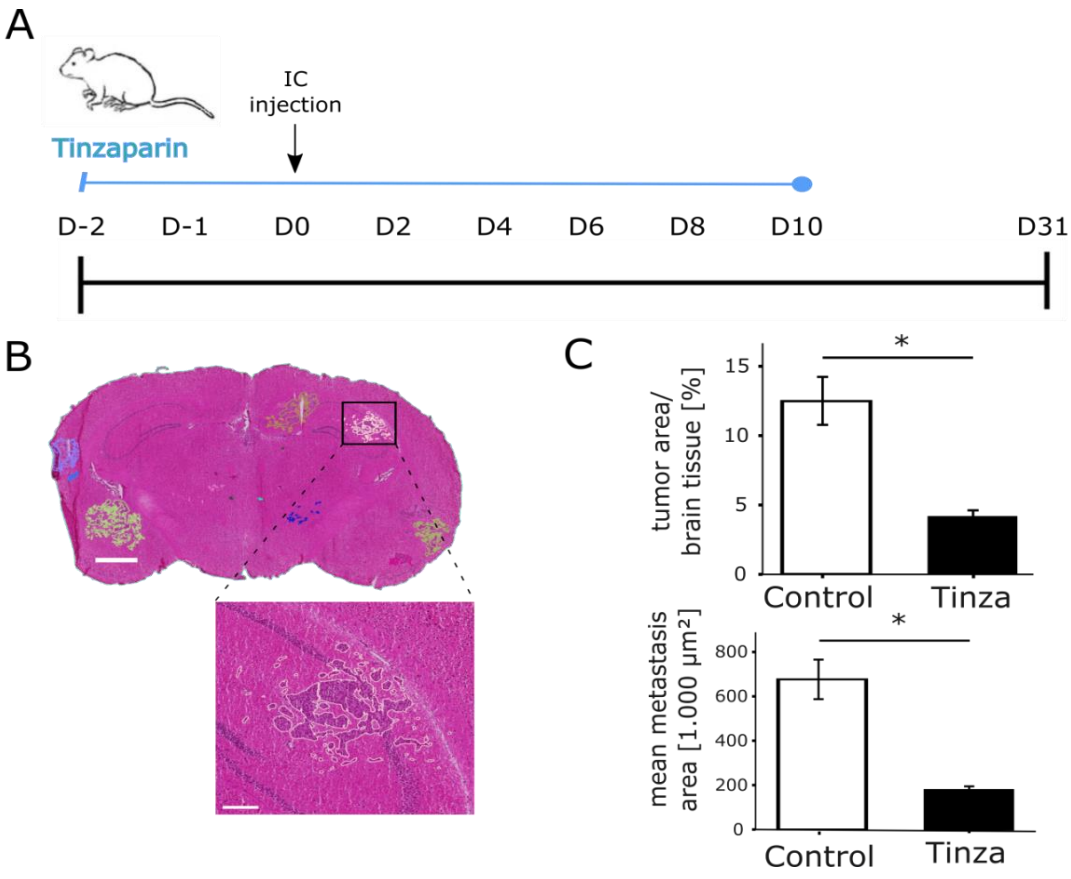

Figure 33. Anticoagulation with Tinzaparin reduces platelet activation and attenuates brain metastasis formation. A. To assess the effect of Tinzaparin on the formation of brain metastasis, an intracardiac injection (i.c.) of melanoma cells was implemented: Tinzaparin (0.6 U/kg daily) was administrated 2 days prior to heart injection of melanoma cells (A2058) and continued with daily application until day 10 after the injection. **B.** H&E staining was performed to quantify the tumor load at day 31. Magnifications show melanoma brain metastases and the outline used for area calculations. **C.** mean metastasis area and tumor area per brain tissue was quantified in Tinzaparin-treated (Tinza) and non-treated (control) mice (n= at least 3 animals per group); *, $P < 0.05$ (Student's t-test). Data are presented as mean ± SD. Scale bars: 1mm (overview); 200µm (magnification).

In summary, our *in vivo* findings suggest that the formation of platelet-derived luminal VWF strings play an important contribution in platelet aggregation and thrombus generation in the context of brain metastasis. Importantly, blocking platelet activation and α-granule-VWF secretion by the LMWH Tinzaparin reduces the thrombus formation and decreases the metastatic load in the brain.

5. Discussion

This study intends to understand the role of von Willebrand factor (VWF) in tumor progression and brain metastasis-associated thrombosis. In summary, our results reveal: (I) Brain microvascular endothelial cells (ECs) show a low expression of VWF and a restricted formation of luminal VWF fibers. (II) Immunofluorescence analyses indicate that platelet activation and subsequent secretion of α-granule-stored VWF accounts for the luminal VWF fibers observed in the brains of ret transgenic mice, which spontaneously develop melanoma with brain metastasis. (III) Platelet-derived VWF mediates the formation of thrombocyte aggregates generating a local increase of VEGF-A which mediates the disruption of the brain endothelium and promotes the transmigration of tumor cells. (IV) The anticoagulant low molecular weight heparin (LMWH) Tinzaparin inhibits platelet activation and subsequent aggregation, reducing the local increase of VEGF-A. (V) Anticoagulation with Tinzaparin reduces the formation of intravascular VWF-platelet aggregates in the brains of ret transgenic mice. (VI) Treatment with the anticoagulant LMWH Tinzaparin attenuates the metastatic load in the brain upon intracardial injection of melanoma cells.

5.1. Von Willebrand factor in cancer and thrombosis

As previously mentioned, thromboembolic events, principally venous thromboembolism (VTE) are frequent complications in malignant melanoma patients (Sparsa, et al. 2011). Particularly, the incidence of VTE increases in patients suffering from melanoma brain metastasis (Alvarado et al. 2012). Given its main role in blood hemostasis and coagulation, it has been suggested that VWF may play a relevant contribution to cancer-associated thrombogenicity (Pépin et al. 2016). Indeed, multiple types of cancer characterized by an high risk of VTE, such as breast cancer, pancreatic cancer, gastrointestinal cancers, ovarian carcinoma or bladder carcinoma are also associated with elevated levels of plasmatic VWF, suggesting the contribution of VWF in the thrombotic complications (Franchini et al. 2013; Röhsig et

al. 2001). Besides, it has been suggested that the prothrombotic activity observed in cancer patients may increase the risk of metastasis (O'Sullivan et al. 2018). Consistent with this, elevated levels of plasmatic VWF have been correlated with the presence of metastases in different types of cancers such as gastric cancer, metastatic colorectal carcinoma or metastatic larynx cancer (Paczuski et al. 1999;. Wang et al. 2005; Yang et al. 2018). These data highlight the potential involvement of VWF in tumor progression.

Despite the increasing number of clinical evidence showing the contribution of VWF in cancer progression, the underlying mechanisms of how VWF is involved in metastasis are still not clear. To address this question, different experimental animal models have been implemented to elucidate the role of VWF in tumor progression. On the one hand, it has been described that VWF regulates tumor vascularization, since VWF controls ECs proliferation by downregulation of angiopoietin 2 (Ang-2) (Yuan et al. 2016). Indeed, isolated ECs from patients with von Willebrand disease type 3 (entailed a complete lack of VWF expression) show an enhanced expression and release of angiopoietin 2 (Ang-2) (Starke et al. 2013). Moreover, VWF also promotes VEGFR-2-αvβ3 integrin interaction, which reduces the affinity of VEGF-R2 for its ligands (Randi and Laffan 2017a). Consequently, the genetic depletion of VWF in mice leads to an enhanced tumor vascularization (Goertz, et al. 2016; Randi and Laffan 2017b). Taken together, these findings suggest that VWF might play an anti-tumor role decreasing tumor angiogenesis. In line with this, in 2006 Terraube and colleagues showed that VWF-deficient animals exhibited an increased pulmonary metastasis compared to wild type (Wt) mice (Terraube et al. 2006) a process related to increased vascular permeability (Wolf et al. 2012). Consistent with this, a recent study from our group showed a similar increased in the number of lung metastatic foci in VWF-deficient mice (Goertz, et al. 2016). Interestingly, in the same study a disintegrin and metalloproteinase with a thrombospondin type 1 motif, member 13 (ADAMTS13)-deficient mouse, characterized by prolonged lifetime of luminal VWF fibers showed an enhanced lung metastasis compared to VWF-deficient mice. Similarly, in other studies the specific depletion of VWF with antibodies reduced the metastasis in different experimental mouse models (Karpatkin et al. 1988; O'Sullivan et al. 2018) supporting the prometastatic role of VWF in tumor progression.

These contrasting data could be explained by the fact that VWF plays a critical role in the formation of Weibel-Palade bodies (WPBs) (Peyvandi, Garagiola, and Baronciani 2011). Indeed, the absence of VWF is associated with the complete lack of WPBs (de Wit and van Mourik 2001). Consequently, VWF deficient mice suffer a dysregulation of WPB constituents, such as P-selectin, Ang-2 and interleukin 8 which regulate the integrity of the vasculature (Starke et al., 2011). This alters the physiology of the endothelium and increases its permeability (Melgar-Lesmes et al. 2009) and might contribute to the enhanced metastasis observed in VWF-deficient mice (Suidan et al. 2013). Therefore, the absence of VWF should not be considered the main responsible for the enhanced metastasis observed in VWF-deficient mice. Indeed, *in vitro* studies have shown that melanoma cells induce a profound secretion of endothelial WPBs containing VWF, which results in the formation of luminal VWF strings (Desch et al. 2012; Kerk et al. 2010). Moreover, it was shown that those strings mediate the adhesion of thrombocytes (Huck et al. 2014a). *In vivo* studies have also revealed that the tumor microenvironment induces the activation of ECs, reflected by the formation of intraluminal VWF networks and the formation of platelet aggregates and subsequent vessel occlusion (Bauer, et al. 2015). Importantly, the activation of ECs is also promoted in distal organs, where the formation of luminal VWF networks is correlated with enhanced metastasis suggesting the contribution of VWF in tumor cell extravasation (Goertz, et al. 2016). Indeed, it has been demonstrated that the formation of VWF-thrombocyte aggregates increases the vascular permeability and facilitates extravasation of leukocytes (Petri et al. 2010).

These findings support a model wherein VWF might promote tumor cell extravasation and thrombus formation through the activation of ECs and the generation of luminal VWF fibers. Luminal VWF networks mediate platelet aggregation and the binding of tumor cells to the vessel wall. The formation of a thrombus increases the permeability of the vessel wall and favors the extravasation of metastatic cells (**Figure 34**).

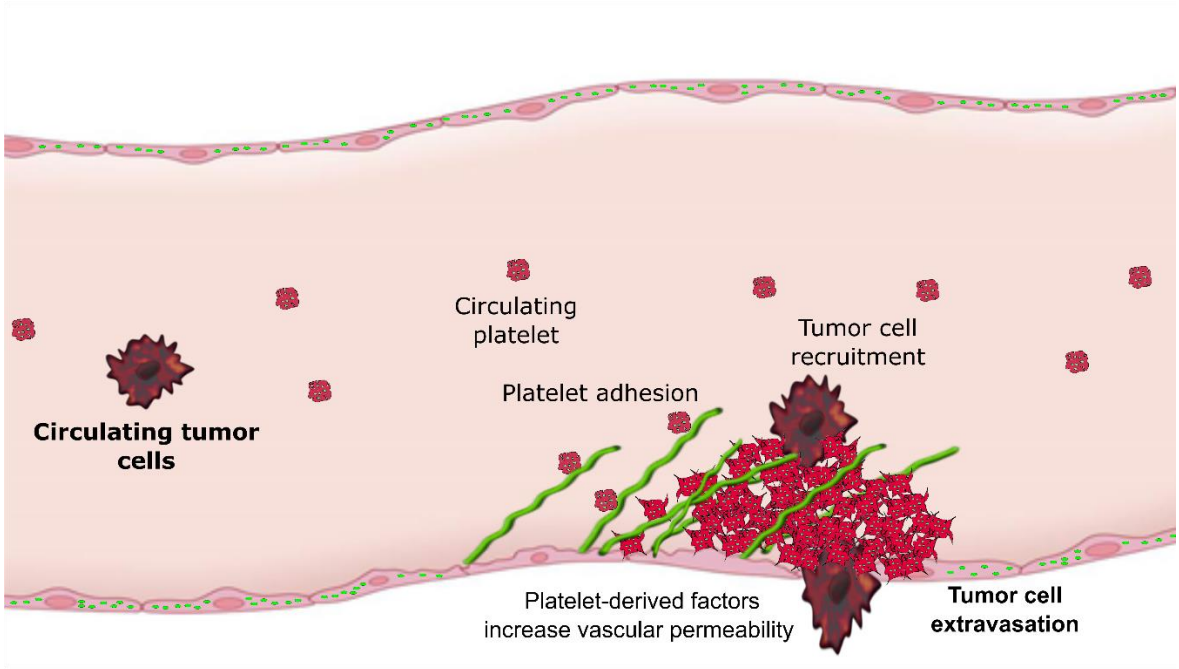

Figure 34. Contribution of VWF fibers to thrombosis and cancer metastasis. Tumor cells promote the activation of ECs at distant organs. The subsequent secretion and activation of VWF leads to the formation of luminal VWF fibers, which in turn mediates the recruitment of platelets and the formation of thrombocyte aggregates. Platelet-VWF aggregates promote the arrest of circulating tumor cells. The secretion of platelet derived factors increases vascular permeability and facilitates tumor cell extravasation.

5.2 Role of von Willebrand factor in pathologies of the central nervous system

Despite patients with brain tumor exhibit one of the highest incidence of VTE (Ay et al. 2010; Pabinger, Thaler, and Ay 2013), the contribution of VWF in intracranial hypercoagulation and brain metastasis is still unclear.

In 2008 Noubade and colleagues described the impact of VWF on Pertussis toxin (PTX)-mediated encephalomyelitis. They observed that the disruption of the blood-brain barrier (BBB) upon PTX insults was more severe in VWF-deficient mice than in Wt mice, suggesting a protective role of VWF in the maintenance of BBB integrity (Noubade et al. 2008). However, many studies report the opposite effect of VWF in diverse cerebral pathologies. For instance, it was described that the absence of VWF decreases the flexibility and the permeability of the BBB in experimental mouse models of hypoxia/reoxygenation and pilocarpine-induced status epilepticus (Suidan et al. 2013b). In line with this, the absence of VWF in transgenic mice was shown to decrease the infarct volume and reduce the concentration of inflammatory mediators after ischemic insults (Zhu et al. 2016a). Consequently, the restoration of VWF expression, by hydrodynamic infusion of a plasmid encoding for VWF recovers the susceptibility for strokes in VWF-deficient mice, increasing the infarct volume to comparable levels observed in Wt mice (Kleinschnitz et al. 2009). Similar results were obtained in a study where the degradation of luminal VWF was enhanced by the infusion of recombinant ADAMTS13, decreasing the volume of the infarct in an experimental stroke model (Canault et al. 2009). Strikingly, Fujioka and coworkers reported the prothrombotic potential of VWF in the brain vasculature showing the increased susceptibility of ADAMTS13-deficient mice to suffer thrombotic episodes in a mouse model of transient cerebral ischemia (Fujioka et al. 2010).

Given that most of the recent data sustain a model where VWF comprises the integrity of the BBB and contributes in the occlusion of brain microvessels, it is tempting to think that VWF might play a prometastatic role in the brain, mediating the formation of thrombi within the brain vasculature which increases the vascular permeability and facilitating the arrest of circulating tumor cells (CTCs).

5.3 Distinct expression of von Willebrand factor in different vascular beds

The expression of VWF is considered a major biomarker for ECs (Goncharov et al. 2017). However, ECs represent a heterogeneous population, whose biological properties differ not only between distinct tissues but also within the different types of vessels in the same organ (Cines et al. 1998). Therefore, is tempting to speculate that heterogeneity of the distinct vascular beds may modulate the expression and functionality of VWF.

Only a few studies have outlined the differences in the expression and distribution of VWF between the distinct vascular beds. In 1998, Yamamoto and colleagues performed a systemic analysis of VWF mRNA and antigen expression along the different vasculatures of the mouse: they found significant differences in VWF levels between ECs from different tissues and also between venous and arterial ECs (Yamamoto et al. 1998). This finding was supported by another study showing that VWF distribution is heterogeneous in the murine vasculature. Interestingly they described the correlation between the individual size of the vessels and the expression of VWF (Müller et al. 2002b). This particular distribution of endothelial VWF has been also confirmed in distinct human tissues showing a heterogeneous distribution of VWF within individual vessels and even in different sections of the same organ (Pusztaszeri, Seelentag, and Bosman 2006).

In line with this, our results showed notables differences in the abundance and distribution of VWF between macrovascular human umbilical vein ECs (HUVECs) and human brain microvascular ECs (HBMECs). We observed that the number of HBMECs storing intracellular VWF was significantly lower than in HUVECs (**Figure 12 A-C**). Additionally, the number of Weibel-Palade bodies (WPBs) storing VWF per cell was also significantly reduced in HBMECs compared to HUVECs (**Figure 12 D**). *In vivo a*nalyses of VWF expression in the brain vasculature of wild type (Wt) mouse brains also confirmed a segregated distribution of VWF in brain vessels: VWF was expressed predominantly in vessels with large diameters (≥ 50 µm), while in smaller capillaries (≤ 10 µm) the presence of VWF was only marginal (**Figure 13 and Table**

2). This pattern of VWF distribution suggests the local specialization of brain ECs to perform distinct functions within the brain vasculature. Consistent with this, it has been described that the low expression of VWF in small capillaries is associated with sites of regulated transport processes, while bigger vessels with abundant VWF are related to inflammation and cell extravasation (Macdonald, Murugesan, and Pachter 2010).

Based on these findings we wondered if the particular expression of VWF in the brain vasculature might affect the tumor-induced procoagulant activity of brain microvascular ECs.

5.3.1 Distinct molecular mechanisms in brain endothelial cell activation.

The interaction between tumor cells and the endothelium is an essential prerequisite in the pathogenesis of tumor metastasis. Earlier studies from our group demonstrated that tumor cell-mediated thrombin generation and the secretion of VEGF-A induce the activation of ECs and the exocytosis of WPB containing VWF (Desch et al. 2012; Kerk et al. 2010). Own results show that thrombin-, as well as VEGF-A- and Ret supernatant induce an acute activation of macrovascular human umbilical vein ECs (HUVECs), reflected by increased levels of secreted VWF (**Figure 14**; HUVECs) and the formation of luminal VWF strings on the luminal surface of HUVEC monolayers (**Figure 16**; HUVECs). In strong agreement with other authors reporting the procoagulant role of thrombin and VEGF-A in cancer spreading (Borensztajn et al. 2009; Mahecha and Wang 2017), here it is shown the contribution of these two molecules in tumor-associated hypercoagulability by turning the endothelium into a proinflammatory and procoagulatory surface.

However, the impact of thrombin and VEGF-A on the activation of brain microvascular ECs is notably distinct in comparison to macrovascular ECs: on the one hand, thrombin fails to activate HBMECs (**Figure 14**) and, thus, luminal VWF are barely present after incubation with thrombin (**Figure 16**). This fact might be explained by the limited expression of thrombin receptor protease-activated receptor-1 (PAR-1) in HBMEC compared to HUVECs (**Figure 15**). Interestingly, it is known that the central nervous system (CNS) exhibits a special procoagulant environment

which is defined by an enhanced expression of tissue factor (TF), prothrombin (Dihanich et al. 1991; Mackman et al. 1993) and a low expression of tissue factor pathway inhibitor (TFPI) (Bajaj et al. 1999), together protect the brain against bleedings (Mark 2013). However, an excessive procoagulant activity may enhance the risk of suffering from diffuse microvascular thrombotic complications upon pathophysiological conditions. Therefore, we purpose that the restricted expression of PAR-1 might act as a protective mechanism at the microvascular level against an enhanced activation of brain microvascular ECs. Conversely, we also observed that VEGF-A induces a significant increase of secreted VWF in brain microvascular ECs, suggesting the importance of VEGF-A/VEGFR-2 axis in the activation of brain microvascular ECs (**Figure 14**; HBMECs). This observation is supported by our mRNA analyses showing an upregulation of VEGF-R2 in HBMECs compared to HUVECs (**Figure 15**). This finding indicates the relevance of VEGF-A, rather than thrombin in the crosstalk between tumor cells and the brain vasculature.

Taken together these results reflect the distinct molecular mechanisms regulating the activation of distinct vascular beds. In addition, here is also shown that the low amount of VWF expressed in microvascular brain ECs combined with the restricted secretion of VWF limits the generation of luminal VWF strings *in vitro*, suggesting that brain vasculature regulates the VWF expression to reduce the risk of thrombotic occlusion of brain vessels and support the regular blood flow.

5.4 The formation of luminal von Willebrand factor fibers is associated with melanoma brain metastases

In the *in vivo* situation the micromilieu within a melanoma tumor promotes the activation of ECs, the consequent formation of luminal ultra-large VWF fibers (ULVWF) mediate the aggregation of thrombocytes leading to the thrombotic occlusion of tumor microvessels (Bauer, et al. 2015). The formation of ULVWF fibers is also detected in organs distal to the primary tumors mediating the formation of thrombi, which suggests the role of VWF in the thrombosis related to cancer (Goertz, et al. 2016). Nevertheless, the cerebro-specific regulation of VWF described before raises the question of whether VWF also participates in the hypercoagulability associated with melanoma cerebral metastasis.

Our own results reveal that patients suffering from brain metastasis exhibit elevated levels of plasmatic VWF (**Figure 18 A**) and they are associated with the formation of intraluminal VWF networks mediating the thrombotic occlusion of cerebral vessels (**Figure 18 C and D**). In strong agreement, immunofluorescence analyses of brains from *ret* transgenic mice with cerebral metastasis confirm the formation of luminal VWF fibers. Importantly, intravascular VWF networks are also detected in *ret* brains without visible metastasis, suggesting that the generation of VWF fibers may indicate an early stage of cerebral metastasis (**Figure 21**). This is in line with the growing body of evidence pointing out the link between hypercoagulability and tumor progression (Caine et al. 2002; Falanga, Marchetti, and Vignoli 2013). Indeed, this finding might provide a possible mechanism of how hemostatic factors, such as VWF and thrombocytes serve as a bridge between the pathological hypercoagulation associated with cancer diseases and metastasis. Indeed, it has been reported that VWF fiber-mediated thrombocyte accumulation contributes to the creation of a microenvironment promoting the survival and proliferation of tumor cells (Gay and Felding-Habermann 2011).

5.4.1 Platelet-derived von Willebrand factor contributes to the formation of luminal fibers in the brain vasculature

Considering our previous results showing a heterogeneous expression of VWF in the brain vasculature, the restricted activation and the limited secretion of VWF in brain ECs (**section 4.1**), one might expect that pathophysiological conditions in the brain should not be associated with a strong formation of intraluminal VWF networks and platelet recruitment. By contrast, as described above, a strong formation of intraluminal VWF networks was significantly enhanced in the context of brain metastasis (**section 4.2**).

Therefore, we sought to determine the source of those VWF strings. Our data show that similarly to primary tumor vessels, intratumoral vessels from metastatic tissue in *ret* brains exhibit luminal VWF networks associated with a decrease of VWF stored in the vessel wall. However, the formation of intraluminal VWF fibers in the peripheral tissue surrounding the metastases, as well as in vessels from *ret* brains without visible tumors does not correlate with a decrease of endothelial VWF (**Figure 22**). These data seem to indicate that VWF fibers within the cerebral vessels are not derived from the brain ECs, but rather reflect plasmatic VWF multimers or platelet-secreted VWF strings. Indeed, *ex vivo* perfusion assays with blood from patients suffering type I von Willebrand disease (VWD) with platelets expressing VWF demonstrated the importance of platelet-derived VWF in thrombus formation (Fressinaud et al. 1994). In line with this, Kanaji and coworkers demonstrated that in the absence of endothelial VWF thrombocyte-derived VWF partially restores blood hemostasis in a chimeric mouse expressing VWF only in platelets (Kanaji et al. 2012).

Platelets store VWF in α-granules (Wagner et al. 1991). The secretion of α-granules is induced upon platelet activation (Lenting et al. 2018), a process regulated by the interaction between platelet surface receptors and their agonists (Yun et al. 2016). The heterodimeric transmembrane GpIIb/IIIa (αIIbβ3) integrin is the most abundant integrin receptor in the platelet surface and mediates the interaction between fibrin(ogen) and platelets (Fuchs, Bhandari, and Wagner 2011). Under resting

conditions, GpIIb/IIIa exhibits a low affinity for its binding partner, however, platelet activation induces a conformational change in GpIIb/IIIa that increases its affinity for fibrin(ogen) (Nieswandt, Varga-szabo, and Elvers 2009). In particular, it has been observed that the interaction between platelets and fibrin(ogen) is enhanced in the context of metastasis and it has been shown that platelet-fibrin(ogen) aggregates protect tumor cells from immune surveillance (Palumbo et al. 2005). Our analyses demonstrate a strong interaction between platelets and fibrinogen in *ret* brains in comparison to healthy wild type mouse brains (**Figure 23**). Interestingly, the association between platelets and fibrinogen is already increased in metastasis-free *ret* brains, suggesting that the activation of platelets is enhanced in the premetastatic context. Interestingly, the activation of GpIIb/IIIa in platelets has been also related to the exocytosis of α-granules and the formation of platelet-derived VWF strings (Lonsdorf et al. 2012). To confirm that platelet activation is promoted in brain metastasis, immunofluorescence analyses were performed. The results show how activated platelets, identified by the characteristic emission of pseudopods are identified in close contact with intraluminal VWF fibers, meanwhile, the endothelial-derived VWF remained stored in the vessel wall (**Figure 24 A-D**). This is in strong agreement with the data reported by Verhenne and colleagues describing that whereas platelet-derived VWF is not essential for the normal hemostasis, it plays a relevant role in thrombo-inflammatory complications in the brain (Verhenne et al. 2015).

In addition, it has been reported that specific N-linked glycosylation in thrombocyte-derived VWF confers resistance against the enzymatic degradation by ADAMTS13 (McGrath et al. 2010). This could explain why we observe VWF networks in the brain vessels of patients with brain metastases despite the regular activity of ADAMTS13 found in the plasma of the same patients (**section 4.2.1**). This is consistent with previous clinical studies showing unaffected ADAMTS13 activity in patients bearing brain metastasis (Böhm et al. 2003). Furthermore, platelet-derived VWF is characterized by a strong affinity for activated platelet-GpIIb/IIIa, while endothelial VWF binds to resting platelet-GPIb more efficiently (Williams et al. 1994). This indicates a distinct contribution of endothelial-derived and platelet-derived VWF in the initial stages of the platelet adhesion and thrombosis, respectively. Consistent with this, we observed that the aggregation of thrombocytes is strongly promoted in *ret*

brains, despite the endothelial VWF remains stored in the vessel wall (**Figure 24 E**). These results outline the contribution of platelet-secreted VWF, rather than EC-derived VWF in the prothrombotic activity associated with brain metastasis.

Ex vivo perfusion assays with human thrombocytes support these findings. Our assessments demonstrate that the initial adhesion of platelets to the vasculature and the formation of platelet aggregates are two separated processes, subordinated to distinct regulation: Firstly, EC activation and the formation of luminal VWF strings mediates the recruitment of platelets. Secondly, thrombocyte activation and VWF secretion promote the aggregation of further activated platelets and the formation of a thrombus (**Figure 26 A and B**). As expected, due to the greater expression of VWF in macrovascular ECs, the adhesion of thrombocytes is increased in comparison to microvascular brain ECs. This in line with other studies showing that the abundance of endothelial-VWF in cultured ECs affects the size and adhesive capacity of VWF strings (Ferraro et al. 2016). In spite of this, our analysis shows that the augment of thrombocyte coverage upon platelet aggregation is proportional in both cell types (**Figure 26 C**), suggesting the exclusive contribution of platelet-secreted VWF in the aggregation of platelets. To confirm this, we tested the capacity of platelets lacking VWF ($VWF^{-/-}$) to form microthrombi at the microvasculature of the brain. Our perfusion experiments show that that $VWF^{-/-}$ platelets generate significant smaller platelet plugs than Wt platelets (**Figure 27 A-C**). Indeed, comparable results have been observed in a study reporting that the aggregation of platelets is inhibited when platelets lack α-granules (platelet decoys) (Papa et al. 2019). Similarly, our aggregation assays reveal that the lack of VWF in platelets significantly slows down the aggregation of platelets compared to Wt platelets (**Figure 27 D**). These results indicate the relevant contribution of VWF stored in α-granules in thrombocyte bundling.

Based on these results we postulated that activated thrombocytes promote the formation of microthrombi which compromise the integrity of the BBB and facilitate the cerebral: The inflammatory conditions associated to malignant diseases promotes the activation of brain ECs and the formation of luminal VWF fibers which mediate the recruitment of thrombocytes (1). The activation of thrombocytes and the subsequent secretion of α-granule-stored VWF (2) mediates the aggregation of

platelets (3). Thrombocyte aggregates generate a local increase of permeability factors (4) which increase the permeability of the brain vasculature and favors tumor cell extravasation (5) (**Figure 35**).

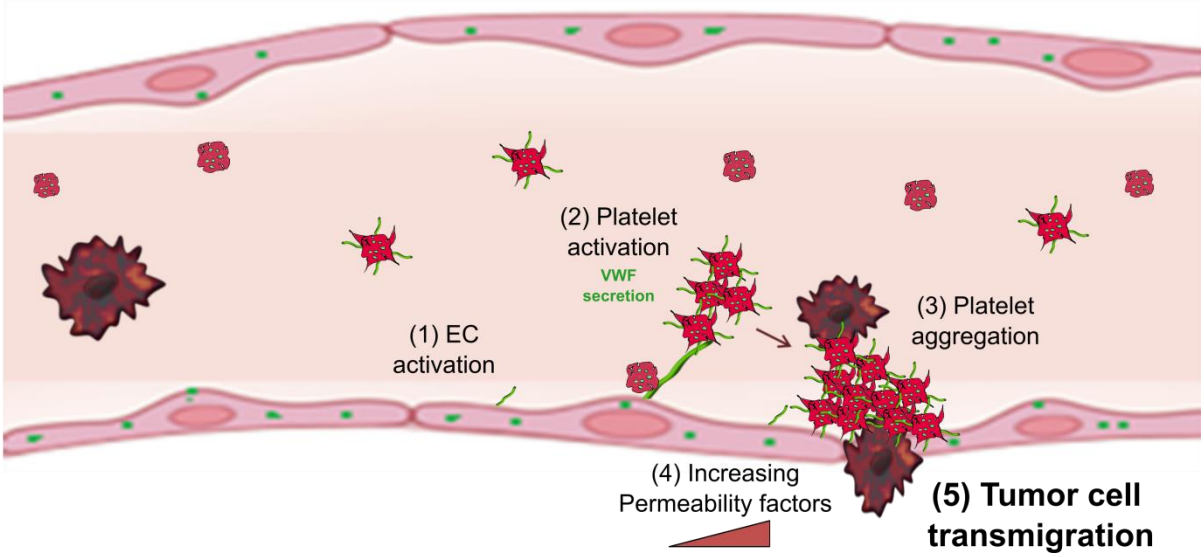

Figure 35. Contribution of activated thrombocytes in cerebral metastastasis: Procoagulant environment associated with malignant diseases promotes the initial adhesion of thrombocytes on brain vessels (1-2). Activation of platelets and the subsequent secretion of VWF induce the aggregation of further platelets (3). The formation of a platelet-rich microthrombus leads to a local increase of permeability factors (4) which disrupt the vascular integrity and promote tumor cell extravasation (5).

5.5 Systemic anticoagulation attenuates the metastatic load in the brain

Our results highlight the impact of VEGF-A on the activation of primary brain microvascular ECs (**section 4.1.3**). Interestingly, thrombocyte α-granules are an important source of bioactive VEGF-A which is known to modulate the endothelial integrity (Salgado et al. 2001; Schumacher et al. 2013).

Indeed, many studies have reported the contribution of VEGF-A in such diverse cerebral pathologies as ischemic stroke or Alzheimer (Greenberg and Jin 2013; Harris et al. 2017). In the context of cerebral metastasis, it has been reported that the expression of VEGF-A by breast cancer cells is associated with an enhanced risk of suffering from metastasis in the brain (Lee et al. 2004; Yang, Wang, and Ma 2018). Own findings demonstrate that VEGF-A secreted by activated platelets comprises the integrity of brain EC monolayer and promotes the extravasation of tumor cells (**Figure 29**). This is in line with a previous study showing that platelet activation and α-granule secretion promote vascular disruption and tumor cell transmigration (Schumacher et al. 2013). Others authors have confirmed *in vivo* the contribution of VEGF-A in cerebral malignancy by showing that antiangiogenic therapy with VEGFR-2 inhibitors resulted in less metastasis and tumor growth retardation due to an impaired development of tumor vasculature (Bohn et al. 2017; Boult et al. 2017; Farzaneh Behelgardi et al. 2018). The angiogenic process regulated by VEGF-A entails a series of morphological and intracellular changes which transiently disrupt the integrity of the endothelial barrier (Song et al. 2014) this situation facilitates the cell extravasation and promotes the metastatic invasion of the brain (Suzuki, Nagai, and Umemura 2016; Zhang et al. 2000).

Therefore, a VEGF-A-targeted therapy sounds like a promising approach to reduce the contribution of activated platelets in brain metastasis. In line with this, it was shown that the depletion of VEGF-A with specific antibodies reduces the growth of tumor vasculature and induces the dormancy of intracranial metastasis (Kienast et al. 2010). However, an anti-VEGF-A treatment implies side effects as bleedings or thrombotic events due to the physiological role of VEGF in vessel maturation (Nalluri et al. 2008b; Y. Yang et al. 2013). Therefore, is important to find alternative

approaches to mitigate the activity of VEGF-A without entailing any risk for bleedings or thrombotic complications for the patients.

5.5.1 The low molecular weight heparin Tinzaparin prevents tumor cell transmigration by blocking platelet-secreted VEGF-A

Low molecular weight heparins (LMWHs) are a class of anticoagulant medication, which are widely implemented in the treatment of thrombotic complications: blood clots and VTEs (including deep vein thrombosis and pulmonary embolism) and in the treatment of myocardial infarctions (V. V Kakkar et al.2000; Solari and Varacallo 2019). Importantly, many studies have shown the benefits of LMWHs preventing thrombotic complications with minimal impact on bleedings (Quinlan, McQuillan, and Eikelboom 2004).

LMWHS are generated by the depolymerization of full-length unfractionated heparins (UFHs) chains, which are a large variety of biomolecules with size ranges from 3 to 30 kDa (Johnson and Mulloy 1976). The anticoagulant functions of heparins are known for at least four decades and are based on the affinity of their pentasaccharide molecular structure for Antithrombin III (AT III), an important inhibitor of FXa and thrombin (Danielsson et al. 1986; Rosenberg and Damus 1973). Indeed, the interaction between AT III and the pentasaccharide structure of heparins enhances the activity of AT III 1000-fold (Olson et al. 1992). The benefits of using LMWHs over UFH are based on its reduced cost-effective compared to UFH (Hatam et al. 2017), their greater bioavailability by subcutaneous injection (Weitz 1997) and their longer half-life (Bradbrook et al. 1987). Moreover, it has been shown that LMWHs exhibit additional functions due to the variability of the structures obtained after UFH fractionation (Rutering et al. 2016). Some of these additional properties include the induction of TFPI release from endothelial cells (Ma et al. 2007) or the inhibition of angiogenesis (Norrby 2006; Villares, Zigler, and Bar-Eli 2011).

In the context of cancer disease, LMWHs are often used to ameliorate the hypercoagulable state of the patients (Kakkar 2009). Some clinical studies have shown the benefits of anticoagulant therapy with LMWHs improving the prognosis

and the survival of cancer patients (Kuderer, Ortel, and Francis 2009). Nowadays many anti-cancer properties have been attributed to LMWHs, such as the inhibition of angiogenesis associated to tumor progression (Norrby 2006) or the impairment of the interaction between tumor cells and P-selectin reducing significantly tumor colonization of new tissue (Läubli, Varki, and Borsig 2016). In line with this, our group has identified an additional antimetastatic property of the LMWH Tinzaparin blocking tumor-secreted VEGF-A (Bauer 2015).

Based on this, we used Tinzaparin to understand the underlying mechanism of platelet activation and the impact of platelet-secreted VEGF-A on this process, the thrombocyte aggregation in the absence of coagulation factors was tested in the presence of Tinzaparin or Fondaparinux. Fondaparinux is a synthetic pentasaccharide that inhibits factor Xa-mediated thrombin generation, but unlike Tinzaparin exhibits low affinity for VEGF-A (Bauer, et al. 2015; Buyue, Misenheimer, and Sheehan 2012). The results show that Fondaparinux did not show any effect on platelet aggregation (**Figure 28 A;** Fonda). As expected, the absence of coagulation factors in our *in vitro* settings explains the lack of effect of Fondaparinux. In contrast, platelet aggregation was completely abrogated by Tinzaprin (**Figure 28 A;** Tinza). Since the plasmatic coagulation factors are absence, it is reasonable to think that platelets mediate their activation in an autocrine fashion through the secretion of α-granule constituents. It is known that platelets expressed VEGFR-2 on their surface (Yang, Wang, and Ma 2018) and our results show that thrombocyte activation leads to the secretion of VEGF-A (**Figure 28 B**). Therefore, we speculate that secretion of VEGF-A by the initial activation of thrombocytes fosters the activation of further platelets. Nevertheless, in the presence of Tinzaparin, platelet-derived VEGF-A is rapidly blocked due to the strong affinity exhibited by these two molecules (Bauer, et al. 2015) and, thus, further platelet activation is inhibited. In line with this, a recent publication showed the inhibitory effect of Tinzaparin on platelet activation by coagulation factors-independent pathways (Gockel et al. 2018).

As has been already mentioned, platelet-derived releasates mediate the disruption of a brain EC barrier which increases the number of transmigrated tumor cells (**section 4.3.3**). The contribution of platelets mediating the vascular permeability is well established (Leblanc and Peyruchaud 2016a; Li 2016). Platelets store a big plethora

of permeability mediators, such as matrix metalloproteinases (MMPs), adenosine triphosphate (ATP) and diverse growth factors like VEGF or interleukins (Gay and Felding-Habermann 2011). Here, using the anti-VEGF-A antibody Bevacizumab, we identify platelet-secreted VEGF-A as the main mediator of brain EC disruption and tumor cell extravasation. In the same extent, Tinzaparin reduces the permeability and tumor cell transmigration mediated by platelet releasates, evidencing the inhibitory effect of Tinzaparin on platelet-secreted VEGF-A (**Figure 29**).

These results highlight the relevance of platelet-derived VEGF-A mediating tumor cell transmigration through the BBB and suggest the benefits of a systemic anticoagulation therapy with Tinzaprin to prevent platelet contribution in cerebral metastasis.

5.5.2 Anticoagulant therapy with Tinzaparin reduces brain metastasis-associated thrombosis and attenuates brain metastasis

Anticoagulation with LMWHs is one of the most common first line treatment for the prevention of thrombotic complications in cancer patients (Kearon et al. 2016). During the last years, a great number of clinical studies have examined whether besides their anticoagulant function, LMWHs also exhibit anti-metastatic properties. However the results obtained are conflictive.

For instance, in a meta-analysis including more than 700 studies the impact of LMWHs on the overall survival of patients was examined and the results concluded that LMWHs do not influence the outcome of patients (Sanford et al. 2014). However, in this study the data were not treated consistently, cancer patients with different tumor types, in different stages and treated with different LMWHs were included in the meta-analysis. Thus, one cannot exclude the different properties of distinct LMWHs and their effect on distinct types of cancer (Läubli, Varki, and Borsig 2016). And this is in line with the distinct anti-tumorigenic effects obtained by the implementation of different clinical approved LMWHs. For example, Dalteparin (*CLOT* trial) and Tinzaarin (*CATCH* trial) demonstrated their benefits versus oral anticoagulants reducing the thrombotic events in cancer patients(Lee 2003; Lee et

al. 2015). However, regarding their anti-tumorigenic impact, on the hand, Dalteparin demonstrated only a moderate survival benefit in certain subpopulations of cancer patients (*FAMOUS* trial) (Kakkar et al. 2004). On the other, Tinzaparin shows contradictoy effects. The first clinical trial which revealed a significant survival benefit in tumor patients implemented Logiparin, which was later known as Tinzaparin (Hull et al. 1992). However, recently it was shown that Tinzaparin has no impact on the survival of patients with pulmonary metastasis (Meyer et al. 2018).

Therefore, these controversial results suggest that further investigation of the distinct properties of different LMWHs must be performed to elucidate the specific therapeutic limitations of each LMWH. Consistent with this, here it has been tested the distinct properties of different anticoagulants. As described, Fondaparinux has no direct effect on platelet activation compared to Tinzaparin. This is in line with recent findings from our group showing that Fondaparinux has a reduced impact on the inhibition of tumor angiogenesis compared Tinzaparin (Goertz, et al. 2016). Another example is the distinct effect of different LMWHs on VEGF-A activity. Our group reported that Tinzaparin exhibits a strong affinity for VEGF-A, blocking its activity (Bauer, et al. 2015). By contrast, it is known that the LMWH Dalteparin increases the activity of VEGF-A enhancing tumor angiogenesis *in vivo* (Norrby and Nordenhem 2010).

Furthermore, the treatment of thromboembolic complications in patients bearing brain metastases is especially challenging because of the high risk of suffering intracranial hemorrhages (Donato et al. 2015). During the last years, LMWHs have demonstrated their therapeutic potential improving the outcome of the patients without increasing the risk of intracranial bleedings (Alvarado et al. 2012; Lin, Green, and Shah 2018). However, as it was mention before the identification of effective anticoagulant treatments is crucial for a successful therapy. Thus, in this study we have examined the impact of Tinzaparin on the hypercoagulability associated with brain metastasis.

Our *in vivo* assays show that Tinzaparin therapy reduces platelet activation in the brain of *ret* transgenic mice (**Figure 30**). Consequently, platelet inhibition leads to a lower secretion of α-granule-derived VWF from activated platelets (**Figure 31**) and therefore the aggregation of platelets and the subsequent occlusion of brain vessels is reduced compared with *ret* mice treated with a saline solution (**Figure 32**). These

findings provide more evidence that demonstrate the pivotal role of platelet-derived VWF in the formation of microthrombi associated with brain metastasis and support the benefits of Tinzaprin inhibiting platelet-aggregation *in vivo*. To prove the impact of Tinzaparin treatment on the formation of brain metastases, mice daily treated with Tinzaparin or with a saline solution were intracardially injected with melanoma cells to induce the formation of intracerebral metastases. The formation of brain metastases was quantified at the end of the experiment revealing that the metastatic load in the brain was significantly reduced in Tinzaparin-treated mice (**Figure 33**). These results suggest that the activation of platelets and the subsequent formation of intracranial microthrombi promote the invasion and proliferation of metastatic cells in the brain, however, the implementation of an anticoagulant treatment with the LMWH Tinzaparin ameliorates the formation of platelet aggregates and attenuates the metastasis in the brain.

.

6. Conclusions

Based on previous studies showing the influence of platelets on transendothelial permeability (Fang et al. 2014; Schumacher et al. 2013), our results indicate that platelets contribute to the opening of the blood-brain barrier and promote tumor cell extravasation principally by the secretion of VEGF-A. Previous studies suggest that inhibition of VEGF-A with a specific antibody prevents angiogenic growth and intracranial metastasis (Kienast et al. 2010). Therefore, VEGF-A-targeted therapy sounds like a promising approach to interfere with the prometastatic activity of platelets, but entails the risk of compromising the hemostasis and promote thrombotic complications (Nalluri et al. 2008a; Y. Yang et al. 2013). An alternative approach to treat brain metastases could be to target the coagulation on the one hand and the secretion of platelet-derived VEGF-A on the other hand, with only one drug. For instance, with LMWH that attenuate the activation of platelets and thus the secretion of angiogenic proteins, such as VEGF-A (Battinelli et al. 2014). Here, we show that the LMWH Tinzaparin reduces platelet-mediated transmigration of melanoma cells, tumor-associated thrombotic vessel occlusion and the formation of intracranial macrometastases.

In summary, our data provide a new insight into the role of platelet-secreted VWF and increase our knowledge about the mechanisms underlying thrombotic complications associated with cerebral metastasis. Thus, cancer patients with high risk for suffering thrombotic complications and brain metastases may benefit from an anticoagulant treatment with LMWHs (**Figure 36**).

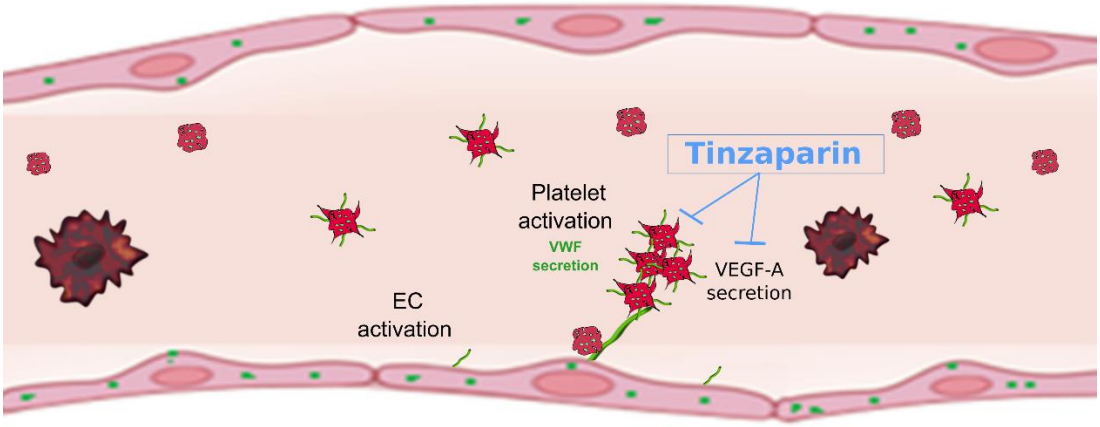

Figure 36. Tinzaparin-mediated inhibition of platelet activation attenuates brain metastasis: Thrombocyte activation and the subsequent secretion of VWF promotes the formation of platelet aggregates in the brain. Tinzaparin inhibits platelet activation and reduces the formation of platelet aggregates protecting the integrity of the BBB.

.

7. References

Abdol Razak, Norbaini et al. 2018. “Cancer-Associated Thrombosis: An Overview of Mechanisms, Risk Factors, and Treatment.” *Cancers* 10(10): 380. http://www.mdpi.com/2072-6694/10/10/380 (July 23, 2019).

Agosto-Arroyo, Emmanuel, Marilin Rosa, Alec Chau, and Laila Khazai. 2017. “Concurrent BRAF and PTEN Mutations in Melanoma of Unknown Origin Presenting as a Breast Mass.” *SAGE open medical case reports* 5: 2050313X17711064. http://www.ncbi.nlm.nih.gov/pubmed/28607685 (June 24, 2019).

Alvarado, Gladys et al. 2012. “Risk of Intracranial Hemorrhage with Anticoagulation Therapy in Melanoma Patients with Brain Metastases.” *Melanoma research* 22(4): 310–15. http://www.ncbi.nlm.nih.gov/pubmed/22584956 (October 21, 2016).

“American Cancer Society | Information and Resources about for Cancer: Breast, Colon, Lung, Prostate, Skin.” https://www.cancer.org/ (July 8, 2019).

Andrikopoulos, Petros et al. 2015. “Endothelial Angiogenesis and Barrier Function in Response to Thrombin Require Ca2+ Influx through the Na+/Ca2+ Exchanger.” *The Journal of biological chemistry* 290(30): 18412–28. http://www.ncbi.nlm.nih.gov/pubmed/25979335 (July 25, 2019).

Antoni, Sebastien et al. 2016. “An Assessment of GLOBOCAN Methods for Deriving National Estimates of Cancer Incidence.” *Bulletin of the World Health Organization* 94(3): 174–84. http://www.who.int/entity/bulletin/volumes/94/3/15-164384.pdf (June 17, 2019).

Arlo J. Miller and Martin C. Mihm, Jr. 2008. “Melanoma.” *English Studies* 60(4): 516–22.

Ay, Cihan et al. 2010. “Prediction of Venous Thromboembolism in Cancer Patients.” *Blood* 116(24): 5377–82. http://www.ncbi.nlm.nih.gov/pubmed/20829374 (July 16, 2019).

Bajaj, Madhu S., M. N. Kuppuswamy, A. N. Manepalli, and S. P. Bajaj. 1999. “Transcriptional Expression of Tissue Factor Pathway Inhibitor, Thrombomodulin and von Willebrand Factor in Normal Human Tissues.” *Thrombosis and Haemostasis*.

Bald, Tobias et al. 2014. “Ultraviolet-Radiation-Induced Inflammation Promotes Angiotropism and Metastasis in Melanoma.” *Nature*.

Battinelli, Elisabeth M. et al. 2014. “Anticoagulation Inhibits Tumor Cell–Mediated Release of Platelet Angiogenic Proteins and Diminishes Platelet Angiogenic Response.” *Blood* 123(1). http://www.bloodjournal.org/content/123/1/101?sso-checked=true (May 31, 2017).

Bauer, Alexander T., Jan Suckau, Kathrin Frank, Anna Desch, Lukas Goertz, Andreas H. Wagner, Markus Hecker, Tobias Goerge, Ludmila Umansky, Philipp Beckhove, Jochen Utikal, Christian Gorzelanny, Nancy Diaz-Valdes, et al. 2015. “Von Willebrand Factor Fibers Promote Cancer-Associated Platelet Aggregation in Malignant Melanoma of Mice and Humans.” *Blood* 125(20): 3153–63.

Bauer, Alexander T, Jan Suckau, Kathrin Frank, Anna Desch, Lukas Goertz, Andreas H Wagner, Markus Hecker, Tobias Goerge, Ludmila Umansky, Philipp Beckhove, Jochen Utikal, Christian Gorzelanny, Nancy Diaz-valdes, et al. 2015. “Von Willebrand Factor Fi Bers Promote Cancer-Associated Platelet Aggregation in Malignant Melanoma of Mice and Humans.” 125(20): 3153–64.

Belhocine, Tarik Z et al. 2006. “Role of Nuclear Medicine in the Management of Cutaneous Malignant Melanoma.” *Journal of nuclear medicine : official publication, Society of Nuclear Medicine*.

Bendas, Gerd, and Lubor Borsig. 2012. “Cancer Cell Adhesion and Metastasis: Selectins, Integrins, and the Inhibitory Potential of Heparins.” *International Journal of Cell Biology* 2012: 1–10. http://www.hindawi.com/journals/ijcb/2012/676731/ (August 15, 2019).

Betti, Roberto et al. 2016. “An Observational Study Regarding the Rate of Growth in Vertical and Radial Growth Phase Superficial Spreading Melanomas.” *Oncology letters* 12(3): 2099–2102. http://www.ncbi.nlm.nih.gov/pubmed/27602146 (July 23, 2019).

Blann, Andrew D. 2012. “Endothelial Cell Activation Markers in Cancer.” *Thrombosis Research* 129: S122–26. https://www.sciencedirect.com/science/article/pii/S0049384812700312 (July 9, 2019).

Blecharz, Kinga G., Ruben Colla, Veit Rohde, and Peter Vajkoczy. 2015. “Control of the Blood-Brain Barrier Function in Cancer Cell Metastasis.” *Biology of the Cell* 107(10): 342–71.

Bode, Michael, and Nigel Mackman. 2014. “Regulation of Tissue Factor Gene Expression in Monocytes and Endothelial Cells: Thromboxane A2 as a New Player.” *Vascular pharmacology* 62(2): 57–62. http://www.ncbi.nlm.nih.gov/pubmed/24858575 (August 18, 2019).

Böhm, Martina et al. 2003. “ADAMTS-13 Activity in Patients with Brain and Prostate Tumors Is Mildly Reduced, but Not Correlated to Stage of Malignancy and Metastasis.” *Thrombosis Research* 111(1–2): 33–37.

Bohn, Kaci A., Chris E. Adkins, Mohamed I. Nounou, and Paul R. Lockman. 2017. “Inhibition of VEGF and Angiopoietin-2 to Reduce Brain Metastases of Breast Cancer Burden.” *Frontiers in Pharmacology*.

7. References

Borensztajn, Keren et al. 2009. “A Mechanism for Thrombin-Dependent Lung Metastasis in Patients with Osteosarcoma.” *British Journal of Haematology* 145(4): 548–50. http://doi.wiley.com/10.1111/j.1365-2141.2009.07643.x (August 20, 2019).

Boult, Jessica K.R. et al. 2017. “Evaluation of the Response of Intracranial Xenografts to VEGF Signaling Inhibition Using Multiparametric MRI.” *Neoplasia (United States)*.

Bradbrook, ID et al. 1987. “ORG 10172: A Low Molecular Weight Heparinoid Anticoagulant with a Long Half-life in Man.” *British Journal of Clinical Pharmacology*.

Bradford, Porcia T. 2009. “Skin Cancer in Skin of Color.” *Dermatology nursing* 21(4): 170–77, 206; quiz 178. http://www.ncbi.nlm.nih.gov/pubmed/19691228 (July 31, 2019).

Brass, Skip. 2001. “Small Cells, Big Issues.” *Nature* 409(6817): 145–47. http://www.nature.com/articles/35051688 (July 10, 2019).

Brenner, Michaela, and Vincent J Hearing. 2008. “The Protective Role of Melanin against UV Damage in Human Skin.” *Photochemistry and photobiology* 84(3): 539–49. http://www.ncbi.nlm.nih.gov/pubmed/18435612 (July 23, 2019).

“Breslow Depth and Clark Level - Melanoma Research Alliance.” https://www.curemelanoma.org/about-melanoma/melanoma-staging/breslow-depth-and-clark-level/ (July 21, 2019).

Butenas, Saulius et al. 2005. “Tissue Factor Activity in Whole Blood.” *Blood* 105(7): 2764–70. http://www.ncbi.nlm.nih.gov/pubmed/15604222 (August 18, 2019).

Buyue, Y., T. M. Misenheimer, and J. P. Sheehan. 2012. “Low Molecular Weight Heparin Inhibits Plasma Thrombin Generation via Direct Targeting of Factor IXa: Contribution of the Serpin-Independent Mechanism.” *Journal of Thrombosis and Haemostasis*.

C., Kearon et al. 2016. “Antithrombotic Therapy for VTE Disease: CHEST Guideline and Expert Panel Report.” *Chest*.

Caine, Graham J, Paul S Stonelake, Gregory Y H Lip, and Sean T Kehoe. 2002. “The Hypercoagulable State of Malignancy: Pathogenesis and Current Debate.” *Neoplasia (New York, N.Y.)* 4(6): 465–73. http://www.ncbi.nlm.nih.gov/pubmed/12407439 (January 23, 2019).

Canault, M. et al. 2009. “Von Willebrand Factor-Cleaving Protease ADAMTS13 Reduces Ischemic Brain Injury in Experimental Stroke.” *Blood* 114(15): 3329–34.

Chaffer, C. L., and R. A. Weinberg. 2011. “A Perspective on Cancer Cell Metastasis.” *Science* 331(6024): 1559–64. http://www.sciencemag.org/cgi/doi/10.1126/science.1203543 (September 4, 2019).

Chaudhry, Raheel, and Hani M. Babiker. 2019. “Physiology, Coagulation Pathways.” https://www.ncbi.nlm.nih.gov/books/NBK482253/ (September 5, 2019).

Cines, D B et al. 1998. “Endothelial Cells in Physiology and in the Pathophysiology of Vascular Disorders.” *Blood*.

Clark, B. C. et al. 1984. “Clark et Al. and McNeil et Al. Respond.” *Physical Review Letters* 53(3): 302–302. https://link.aps.org/doi/10.1103/PhysRevLett.53.302 (July 8, 2019).

Cloutier, Nathalie et al. 2012. “Platelets Can Enhance Vascular Permeability Platelets Can Enhance Vascular Permeability.” 120(6): 1334–43.

Conway, Dwayne S.G. et al. 2003. “Prognostic Value of Plasma von Willebrand Factor and Soluble P-Selectin as Indices of Endothelial Damage and Platelet Activation in 994 Patients with Nonvalvular Atrial Fibrillation.” *Circulation*.

Coughlin, Shaun R. 2000. “Thrombin Signalling and Protease-Activated Receptors.” *Nature* 407(6801): 258–64. http://www.nature.com/doifinder/10.1038/35025229 (September 1, 2016).

Crawley, James T.B. et al. 2011. “Unraveling the Scissile Bond: How ADAMTS13 Recognizes and Cleaves von Willebrand Factor.” *Blood*.

Cudmore, Melissa J. et al. 2012. “The Role of Heterodimerization between VEGFR-1 and VEGFR-2 in the Regulation of Endothelial Cell Homeostasis.” *Nature Communications* 3(1): 972. http://www.nature.com/articles/ncomms1977 (April 1, 2019).

Cugno, Massimo, and Alberto Tedeschi. 2013. Autoantibodies: Third Edition *Coagulation Factor Autoantibodies*. Third Edit. Elsevier. http://dx.doi.org/10.1016/B978-0-444-56378-1.00059-9.

Damin, Daniel C et al. 2002. “Von Willebrand Factor in Colorectal Cancer.” *Int J Colorectal Dis* 17: 42–45. https://www.researchgate.net/profile/Daniel_Damin/publication/11354221_Von_Willebrand_factor_in_colorectal_cancer/links/54e760600cf2b199060c2574/Von-Willebrand-factor-in-colorectal-cancer.pdf (November 30, 2017).

Daneman, Richard, and Alexandre Prat. 2015. “The Blood-Brain Barrier.” *Cold Spring Harbor perspectives in biology* 7(1): a020412. http://www.ncbi.nlm.nih.gov/pubmed/25561720 (June 25, 2019).

Danielsson, A., E. Raub, U. Lindahl, and I. Bjork. 1986. “Role of Ternary Complexes, in Which Heparin Binds Both Antithrombin and Proteinase, in the Acceleration of the Reactions between Antithrombin and Thrombin or Factor Xa.” *Journal of Biological Chemistry*.

Darbousset, Roxane et al. 2012. “Tissue Factor-Positive Neutrophils Bind to Injured Endothelial Wall and Initiate Thrombus Formation.” *Blood* 120(10): 2133–43. http://www.ncbi.nlm.nih.gov/pubmed/22837532 (August 18, 2019).

Das, Suvendu et al. 2013. “Tumor Cell Entry into the Lymph Node Is Controlled by CCL1 Chemokine Expressed by Lymph Node Lymphatic Sinuses.” *The Journal of experimental medicine* 210(8): 1509–28. http://www.ncbi.nlm.nih.gov/pubmed/23878309 (June 25, 2019).

Davies, Michael A. et al. 2011. “Prognostic Factors for Survival in Melanoma Patients with Brain Metastases.” *Cancer* 117(8): 1687–96. http://doi.wiley.com/10.1002/cncr.25634 (January 24, 2017).

Davis, Faith G., Therese A. Dolecek, Bridget J. McCarthy, and John L. Villano. 2012. “Toward Determining the Lifetime Occurrence of Metastatic Brain Tumors Estimated from 2007 United States Cancer Incidence Data.” *Neuro-Oncology*.

Desch, Anna et al. 2012. “Highly Invasive Melanoma Cells Activate the Vascular Endothelium via an MMP-2/Integrin Avβ5-Induced Secretion of VEGF-A.” *American Journal of Pathology* 181(2): 693–705. http://dx.doi.org/10.1016/j.ajpath.2012.04.012.

Dihanich, Melitta et al. 1991. “Prothrombin MRNA Is Expressed by Cells of the Nervous System.” *Neuron*.

Domingues, Beatriz, José Manuel Lopes, Paula Soares, and Helena Pópulo. 2018. “Melanoma Treatment in Review.” *ImmunoTargets and therapy* 7: 35–49. http://www.ncbi.nlm.nih.gov/pubmed/29922629 (June 24, 2019).

Donato, Jessica et al. 2015. “Intracranial Hemorrhage in Patients with Brain Metastases Treated with Therapeutic Enoxaparin : A Matched Cohort Study.” 126(4): 494–500.

Dongre, Anushka, and Robert A. Weinberg. 2019. “New Insights into the Mechanisms of Epithelial–Mesenchymal Transition and Implications for Cancer.” *Nature Reviews Molecular Cell Biology* 20(2): 69–84. http://www.nature.com/articles/s41580-018-0080-4 (June 24, 2019).

Eming, Sabine A., Thomas Krieg, and Jeffrey M. Davidson. 2007. “Inflammation in Wound Repair: Molecular and Cellular Mechanisms.” *Journal of Investigative Dermatology* 127(3): 514–25. https://www.sciencedirect.com/science/article/pii/S0022202X15332917 (July 20, 2019).

FALANGA, A., M. MARCHETTI, and A. VIGNOLI. 2013. “Coagulation and Cancer: Biological and Clinical Aspects.” *Journal of Thrombosis and Haemostasis* 11(2): 223–33. http://www.ncbi.nlm.nih.gov/pubmed/23279708 (July 31, 2018).

Fang, Weirong et al. 2014. “Platelet Activating Factor Induces Transient Blood-Brain Barrier Opening to Facilitate Edaravone Penetration into the Brain.” *Journal of Neurochemistry* 128(5): 662–71.

Fankhauser, Manuel et al. 2017. “Tumor Lymphangiogenesis Promotes T Cell Infiltration and Potentiates Immunotherapy in Melanoma.” *Science Translational Medicine* 9(407): eaal4712. https://stm.sciencemag.org/content/9/407/eaal4712 (June 24, 2019).

Farzaneh Behelgardi, Maryam et al. 2018. “A Peptide Mimicking the Binding Sites of VEGF-A and VEGF-B Inhibits VEGFR-1/-2 Driven Angiogenesis, Tumor Growth and Metastasis.” *Scientific Reports* 8(1): 17924. http://www.nature.com/articles/s41598-018-36394-0 (July 15, 2019).

Federici, Augusto B. 2006. “Acquired von Willebrand Syndrome: An Underdiagnosed and Misdiagnosed Bleeding Complication in Patients With Lymphoproliferative and Myeloproliferative Disorders.” *Seminars in Hematology* 43: S48–58. https://www.sciencedirect.com/science/article/abs/pii/S0037196305002106?via%3Dihub (July 9, 2019).

Ferrari, Silvia, Hanspeter Rottensteiner, and Friedrich Scheiflinger. 2013. “ADAMTS13: Von Willebrand Factor-Cleaving Protease.” *Handbook of Proteolytic Enzymes* 1(M): 1199–1206.

Ferraro, Francesco et al. 2016. “Weibel-Palade Body Size Modulates the Adhesive Activity of Its von Willebrand Factor Cargo in Cultured Endothelial Cells.” *Scientific Reports* 6(March): 1–15. http://dx.doi.org/10.1038/srep32473.

Fidler, Isaiah J. 2015. “The Biology of Brain Metastasis: Challenges for Therapy.” *Cancer journal (Sudbury, Mass.)* 21(4): 284–93. http://www.ncbi.nlm.nih.gov/pubmed/26222080.

Fisher, Mark J. 2013. “Brain Regulation of Thrombosis and Hemostasis: From Theory to Practice.” *Stroke; a journal of cerebral circulation* 44(11): 3275–85. http://www.pubmedcentral.nih.gov/articlerender.fcgi?artid=3954774&tool=pmcentrez&rendertype=abstract (April 6, 2016).

Flaherty, Keith T. et al. 2012. “Combined BRAF and MEK Inhibition in Melanoma with BRAF V600 Mutations.” *New England Journal of Medicine*.

Flørenes, Vivi Ann et al. 2000. “Clinical Cancer Research.” *Clin. Cancer Res.* 5(10): 2810–19. http://clincancerres.aacrjournals.org/content/6/9/3614.long (July 8, 2019).

Floyd, C M, K Irani, P D Kind, and C M Kessler. 1992. “Von Willebrand Factor Interacts with Malignant Hematopoietic Cell Lines: Evidence for the Presence of Specific Binding Sites and Modification of von

Willebrand Factor Structure and Function." *The Journal of laboratory and clinical medicine* 119(5): 467–76. http://www.ncbi.nlm.nih.gov/pubmed/1583402 (July 9, 2019).

Folsom, A R et al. 1999. "Prospective Study of Markers of Hemostatic Function with Risk of Ischemic Stroke. The Atherosclerosis Risk in Communities (ARIC) Study Investigators." *Circulation*.

Franchini, Massimo et al. 2013. "Von Willebrand Factor and Cancer: A Renewed Interest." *Thrombosis Research* 131(4): 290–92. http://www.ncbi.nlm.nih.gov/pubmed/23394808 (January 4, 2018).

Franchino, Federica, Roberta Rudà, and Riccardo Soffietti. 2018. "Mechanisms and Therapy for Cancer Metastasis to the Brain." *Frontiers in oncology* 8: 161. http://www.ncbi.nlm.nih.gov/pubmed/29881714 (June 17, 2019).

Fressinaud, Edith et al. 1994. "The Role of Platelet von Willebrand Factor in Platelet Adhesion and Thrombus Formation: A Study of 34 Patients with Various Subtypes of Type I von Willebrand Disease." *British Journal of Haematology* 86(2): 327–32. http://doi.wiley.com/10.1111/j.1365-2141.1994.tb04734.x (August 23, 2019).

Fuchs, Tobias A., Ashish A. Bhandari, and Denisa D. Wagner. 2011. "Histones Induce Rapid and Profound Thrombocytopenia in Mice." *Blood* 118(13): 3708–14.

Fujioka, Masayuki et al. 2010. "ADAMTS13 Gene Deletion Aggravates Ischemic Brain Damage: A Possible Neuroprotective Role of ADAMTS13 by Ameliorating Postischemic Hypoperfusion." *Blood* 115(8): 1650–53.

Gale, Andrew J. 2011. "Continuing Education Course #2: Current Understanding of Hemostasis." *Toxicologic pathology* 39(1): 273–80. http://www.ncbi.nlm.nih.gov/pubmed/21119054 (July 9, 2019).

Ganapathy, Vidya, Prabhas V. Moghe, and Charles M. Roth. 2015. "Targeting Tumor Metastases: Drug Delivery Mechanisms and Technologies." *Journal of Controlled Release* 219: 215–23. https://www.sciencedirect.com/science/article/pii/S0168365915301437 (September 5, 2019).

Garam, Nóra et al. 2018. "Platelet Count, ADAMTS13 Activity, von Willebrand Factor Level and Survival in Patients with Colorectal Cancer: 5-Year Follow-up Study." *Thrombosis and Haemostasis* 118(01): 123–31. http://www.thieme-connect.de/DOI/DOI?10.1160/TH17-07-0548 (May 3, 2019).

Gasser, Stephan, Lina H K Lim, and Florence S G Cheung. 2017. "The Role of the Tumour Microenvironment in Immunotherapy." *Endocrine-Related Cancer* 24(12): T283–95. http://www.ncbi.nlm.nih.gov/pubmed/28754821 (August 13, 2019).

Gay, Laurie J., and Brunhilde Felding-Habermann. 2011. "Contribution of Platelets to Tumour Metastasis." *Nature Reviews Cancer* 11(2): 123–34. http://www.nature.com/doifinder/10.1038/nrc3004.

Gerotziafas, Grigoris T. et al. 2012. "Tissue Factor Over-Expression by Human Pancreatic Cancer Cells BXPC3 Is Related to Higher Prothrombotic Potential as Compared to Breast Cancer Cells MCF7." *Thrombosis Research*.

Glanz, Karen, David B. Buller, and Mona Saraiya. 2007. "Reducing Ultraviolet Radiation Exposure among Outdoor Workers: State of the Evidence and Recommendations." *Environmental Health: A Global Access Science Source*.

Gloster, Hugh M., and Kenneth Neal. 2006. "Skin Cancer in Skin of Color." *Journal of the American Academy of Dermatology* 55(5): 741–60. http://www.ncbi.nlm.nih.gov/pubmed/17052479 (July 23, 2019).

Gockel, Lukas Maria et al. 2018. "The Low Molecular Weight Heparin Tinzaparin Attenuates Platelet Activation in Terms of Metastatic Niche Formation by Coagulation-Dependent and Independent Pathways." *Molecules (Basel, Switzerland)* 23(11). http://www.ncbi.nlm.nih.gov/pubmed/30356007 (July 16, 2019).

Goertz, Lukas, Stefan Werner Schneider, et al. 2016. "Heparins That Block VEGF-A-Mediated von Willebrand Factor Fiber Generation Are Potent Inhibitors of Hematogenous but Not Lymphatic Metastasis." *Oncotarget* 7(42): 68527–45.

Goertz, Lukas, Stefan Werner Schneider, et al. 2016. "Heparins That Block VEGF-A-Mediated von Willebrand Factor Fiber Generation Are Potent Inhibitors of Hematogenous but Not Lymphatic Metastasis." *Oncotarget* 7(42): 68527–45. http://www.oncotarget.com/abstract/11832 (January 10, 2017).

Gomes, Noëlia, Chantal Legrand, and Françoise Fauvel- Lafeve. 2005. "Shear Stress Induced Release of Von Willebrand Factor and Thrombospondin-1 in Uvec Extracellular Matrix Enhances Breast Tumour Cell Adhesion." *Clinical & Experimental Metastasis* 22(3): 215–23. http://www.ncbi.nlm.nih.gov/pubmed/16158249 (July 15, 2019).

Goncharov, Nikolay V., Alexander D. Nadeev, Richard O. Jenkins, and Pavel V. Avdonin. 2017. "Markers and Biomarkers of Endothelium: When Something Is Rotten in the State." *Oxidative Medicine and Cellular Longevity* 2017.

Gragnano, Felice et al. 2017. "The Role of von Willebrand Factor in Vascular Inflammation: From Pathogenesis to Targeted Therapy." *Mediators of Inflammation* 2017: 1–13.

Greenberg, David A, and Kunlin Jin. 2013. "Vascular Endothelial Growth Factors (VEGFs) and Stroke." *Cellular*

and molecular life sciences : CMLS 70(10): 1753–61. http://www.ncbi.nlm.nih.gov/pubmed/23475070 (July 16, 2019).

Guan, Xiangming. 2015. "Cancer Metastases: Challenges and Opportunities." *Acta Pharmaceutica Sinica B* 5(5): 402–18. https://www.sciencedirect.com/science/article/pii/S2211383515001094 (September 6, 2019).

Guy, Gery P et al. 2015. "Vital Signs: Melanoma Incidence and Mortality Trends and Projections - United States, 1982-2030." *MMWR. Morbidity and mortality weekly report* 64(21): 591–96. http://www.ncbi.nlm.nih.gov/pubmed/26042651 (June 16, 2019).

Hamid, Omid et al. 2013. "Safety and Tumor Responses with Lambrolizumab (Anti-PD-1) in Melanoma." *New England Journal of Medicine*.

Harary, Maya, David A Reardon, and J Bryan Iorgulescu. 2019. "Efficacy and Safety of Immune Checkpoint Blockade for Brain Metastases." *CNS Oncology* 8(2): CNS33. https://www.futuremedicine.com/doi/10.2217/cns-2018-0018 (September 5, 2019).

Harris, Rachel, James Scott Miners, Shelley Allen, and Seth Love. 2017. "VEGFR1 and VEGFR2 in Alzheimer's Disease." *Journal of Alzheimer's Disease*.

Hatam, Nahid et al. 2017. "Cost-Effectiveness Analysis of the Unfractionated Heparin versus Low–Molecular-Weight Heparin in Hospitalized Patients with Stroke Due to Atrial Fibrillation in Shiraz, South of Iran." *Journal of Vascular and Interventional Neurology* 9(4): 6. https://www.ncbi.nlm.nih.gov/pmc/articles/PMC5501122/ (July 14, 2019).

Huck, Volker, Matthias F. Schneider, Christian Gorzelanny, and Stefan W. Schneider. 2014a. "The Various States of von Willebrand Factor and Their Function in Physiology and Pathophysiology." *Thrombosis and Haemostasis*.

Huck, Volker, Matthias Schneider, Christian Gorzelanny, and Stefan Schneider. 2014b. "The Various States of von Willebrand Factor and Their Function in Physiology and Pathophysiology." *Thrombosis and Haemostasis* 111(04): 598–609. http://www.ncbi.nlm.nih.gov/pubmed/24573248 (July 23, 2019).

Hull, Russell D. et al. 1992. "Subcutaneous Low-Molecular-Weight Heparin Compared with Continuous Intravenous Heparin in the Treatment of Proximal-Vein Thrombosis." *New England Journal of Medicine* 326(15): 975–82. http://www.nejm.org/doi/abs/10.1056/NEJM199204093261502 (September 9, 2019).

Ji, Rui-Cheng. 2006. "Lymphatic Endothelial Cells, Lymphangiogenesis, and Extracellular Matrix." *Lymphatic Research and Biology* 4(2): 83–100. http://www.liebertpub.com/doi/10.1089/lrb.2006.4.83 (June 24, 2019).

Johnson, Edward A., and Barbara Mulloy. 1976. "The Molecular-Weight Range of Mucosal-Heparin Preparations." *Carbohydrate Research*.

Joyce, Johanna A., and Jeffrey W. Pollard. 2009. "Microenvironmental Regulation of Metastasis." *Nature Reviews Cancer* 9(4): 239–52. http://www.nature.com/articles/nrc2618 (June 24, 2019).

Kakkar, A.K. 2009. "Antithrombotic Therapy and Survival in Cancer Patients." *Best Practice & Research Clinical Haematology* 22(1): 147–51. https://www.sciencedirect.com/science/article/pii/S152169260900005X?via%3Dihub (May 3, 2018).

Kakkar, Ajay K. et al. 2004. "Low Molecular Weight Heparin, Therapy with Dalteparin, and Survival in Advanced Cancer: The Fragmin Advanced Malignancy Outcome Study (FAMOUS)." *Journal of Clinical Oncology*.

Kakkar, V V et al. "Low Molecular Weight Heparin for Treatment of Acute Myocardial Infarction (FAMI): Fragmin (Dalteparin Sodium) in Acute Myocardial Infarction." *Indian heart journal* 52(5): 533–39. http://www.ncbi.nlm.nih.gov/pubmed/11256775 (August 16, 2019).

Kanaji, S. et al. 2012. "Contribution of Platelet vs. Endothelial VWF to Platelet Adhesion and Hemostasis." *Journal of Thrombosis and Haemostasis* 10(8): 1646–52.

Karlsson, Mikael C., Santiago F. Gonzalez, Josefin Welin, and Jonas Fuxe. 2017. "Epithelial-Mesenchymal Transition in Cancer Metastasis through the Lymphatic System." *Molecular Oncology* 11(7): 781–91.

Karpatkin, S., E. Pearlstein, C. Ambrogio, and B. S. Coller. 1988. "Role of Adhesive Proteins in Platelet Tumor Interaction in Vitro and Metastasis Formation in Vivo." *Journal of Clinical Investigation* 81(4): 1012–19.

Kato, M et al. 1998. "Transgenic Mouse Model for Skin Malignant Melanoma." *Oncogene* 17(14): 1885–88.

Kerk, Nina, Elwira a Strozyk, Birgit Pöppelmann, and Stefan W Schneider. 2010. "The Mechanism of Melanoma-Associated Thrombin Activity and von Willebrand Factor Release from Endothelial Cells." *The Journal of investigative dermatology* 130(9): 2259–68.

Kienast, Yvonne et al. 2010. "Real-Time Imaging Reveals the Single Steps of Brain Metastasis Formation." *Nature Medicine* 16(1): 116–22. http://www.nature.com/doifinder/10.1038/nm.2072 (July 11, 2016).

Kimpfler, S. et al. 2009. "Skin Melanoma Development in Ret Transgenic Mice Despite the Depletion of CD25+Foxp3+ Regulatory T Cells in Lymphoid Organs." *The Journal of Immunology*.

Kleinschnitz, C. et al. 2009. "Deficiency of von Willebrand Factor Protects Mice from Ischemic Stroke." *Blood* 113(15): 3600–3603. http://www.ncbi.nlm.nih.gov/pubmed/19182208 (July 9, 2019).

KM, Valentijn et al. 2010. “Multigranular Exocytosis of Weibel-Palade Bodies in Vascular Endothelial Cells.” *Blood* 116(10): 1807–16. http://bloodjournal.hematologylibrary.org/content/116/10/1807.abstract.

Kuderer, Nicole M., Thomas L. Ortel, and Charles W. Francis. 2009. “Impact of Venous Thromboembolism and Anticoagulation on Cancer and Cancer Survival.” *Journal of Clinical Oncology* 27(29): 4902. http://www.ncbi.nlm.nih.gov/pubmed/19738120 (July 7, 2019).

Kunz, Manfred. 2014. “Oncogenes in Melanoma: An Update.” *European Journal of Cell Biology* 93(1–2): 1–10. https://www.sciencedirect.com/science/article/pii/S0171933513000976?via%3Dihub (June 18, 2019).

Kwak, Minyoung et al. 2019. “Updates in Adjuvant Systemic Therapy for Melanoma.” *Journal of Surgical Oncology* 119(2): 222–31. https://onlinelibrary.wiley.com/doi/abs/10.1002/jso.25298 (August 13, 2019).

Labelle, Myriam et al. “Platelets Guide the Formation of Early Metastatic Niches.” https://www.ncbi.nlm.nih.gov/pmc/articles/PMC4121772/pdf/pnas.201411082.pdf (April 25, 2018).

Lambert, Arthur W., Diwakar R. Pattabiraman, and Robert A. Weinberg. 2017. “Emerging Biological Principles of Metastasis.” *Cell* 168(4): 670–91. http://www.ncbi.nlm.nih.gov/pubmed/28187288 (June 24, 2019).

Larkin, James et al. 2018. “Overall Survival in Patients with Advanced Melanoma Who Received Nivolumab versus Investigator’s Choice Chemotherapy in CheckMate 037: A Randomized, Controlled, Open-Label Phase III Trial.” In *Journal of Clinical Oncology*,.

Läubli, Heinz, Ajit Varki, and Lubor Borsig. 2016. “Antimetastatic Properties of Low Molecular Weight Heparin.” *Journal of Clinical Oncology* 34(21): 2560–61. http://www.ncbi.nlm.nih.gov/pubmed/27185851 (July 16, 2019).

Leblanc, Raphael, and Olivier Peyruchaud. 2016a. “Metastasis: New Functional Implications of Platelets and Megakaryocytes.” *Blood* 128(1). http://www.bloodjournal.org/content/128/1/24.long?sso-checked=true (May 9, 2017).

———. 2016b. “Metastasis: New Functional Implications of Platelets and Megakaryocytes.” *Blood* 128(1): 24–31. http://www.bloodjournal.org/cgi/doi/10.1182/blood-2016-01-636399.

Lee, Agnes Y. Y. et al. 2015. “Tinzaparin vs Warfarin for Treatment of Acute Venous Thromboembolism in Patients With Active Cancer.” *JAMA* 314(7): 677. http://jama.jamanetwork.com/article.aspx?doi=10.1001/jama.2015.9243 (September 3, 2019).

Lee, Agnes YY. 2003. “Anti-Thrombotic Therapy in Cancer Patients.” *Expert Opinion on Pharmacotherapy* 4(12): 2213–20. http://www.ncbi.nlm.nih.gov/pubmed/14640920 (March 24, 2017).

Lee, Su Kim et al. 2004. “Vascular Endothelial Growth Factor Expression Promotes the Growth of Breast Cancer Brain Metastases in Nude Mice.” *Clinical and Experimental Metastasis*.

Lenting, Peter J et al. 2018. “Von Willebrand Factor Biosynthesis , Secretion & Clearance : Connecting the Far Ends.” *Bloodjournal* 125(13): 2019–29.

Lenting, Peter J, Olivier D Christophe, and Cécile V Denis. 2015. “Von Willebrand Factor Biosynthesis, Secretion, and Clearance: Connecting the Far Ends.” *Blood* 125(13): 2019–28. http://www.ncbi.nlm.nih.gov/pubmed/25712991 (July 9, 2019).

Leonardi, Giulia et al. 2018. “Cutaneous Melanoma: From Pathogenesis to Therapy (Review).” *International Journal of Oncology* 52(4): 1071–80. http://www.spandidos-publications.com/10.3892/ijo.2018.4287 (July 22, 2019).

Li, Nailin. 2016. “Platelets in Cancer Metastasis: To Help the ‘Villain’ to Do Evil.” *International Journal of Cancer* 138(9): 2078–87.

Lima, Luize G., and Robson Q. Monteiro. 2013. “Activation of Blood Coagulation in Cancer: Implications for Tumour Progression.” *Bioscience Reports* 33(5): 701–10. http://bioscirep.org/cgi/doi/10.1042/BSR20130057.

Lima, Luize G. et al. 2011. “Malignant Transformation in Melanocytes Is Associated with Increased Production of Procoagulant Microvesicles.” *Thrombosis and Haemostasis*.

Lin, Richard J, David L Green, and Gunjan L Shah. 2018. “Therapeutic Anticoagulation in Patients with Primary Brain Tumors or Secondary Brain Metastasis.” *The oncologist* 23(4): 468–73. http://www.ncbi.nlm.nih.gov/pubmed/29158366 (July 16, 2019).

Liu, L. et al. 2014. “Notch3 Is Important for TGF-β-Induced Epithelial-Mesenchymal Transition in Non-Small Cell Lung Cancer Bone Metastasis by Regulating ZEB-1.” *Cancer Gene Therapy*.

Liu, Wei-Ye et al. 2012. “Tight Junction in Blood-Brain Barrier: An Overview of Structure, Regulation, and Regulator Substances.” *CNS neuroscience & therapeutics* 18(8): 609–15. http://www.ncbi.nlm.nih.gov/pubmed/22686334 (June 25, 2016).

Liu, Yanting et al. 2017. “Downregulation of Bmi-1 Suppresses Epithelial-Mesenchymal Transition in Melanoma.” *Oncology Reports*.

Lonsdorf, Anke S. et al. 2012. “Engagement of AIIbβ3 (GPIIb/IIIa) with Avβ3 Integrin Mediates Interaction of Melanoma Cells with Platelets: A Connection to Hematogenous Metastasis.” *Journal of Biological*

Chemistry 287(3): 2168–78.
M.J., Wolf et al. 2012. “Endothelial CCR2 Signaling Induced by Colon Carcinoma Cells Enables Extravasation via the JAK2-Stat5 and P38MAPK Pathway.” In *Cancer Cell*,.
Ma, Qing et al. 2007. “Molecular Weight Dependent Tissue Factor Pathway Inhibitor Release by Heparin and Heparin Oligosaccharides.” *Thrombosis Research*.
Macdonald, Jennifer A., Nivetha Murugesan, and Joel S. Pachter. 2010. “Endothelial Cell Heterogeneity of Blood-Brain Barrier Gene Expression along the Cerebral Microvasculature.” *Journal of Neuroscience Research*.
Mackman, Nigel. 2009. “The Role of Tissue Factor and Factor VIIa in Hemostasis.” *Anesthesia and analgesia* 108(5): 1447. http://www.ncbi.nlm.nih.gov/pubmed/19372318 (July 7, 2019).
Mackman, Nigel, Michael S. Sawdey, Mark R. Keeton, and David J. Loskutoff. 1993. “Murine Tissue Factor Gene Expression in Vivo: Tissue and Cell Specificity and Regulation by Lipopolysaccharide.” *American Journal of Pathology*.
Mahecha, Anna M., and Hongbo Wang. 2017. “The Influence of Vascular Endothelial Growth Factor-A and Matrix Metalloproteinase-2 and -9 in Angiogenesis, Metastasis, and Prognosis of Endometrial Cancer.” *OncoTargets and Therapy* 10: 4617–24.
Mannucci, Pier Mannuccio, and Flora Peyvandi. 2007. “TTP and ADAMTS13: When Is Testing Appropriate?” *Hematology. American Society of Hematology. Education Program* 2007(1): 121–26. http://www.ncbi.nlm.nih.gov/pubmed/18024619 (July 25, 2019).
Mark, Fisher. 2013. “Brain Regulation of Thrombosis and Hemostasis: From Theory to Practice.” *Stroke* 44(11): 3275–85.
Matthews, Natalie H. et al. 2017. Cutaneous Melanoma: Etiology and Therapy *Epidemiology of Melanoma*. Codon Publications. http://www.ncbi.nlm.nih.gov/pubmed/29461782 (June 16, 2019).
McCain, Jack. 2013. “The MAPK (ERK) Pathway: Investigational Combinations for the Treatment Of BRAF-Mutated Metastatic Melanoma.” *P & T : a peer-reviewed journal for formulary management* 38(2): 96–108. http://www.ncbi.nlm.nih.gov/pubmed/23599677 (June 24, 2019).
McGrath, Rachel T., Emily McRae, Owen P. Smith, and James S. O’Donnell. 2010. “Platelet von Willebrand Factor - Structure, Function and Biological Importance.” *British Journal of Haematology* 148(6): 834–43.
Meeran, Syed M., Thejass Punathil, and Santosh K. Katiyar. 2008. “IL-12 Deficiency Exacerbates Inflammatory Responses in UV-Irradiated Skin and Skin Tumors.” *Journal of Investigative Dermatology*.
Meikle, Claire K S et al. 2016. “Cancer and Thrombosis: The Platelet Perspective.” *Frontiers in cell and developmental biology* 4: 147. http://www.ncbi.nlm.nih.gov/pubmed/28105409 (July 6, 2018).
Melgar-Lesmes, P. et al. 2009. “Vascular Endothelial Growth Factor and Angiopoietin-2 Play a Major Role in the Pathogenesis of Vascular Leakage in Cirrhotic Rats.” *Gut* 58(2): 285–92.
Meyer, Guy et al. 2018. “Anti-Tumour Effect of Low Molecular Weight Heparin in Localised Lung Cancer: A Phase III Clinical Trial.” *The European respiratory journal* 52(4): 1801220. http://www.ncbi.nlm.nih.gov/pubmed/30262574 (September 3, 2019).
Michaux, Grégoire et al. 2006. “The Physiological Function of von Willebrand’s Factor Depends on Its Tubular Storage in Endothelial Weibel-Palade Bodies.” *Developmental Cell*.
Miller, Arlo J., and Martin C. Mihm. 2006. “Melanoma.” *New England Journal of Medicine* 355(1): 51–65. http://www.nejm.org/doi/abs/10.1056/NEJMra052166 (June 17, 2019).
Morange, P E et al. 2004. “Endothelial Cell Markers and the Risk of Coronary Heart Disease: The Prospective Epidemiological Study of Myocardial Infarction (PRIME) Study.” *Circulation* 109(11): 1343–48. https://www.ahajournals.org/doi/10.1161/01.CIR.0000120705.55512.EC (July 24, 2019).
Mrozik, Krzysztof Marek et al. 2018. “N-Cadherin in Cancer Metastasis, Its Emerging Role in Haematological Malignancies and Potential as a Therapeutic Target in Cancer.” *BMC Cancer* 18(1): 939. https://bmccancer.biomedcentral.com/articles/10.1186/s12885-018-4845-0 (June 24, 2019).
Mueller, B M, R A Reisfeld, T S Edgington, and W Ruf. 1992. “Expression of Tissue Factor by Melanoma Cells Promotes Efficient Hematogenous Metastasis.” *Proceedings of the National Academy of Sciences of the United States of America* 89(24): 11832–36. http://www.ncbi.nlm.nih.gov/pubmed/1465406 (June 24, 2019).
Müller, Annette M., Carmen Skrzynski, Guido Skipka, and Klaus-Michael Müller. 2002a. “Expression of von Willebrand Factor by Human Pulmonary Endothelial Cells in Vivo<Footref Rid="Foot01">¹</Footref>” *Respiration* 69(6): 526–33. http://www.ncbi.nlm.nih.gov/pubmed/12457006 (July 26, 2019).
Müller, Annette M, Carmen Skrzynski, Guido Skipka, and Klaus-Michael Müller. 2002b. “Expression of von Willebrand Factor by Human Pulmonary Endothelial Cells in Vivo.” *Respiration; international review of thoracic diseases* 69(6): 526–33. http://www.ncbi.nlm.nih.gov/pubmed/12457006 (July 12, 2016).

Nalluri, Shobha Rani et al. 2008a. “Risk of Venous Thromboembolism with the Angiogenesis Inhibitor Bevacizumab in Cancer Patients: A Meta-Analysis.” *JAMA - Journal of the American Medical Association*.

———. 2008b. “Risk of Venous Thromboembolism With the Angiogenesis Inhibitor Bevacizumab in Cancer Patients.” *JAMA* 300(19): 2277. http://www.ncbi.nlm.nih.gov/pubmed/19017914 (July 14, 2019).

Narayanan, Deevya L., Rao N. Saladi, and Joshua L. Fox. 2010. “Review: Ultraviolet Radiation and Skin Cancer.” *International Journal of Dermatology* 49(9): 978–86. http://doi.wiley.com/10.1111/j.1365-4632.2010.04474.x (June 18, 2019).

NIESWANDT, B., D. VARGA-SZABO, and M. ELVERS. 2009. “Integrins in Platelet Activation.” *Journal of Thrombosis and Haemostasis* 7: 206–9. http://doi.wiley.com/10.1111/j.1538-7836.2009.03370.x (May 10, 2019).

Nieswandt, Bernhard, D. Varga-Szabo, and M. Elvers. 2009. “Integrins in Platelet Activation.” *Journal of Thrombosis and Haemostasis* 7(SUPPL. 1): 206–9.

Norrby, Klas. 2006. “Low-Molecular-Weight Heparins and Angiogenesis.” *Apmis* 114(2): 79–102.

Norrby, Klas, and Arvid Nordenhem. 2010. “Dalteparin, a Low-Molecular-Weight Heparin, Promotes Angiogenesis Mediated by Heparin-Binding VEGF-A in Vivo.” *APMIS*.

Noubade, Rajkumar et al. 2008. “Von-Willebrand Factor Influences Blood Brain Barrier Permeability and Brain Inflammation in Experimental Allergic Encephalomyelitis.” *American Journal of Pathology* 173(3): 892–900. http://dx.doi.org/10.2353/ajpath.2008.080001.

O’regan, Niamh et al. 2016. “A Novel Role for von Willebrand Factor in the Pathogenesis of Experimental Cerebral Malaria.” *Blood* 127(9): 1192–1201.

O’Sullivan, Jamie, Roger Preston, Tracy Robson, and James O’Donnell. 2018. “Emerging Roles for von Willebrand Factor in Cancer Cell Biology.” *Seminars in Thrombosis and Hemostasis* 44(02): 159–66. http://www.thieme-connect.de/DOI/DOI?10.1055/s-0037-1607352 (April 24, 2018).

Obermeier, Birgit, Richard Daneman, and Richard M Ransohoff. 2013. “Development, Maintenance and Disruption of the Blood-Brain Barrier.” *Nature medicine* 19(12): 1584–96. http://www.pubmedcentral.nih.gov/articlerender.fcgi?artid=4080800&tool=pmcentrez&rendertype=abstract.

Oiseth, Stanley J., and Mohamed S. Aziz. 2017. “Cancer Immunotherapy: A Brief Review of the History, Possibilities, and Challenges Ahead.” *Journal of Cancer Metastasis and Treatment* 3(10): 250. http://jcmtjournal.com/article/view/2275 (August 13, 2019).

Olson, S. T. et al. 1992. “Role of the Antithrombin-Binding Pentasaccharide in Heparin Acceleration of Antithrombin-Proteinase Reactions. Resolution of the Antithrombin Conformational Change Contribution to Heparin Rate Enhancement.” *Journal of Biological Chemistry*.

Pabinger, I., and C. Ay. 2012. “Risk of Venous Thromboembolism and Primary Prophylaxis in Cancer: Should All Patients Receive Thromboprophylaxis?” *Hamostaseologie*.

Pabinger, Ingrid, Johannes Thaler, and Cihan Ay. 2013. “Biomarkers for Prediction of Venous Thromboembolism in Cancer.” *Blood* 122(12): 2011–18.

Paczuski, R et al. 1999. “Von Willebrand Factor in Plasma of Patients with Advanced Stages of Larynx Cancer.” *Thrombosis research* 95(4): 197–200. http://www.ncbi.nlm.nih.gov/pubmed/10498389 (September 3, 2019).

Page, C, M Rose, M Yacoub, and R Pigott. 1992. “Antigenic Heterogeneity of Vascular Endothelium.” *The American journal of pathology* 141(3): 673–83. http://www.ncbi.nlm.nih.gov/pubmed/1519671 (April 30, 2019).

Palumbo, Joseph S. et al. 2005. “Blood.” *Blood* 96(10): 3302–9. http://www.bloodjournal.org/content/105/1/178?sso-checked=true (August 23, 2019).

Papa, Anne-Laure et al. 2019. “Platelet Decoys Inhibit Thrombosis and Prevent Metastatic Tumor Formation in Preclinical Models.” *Science translational medicine* 11(479): eaau5898. http://www.ncbi.nlm.nih.gov/pubmed/30760580 (March 31, 2019).

Parkinson, Katie et al. 2014. “Calcium-Dependent Regulation of Rab Activation and Vesicle Fusion by an Intracellular P2X Ion Channel.” *Nature cell biology* 16(1): 87–98. http://www.nature.com/articles/ncb2887 (July 9, 2019).

Pearlman, Ross L., Mary Katherine Montes de Oca, Harish Chandra Pal, and Farrukh Afaq. 2017. “Potential Therapeutic Targets of Epithelial–Mesenchymal Transition in Melanoma.” *Cancer Letters*.

Pekkonen, Pirita et al. 2018. “Lymphatic Endothelium Stimulates Melanoma Metastasis and Invasion via MMP14-Dependent Notch3 and B1-Integrin Activation.” *eLife* 7: 1–28.

Pépin, M. et al. 2016. “ADAMTS-13 and von Willebrand Factor Predict Venous Thromboembolism in Patients with Cancer.” *Journal of Thrombosis and Haemostasis*.

Petri, B et al. 2010. “Von Willebrand Factor Promotes Leukocyte Extravasation.” *Blood* 116(22): 4712–19.

Petri, Björn et al. 2010. “Von Willebrand Factor Promotes Leukocyte Extravasation.” *Blood* 116(22): 4712–19. http://www.ncbi.nlm.nih.gov/pubmed/20716766 (September 7, 2016).

Peyvandi, Flora, Isabella Garagiola, and Luciano Baronciani. 2011a. “Role of von Willebrand Factor in the Haemostasis.” *Blood transfusion = Trasfusione del sangue* 9 Suppl 2(Suppl 2): s3-8. http://www.ncbi.nlm.nih.gov/pubmed/21839029 (July 24, 2019).

———. 2011b. “Role of von Willebrand Factor in the Haemostasis.” *Blood transfusion = Trasfusione del sangue* 9 Suppl 2(Suppl 2): s3-8. http://www.ncbi.nlm.nih.gov/pubmed/21839029 (November 2, 2017).

Phillips, Stephanie, John Lazarchick, and Shayla Bergmann. 2016. “Type 3 Von Willebrand Disease: A Case Report of a Rare Entity.” *Blood* 128(22). http://www.bloodjournal.org/content/128/22/4988?sso-checked=true (July 25, 2019).

Pober, Jordan S. 2002. “Endothelial Activation: Intracellular Signaling Pathways.” *Arthritis research* 4 Suppl 3(Suppl 3): S109-16. http://www.ncbi.nlm.nih.gov/pubmed/12110129 (July 9, 2019).

Ponert, Jan Moritz et al. 2018. “The Mechanisms How Heparin Affects the Tumor Cell Induced VEGF and Chemokine Release from Platelets to Attenuate the Early Metastatic Niche Formation.” *PloS one* 13(1): e0191303. http://www.ncbi.nlm.nih.gov/pubmed/29346400 (August 15, 2019).

Pusztaszeri, Marc P., Walter Seelentag, and Fred T. Bosman. 2006. “Immunohistochemical Expression of Endothelial Markers CD31, CD34, von Willebrand Factor, and Fli-1 in Normal Human Tissues.” *Journal of Histochemistry & Cytochemistry* 54(4): 385–95. http://journals.sagepub.com/doi/10.1369/jhc.4A6514.2005 (May 23, 2018).

Quinlan, Daniel J., Andrew McQuillan, and John W. Eikelboom. 2004. “Low-Molecular-Weight Heparin Compared with Intravenous Unfractionated Heparin for Treatment of Pulmonary Embolism.” *Annals of Internal Medicine* 140(3): 175. http://annals.org/article.aspx?doi=10.7326/0003-4819-140-3-200402030-00008 (September 3, 2019).

Randi, A. M., and M. A. Laffan. 2017a. “Von Willebrand Factor and Angiogenesis: Basic and Applied Issues.” *Journal of Thrombosis and Haemostasis* 15(1): 13–20.

———. 2017b. “Von Willebrand Factor and Angiogenesis: Basic and Applied Issues.” *Journal of Thrombosis and Haemostasis* 15(1): 13–20. http://doi.wiley.com/10.1111/jth.13551 (July 10, 2019).

Reymond, Nicolas, Bárbara Borda D’Água, and Anne J. Ridley. 2013. “Crossing the Endothelial Barrier during Metastasis.” *Nature Reviews Cancer*.

Rieger, Manfred et al. 2005. “ADAMTS13 Autoantibodies in Patients with Thrombotic Microangiopathies and Other Immunomediated Diseases.” *Blood* 106(4): 1262–67. http://www.ncbi.nlm.nih.gov/pubmed/15890682 (July 11, 2019).

Röhsig, L M et al. 2001. “Von Willebrand Factor Antigen Levels in Plasma of Patients with Malignant Breast Disease.” *Brazilian journal of medical and biological research = Revista brasileira de pesquisas medicas e biologicas* 34(9): 1125–29. http://www.ncbi.nlm.nih.gov/pubmed/11514835 (July 9, 2019).

Rosenberg, R. D., and P. S. Damus. 1973. “The Purification and Mechanism of Action of Human Antithrombin Heparin Cofactor.” *Journal of Biological Chemistry*.

Ruggeri, Z. M. 2003a. “Von Willebrand Factor, Platelets and Endothelial Cell Interactions.” *Journal of Thrombosis and Haemostasis* 1(7): 1335–42. http://doi.wiley.com/10.1046/j.1538-7836.2003.00260.x (July 11, 2017).

Ruggeri, Z M. 2003b. “Von Willebrand Factor, Platelets and Endothelial Cell Interactions.” *Journal of thrombosis and haemostasis : JTH* 1(7): 1335–42. http://www.ncbi.nlm.nih.gov/pubmed/12871266 (March 23, 2017).

Rutering, Jennifer et al. 2016. “乳鼠心肌提取 HHS Public Access.” *Nature Rev Drug Discovery* 5(6): 1–8.

Sadler, J Evan et al. 2003. “Von Willebrand Disease Type 1: A Diagnosis in Search of a Disease.” *Blood* 101(6): 2089–93. http://www.ncbi.nlm.nih.gov/pubmed/8839833 (July 25, 2019).

Salgado, Roberto et al. 2001. “Platelets and Vascular Endothelial Growth Factor (VEGF): A Morphological and Functional Study.” *Angiogenesis* 4(1): 37–43. http://link.springer.com/10.1023/A:1016611230747 (June 6, 2019).

Sandru, A, S Voinea, E Panaitescu, and A Blidaru. 2014. “Survival Rates of Patients with Metastatic Malignant Melanoma.” *Journal of medicine and life* 7(4): 572–76. http://www.ncbi.nlm.nih.gov/pubmed/25713625 (July 22, 2019).

Sandsmark, Danielle K et al. 2019. “Changes in Plasma von Willebrand Factor and Cellular Fibronectin in MRI-Defined Traumatic Microvascular Injury.” *Frontiers in neurology* 10: 246. http://www.ncbi.nlm.nih.gov/pubmed/30972003 (August 18, 2019).

Sanford, D., A. Naidu, N. Alizadeh, and A. Lazo-Langner. 2014. “The Effect of Low Molecular Weight Heparin on Survival in Cancer Patients: An Updated Systematic Review and Meta-Analysis of Randomized Trials.” *Journal of Thrombosis and Haemostasis* 12(7): 1076–85. http://doi.wiley.com/10.1111/jth.12595 (July 16, 2019).

Schneider, S W et al. 2007. “Shear-Induced Unfolding Triggers Adhesion of von Willebrand Factor Fibers.” *Proceedings of the National Academy of Sciences of the United States of America* 104(19): 7899–7903. http://www.ncbi.nlm.nih.gov/pubmed/17470810 (May 3, 2019).

Schrenk, Gerald et al. 2010. “Binding of FVIII to Recombinant VWF.” *Blood* 116(21).

Schumacher, Dagmar et al. 2013. “Platelet-Derived Nucleotides Promote Tumor-Cell Transendothelial Migration and Metastasis via P2Y2 Receptor.” *Cancer Cell* 24(1): 130–37. http://dx.doi.org/10.1016/j.ccr.2013.05.008.

Sheth, Rahul A et al. 2017. “Thrombosis in Cancer Patients: Etiology, Incidence, and Management.” *Cardiovascular diagnosis and therapy* 7(Suppl 3): S178–85. http://www.ncbi.nlm.nih.gov/pubmed/29399521 (July 8, 2019).

Shirley, Stephanie H et al. 2012. “Slug Expression during Melanoma Progression.” *The American journal of pathology* 180(6): 2479–89. http://www.ncbi.nlm.nih.gov/pubmed/22503751 (July 23, 2019).

Soengas, María S., and Scott W. Lowe. 2003. “Apoptosis and Melanoma Chemoresistance.” *Oncogene*.

Solari, Francesca, and Matthew Varacallo. 2019. StatPearls *Low Molecular Weight Heparin (LMWH)*. StatPearls Publishing. http://www.ncbi.nlm.nih.gov/pubmed/30247832 (August 16, 2019).

Song, Haibo et al. 2014. “Irisin Promotes Human Umbilical Vein Endothelial Cell Proliferation through the ERK Signaling Pathway and Partly Suppresses High Glucose-Induced Apoptosis” ed. Shang-Zhong Xu. *PLoS ONE* 9(10): e110273. https://dx.plos.org/10.1371/journal.pone.0110273 (July 16, 2019).

Sørensen, Henrik Toft, Lene Mellemkjær, Jørgen H. Olsen, and John A. Baron. 2000. “Prognosis of Cancers Associated with Venous Thromboembolism.” *New England Journal of Medicine* 343(25): 1846–50. http://www.nejm.org/doi/abs/10.1056/NEJM200012213432504 (June 27, 2017).

Sparsa, A., H. Durox, V. Doffoel-Hantz, E. M. Munyangango, C. Bédane, et al. 2011. “High Prevalence and Risk Factors of Thromboembolism in Stage IV Melanoma.” *Journal of the European Academy of Dermatology and Venereology* 25(3): 340–44.

Sparsa, A., H. Durox, V. Doffoel-Hantz, E. M. Munyangango, C. B??dane, et al. 2011. “High Prevalence and Risk Factors of Thromboembolism in Stage IV Melanoma.” *Journal of the European Academy of Dermatology and Venereology* 25(3): 340–44.

Spronk, Henri M.H., Hugo ten Cate, and Paola E.J. van der Meijden. 2014. “Differential Roles of Tissue Factor and Phosphatidylserine in Activation of Coagulation.” *Thrombosis Research* 133: S54–56. https://linkinghub.elsevier.com/retrieve/pii/S0049384814001479 (July 20, 2019).

Starke, R. D. et al. 2013. “Cellular and Molecular Basis of von Willebrand Disease: Studies on Blood Outgrowth Endothelial Cells.” *Blood* 121(14): 2773–84. http://www.ncbi.nlm.nih.gov/pubmed/23355534 (July 10, 2019).

Starke, Richard D et al. 2011. “Endothelial von Willebrand Factor Regulates Angiogenesis.” *Blood* 117(3): 1071–80. http://www.ncbi.nlm.nih.gov/pubmed/21048155 (November 16, 2017).

Stelzer, KeithJ. 2017. “Epidemiology and Prognosis of Brain Metastases.” *Surgical Neurology International* 4(5): 192.

Suidan, Georgette L et al. 2013a. “Endothelial Von Willebrand Factor Promotes Blood-Brain Barrier Flexibility and Provides Protection from Hypoxia and Seizures in Mice.” *Arteriosclerosis, thrombosis, and vascular biology* 33(9): 2112–20. http://www.ncbi.nlm.nih.gov/pubmed/23825365 (July 11, 2016).

———. 2013b. “Endothelial Von Willebrand Factor Promotes Blood-Brain Barrier Flexibility and Provides Protection from Hypoxia and Seizures in Mice.” *Arteriosclerosis, thrombosis, and vascular biology* 33(9): 2112–20. http://www.ncbi.nlm.nih.gov/pubmed/23825365 (July 9, 2019).

Suzuki, Yasuhiro, Nobuo Nagai, and Kazuo Umemura. 2016. “A Review of the Mechanisms of Blood-Brain Barrier Permeability by Tissue-Type Plasminogen Activator Treatment for Cerebral Ischemia.” *Frontiers in Cellular Neuroscience*.

Switonski, M., M. Mankowska, and S. Salamon. 2013. “Family of Melanocortin Receptor (MCR) Genes in Mammals—Mutations, Polymorphisms and Phenotypic Effects.” *Journal of Applied Genetics* 54(4): 461–72. http://www.ncbi.nlm.nih.gov/pubmed/23996627 (June 19, 2019).

T. NIGHTINGALE and D. CUTLER. 2013. “The Secretion of von Willebrand Factor from Endothelial Cells; an Increasingly Complicated Story.” *Thromb Haemost* 11: 192–201. https://onlinelibrary.wiley.com/doi/pdf/10.1111/jth.12225 (April 12, 2018).

Tas, Faruk. 2012. “Metastatic Behavior in Melanoma: Timing, Pattern, Survival, and Influencing Factors.” *Journal of Oncology* 2012.

Tejera-Vaquerizo, Antonio et al. 2012. “Prediction of Sentinel Lymph Node Positivity by Growth Rate of Cutaneous Melanoma.” *Archives of Dermatology* 148(5): 577–84. http://archderm.jamanetwork.com/article.aspx?doi=10.1001/archdermatol.2011.2522 (June 24, 2019).

TERRAUBE, V. et al. 2006. “Increased Metastatic Potential of Tumor Cells in von Willebrand Factor-Deficient

Mice." *Journal of Thrombosis and Haemostasis* 4(3): 519–26. http://doi.wiley.com/10.1111/j.1538-7836.2005.01770.x (July 9, 2019).

Terraube, V et al. 2006. "Increased Metastatic Potential of Tumor Cells in von Willebrand Factor-Deficient Mice." *Journal of thrombosis and haemostasis : JTH* 4(3): 519–26. http://www.ncbi.nlm.nih.gov/pubmed/16405520 (July 10, 2016).

TESSELAAR, M. E. T. et al. 2009. "Microparticle-Associated Tissue Factor Activity in Cancer Patients with and without Thrombosis." *Journal of Thrombosis and Haemostasis* 7(8): 1421–23. http://doi.wiley.com/10.1111/j.1538-7836.2009.03504.x (August 13, 2019).

Tinholt, Mari et al. 2015. "Tumor Expression, Plasma Levels and Genetic Polymorphisms of the Coagulation Inhibitor TFPI Are Associated with Clinicopathological Parameters and Survival in Breast Cancer, in Contrast to the Coagulation Initiator TF." *Breast Cancer Research* 17(1): 1–15. ???

Tosetto, Alberto, and Giancarlo Castaman. 2015. "How I Treat Type 2 Variant Forms of von Willebrand Disease." *Blood* 125(6): 907–14. http://www.bloodjournal.org/content/125/6/907 (July 25, 2019).

Tran, T Thanh-Nga, Joshua Schulman, and David E Fisher. 2008. "UV and Pigmentation: Molecular Mechanisms and Social Controversies." *Pigment cell & melanoma research* 21(5): 509–16. http://www.ncbi.nlm.nih.gov/pubmed/18821855 (July 25, 2019).

Trousseau. 1865. "Plegmasia Alba Dolens. Lectures on Clinical Medicine, Delivered at the Hotel-Dieu, Paris." (5): 281–332.

Tsai, Han-Mou. 2007. "Thrombotic Thrombocytopenic Purpura: A Thrombotic Disorder Caused by ADAMTS13 Deficiency." *Hematology/oncology clinics of North America* 21(4): 609–32, v. http://www.ncbi.nlm.nih.gov/pubmed/17666281 (July 25, 2019).

Umansky, Viktor, and Alexandra Sevko. 2013. "Ret Transgenic Mouse Model of Spontaneous Skin Melanoma: Focus on Regulatory T Cells." *Pigment Cell and Melanoma Research* 26(4): 457–63.

Valentijn, Karine M et al. 2011. "Functional Architecture of Weibel-Palade Bodies." *Blood* 117(19): 5033–43. http://www.ncbi.nlm.nih.gov/pubmed/21266719 (July 9, 2019).

Verhenne, Sebastien et al. 2015. "While Not Essential for Normal Thrombosis and Hemostasis , Platelet-Derived VWF Fosters Ischemic Stroke Injury in Mice . Key Points :" 32(0): 1715–23.

Villares, Gabriel J., Maya Zigler, and Menashe Bar-Eli. 2011. "The Emerging Role of the Thrombin Receptor (PAR-1) in Melanoma Metastasis - a Possible Therapeutic Target." *Oncotarget*.

Vosoughi, Elham et al. 2018. "Survival and Clinical Outcomes of Patients with Melanoma Brain Metastasis in the Era of Checkpoint Inhibitors and Targeted Therapies." *BMC Cancer* 18(1): 490. https://bmccancer.biomedcentral.com/articles/10.1186/s12885-018-4374-x (July 8, 2019).

Wagner, Denisa D et al. 1991. "Induction of Specific Storage Organelles by von Willebrand Factor Propolypeptide." *Cell* 64(2): 403–13. http://linkinghub.elsevier.com/retrieve/pii/009286749190648I (April 12, 2018).

Wang, Jiong Wei et al. 2011. "Intracellular Storage and Regulated Secretion of Von Willebrand Factor in Quantitative Von Willebrand Disease." *Journal of Biological Chemistry* 286(27): 24180–88.

Wang, Wei-Shu et al. 2005a. "Plasma von Willebrand Factor Level as a Prognostic Indicator of Patients with Metastatic Colorectal Carcinoma." *World journal of gastroenterology* 11(14): 2166–70. http://www.ncbi.nlm.nih.gov/pubmed/15810086 (January 3, 2018).

———. 2005b. "Plasma von Willebrand Factor Level as a Prognostic Indicator of Patients with Metastatic Colorectal Carcinoma." *World journal of gastroenterology* 11(14): 2166–70. http://www.ncbi.nlm.nih.gov/pubmed/15810086 (September 3, 2019).

Weitz, Jeffrey I. 1997. "Low-Molecular-Weight Heparins" ed. Alastair J.J. Wood. *New England Journal of Medicine* 337(10): 688–99. http://www.nejm.org/doi/10.1056/NEJM199709043371007 (July 14, 2019).

Wilhelm, Imola et al. 2013. "Role of the Blood-Brain Barrier in the Formation of Brain Metastases." *International Journal of Molecular Sciences* 14(1): 1383–1411.

Williams, S. B. et al. 1994. "Purification and Characterization of Human Platelet von Willebrand Factor." *British Journal of Haematology*.

Wilson, Melissa A., and Lynn M. Schuchter. 2016. "Chemotherapy for Melanoma." In *Cancer Treatment and Research*,.

de Wit, T R, and J A van Mourik. 2001. "Biosynthesis, Processing and Secretion of von Willebrand Factor: Biological Implications." *Best practice & research. Clinical haematology* 14(2): 241–55. http://www.ncbi.nlm.nih.gov/pubmed/11686098 (July 21, 2019).

Wun, Ted, and Richard H White. 2009. "Epidemiology of Cancer-Related Venous Thromboembolism." *Best practice & research. Clinical haematology* 22(1): 9–23. http://www.ncbi.nlm.nih.gov/pubmed/19285269 (July 1, 2017).

Yamamoto, Koji, Vivian de Waard, Colleen Fearns, and David J Loskutoff. 1998a. "Tissue Distribution and

Regulation of Murine von Willebrand Factor Gene Expression In Vivo." *Blood* 92(8): 2791–2801. http://www.bloodjournal.org/content/92/8/2791.abstract.

———. 1998b. "Tissue Distribution and Regulation of Murine von Willebrand Factor Gene Expression In Vivo." *Blood* 92(8): 2791–2801. http://www.bloodjournal.org/content/92/8/2791.abstract.

Yan, Shaofeng et al. 2016. "Epithelial-Mesenchymal Expression Phenotype of Primary Melanoma and Matched Metastases and Relationship with Overall Survival." *Anticancer research* 36(12): 6449–56. http://www.ncbi.nlm.nih.gov/pubmed/27919967 (July 21, 2019).

Yang, Ai Jun et al. 2018. "Cancer Cell-Derived von Willebrand Factor Enhanced Metastasis of Gastric Adenocarcinoma." *Oncogenesis* 7(1). http://dx.doi.org/10.1038/s41389-017-0023-5.

Yang, Jin-Gang, Li-Li Wang, and Dong-Chu Ma. 2018. "Effects of Vascular Endothelial Growth Factors and Their Receptors on Megakaryocytes and Platelets and Related Diseases." *British Journal of Haematology* 180(3): 321–34. http://doi.wiley.com/10.1111/bjh.15000 (July 14, 2019).

Yang, Y. et al. 2013. "Anti-VEGF- and Anti-VEGF Receptor-Induced Vascular Alteration in Mouse Healthy Tissues." *Proceedings of the National Academy of Sciences*.

Yokota, Hiroyuki. 2007. "Cerebral Endothelial Damage after Severe Head Injury." *Journal of Nippon Medical School*.

Yokota, N et al. 2009. "Self-Production of Tissue Factor-Coagulation Factor VII Complex by Ovarian Cancer Cells." *British journal of cancer* 101(12): 2023–29. http://www.ncbi.nlm.nih.gov/pubmed/19904262 (August 13, 2019).

Yuan, Lei et al. 2016. "A Role of Stochastic Phenotype Switching in Generating Mosaic Endothelial Cell Heterogeneity." *Nature Communications* 7(1): 10160. http://www.nature.com/articles/ncomms10160 (July 10, 2019).

Yun, Seong-Hoon et al. 2016. "Platelet Activation: The Mechanisms and Potential Biomarkers." *BioMed research international* 2016: 9060143. http://www.ncbi.nlm.nih.gov/pubmed/27403440%5Cnhttp://www.pubmedcentral.nih.gov/articlerender.fcgi?artid=PMC4925965.

Zhang, Zheng Gang et al. 2000. "VEGF Enhances Angiogenesis and Promotes Blood-Brain Barrier Leakage in the Ischemic Brain." *Journal of Clinical Investigation*.

Zhao, Fang et al. 2009. "Activation of P38 Mitogen-Activated Protein Kinase Drives Dendritic Cells to Become Tolerogenic in Ret Transgenic Mice Spontaneously Developing Melanoma." *Clinical Cancer Research* 15(13): 4382–90.

Zhou, Y.-F. et al. 2012. "Sequence and Structure Relationships within von Willebrand Factor." *Blood* 120(2): 449–58. http://www.ncbi.nlm.nih.gov/pubmed/22490677 (July 9, 2019).

Zhu, Ximin et al. 2016a. "Von Willebrand Factor Contributes to Poor Outcome in a Mouse Model of Intracerebral Haemorrhage." *Scientific Reports* 6(1): 35901. http://www.nature.com/articles/srep35901 (July 9, 2019).

———. 2016b. "Von Willebrand Factor Contributes to Poor Outcome in a Mouse Model of Intracerebral Haemorrhage." *Scientific Reports* 6: 1–11.

Zwicker, J. I. et al. 2009. "Tumor-Derived Tissue Factor-Bearing Microparticles Are Associated With Venous Thromboembolic Events in Malignancy." *Clinical Cancer Research* 15(22): 6830–40. http://www.ncbi.nlm.nih.gov/pubmed/19861441 (August 13, 2019).

8. List of tables and figures

9. Acknowledges

This work could not have been possible without the funding and support of the Research Training Group (RTG) 2099 “Hallmarks of Skin Cancer”, the Deutsche Forschungsgemeinschaft (DFG) and the Eric und Gertrud Roggenbuck foundation.

To my supervisors and collaborators…

I would like to start expressing my gratitude to the three members of my thesis advisory committee. In the first place, thanks to my principal supervisor Prof. Stefan Werner Schneider for offering me the opportunity to perform my Ph.D. thesis in his excellent research group, for his motivational spirit and for supporting my work throughout this years. Besides, I would like to thank Prof. Dr. Viktor Umansky, who made this thesis possible being my first supervisor and for providing us the ret transgenic mouse model. Moreover, thanks to Prof. Dr. Frank Winkler, for his excellent collaboration and help in the elaboration of our manuscript.

Besides, I would like to thank Prof. Dr. Peter Angel, Prof. Dr. Daniela Mauceri for enrolling in my thesis defense committee.

My sincere thanks also go to Prof. Dr. Anthony Dorling and his group members of the MRC Centre for Transplantation in the King's College London for giving me the opportunity to join their team for my research stay.

To my colleagues…

Very special gratitude is dedicated to all the members of the Experimental dermatology group, from the former times in Mannheim to our new location in Hamburg. I would like to start remarking the invaluable work of Natalia Halter, our technician in Mannheim, and her helpful spirit and patience. I would also like to thank our technician team in the UKE-Hamburg. New starts are always hard but they made everything easy from the very beginning. Therefore, special thanks to Sabine Vidal-Sy, Pia Houdek and Ewa Wladikoski. Thank you for your inestimable technical support, but more important for your warm welcome in the cold winter of 2018!

Thanks to Dr. Volker Huck, Dr. Christian Gorzelanny and Christian Mess for their scientific support and their friendly treatment. Particularly, I want to express my sincere gratitude to Dr. Alex Thomas Bauer who has been more than a master in the

performance of this work. Thank you for your time, your guidance, your advices, and thank you because you never leave anyone behind.

Thanks to all the students with whom I shared pains and joys during these years, Xiabo Liu (a long time ago since we met in Heidelberg in February 2015), Dr. Gustavo Ramos, Marisse Assong, Dr. Yi Yang, YuanYuan Wang, Tina Wolf, and Lydia von Palubitzki. I wish you all a lot of success in your fore coming career!

Thank you all for making me feel at home! I will miss you!

To my friends…

Special thanks to my friends in Bilbao, for your support and for remaining my friends after these years. Sellan, Cruz, Garde, Manu, Mere, Urce, Jon, Mikelo and particularly to Gabriel el chaman and Gomez super detective en Hollywood.

Also thanks to my friends in Mannheim, Blanca, Samu, Eva, Jesus, Ana, Paski, Merchi, and a long etc… It was a pleasure to share with you my first years in Germany.

To my friends in Hamburg, for their moral support and the good moments in the Cobertizo. Many thanks to Iago, Lluis, Eulalia, Eddie, Javitxu, Alicia, Oscar and all the rest, your friendship during the last year was a turning point to me in Hamburg and I will be always grateful for it.

Thanks to the coolest flatmate one can ever have. Wiebke, our evening talks about how to fix the world would provide enough material to write a second thesis, but it must wait. Your friendly spirit and your unconditional support in the last months have been meaningful for me. I wish you and the Katze all the best

Special thanks to my “brother in arms” Diego Martin. Who taught me how to survive in the most extreme decadence, how to deal with crazy roomies (either mammalians or from the fungi kingdom) and because he has always demonstrated to be a true friend.

And last but not least…

Special thanks to Sophie, for believing in me, for being next to me in every step, for your strength and courageous spirit. I am really grateful for having shared all this time with you. See you soon in Freiburg ☺

And finally thanks to my family, Lourdes, Ignacio, and Gonzalo. For your unconditional support, for your patience and for being there when I needed it.